Western Graduate&PostdoctoralStudies

Western University
Scholarship@Western

Electronic Thesis and Dissertation Repository

4-18-2012 12:00 AM

Applications of Rapid Cardiac Micro-CT

Sarah A. Detombe
The University of Western Ontario

Supervisor
Dr. Maria Drangova
The University of Western Ontario

Graduate Program in Medical Biophysics
A thesis submitted in partial fulfillment of the requirements for the degree in Doctor of Philosophy
© Sarah A. Detombe 2012

Follow this and additional works at: https://ir.lib.uwo.ca/etd

 Part of the Biophysics Commons

Recommended Citation

Detombe, Sarah A., "Applications of Rapid Cardiac Micro-CT" (2012). *Electronic Thesis and Dissertation Repository*. 497.
https://ir.lib.uwo.ca/etd/497

This Dissertation/Thesis is brought to you for free and open access by Scholarship@Western. It has been accepted for inclusion in Electronic Thesis and Dissertation Repository by an authorized administrator of Scholarship@Western. For more information, please contact wlswadmin@uwo.ca.

APPLICATIONS OF RAPID CARDIAC MICRO-CT

(Thesis Format: Integrated-Article)

by

Sarah A. Detombe

Department of
Medical Biophysics
Schulich School of Medicine and Dentistry

Submitted in partial fulfillment
of the requirements for the degree of
Doctor of Philosophy

School of Graduate and Postdoctoral Studies
The University of Western Ontario
London, Ontario

April 2012

© Sarah A. Detombe 2012

THE UNIVERSITY OF WESTERN ONTARIO
SCHOOL OF GRADUATE AND POSTDOCTORAL STUDIES

Certificate of Examination

Chief Advisor

Maria Drangova, Ph.D.

Advisory Committee

David W. Holdsworth, Ph.D.

Qingping Feng, M.D., Ph.D.

Examining Board

James Lacefield, Ph.D.

Ting-Yim Lee, Ph.D.

Morris Karmazyn, Ph.D.

John Sled, Ph.D.

The thesis by

Sarah A. Detombe

entitled:

Applications of Rapid Cardiac Micro-CT

is accepted in partial fulfillment of the
requirements for the degree of
Doctor of Philosophy

Date _____

_____
Chair of Examining Board

Abstract

Mouse models are an important tool in cardiovascular disease research, and a non-invasive imaging method is an advantageous way of monitoring disease progression. Cardiac micro-CT is rapid imaging technique capable of quantifying changes in cardiac structure and function in mice. The goal of this thesis was to demonstrate the utility of this technique in monitoring disease progression in a longitudinal study, as well as its capability for evaluating other methods of measuring cardiac function in mice.

In a longitudinal study, a mouse model of myocardial infarction was scanned weekly for four weeks; left ventricular volume and ejection fraction were measured from the images. Cardiac micro-CT was capable of tracking small changes in cardiac structure and function, with the MI mice demonstrating a significant increase in volume and a significant decrease in ejection fraction. Both inter- and intra-variability was low, indicating the results were highly reproducible.

Contrast agents are essential to evaluating the heart in micro-CT images. A new blood-pool agent was evaluated to determine its suitability for use in cardiac micro-CT studies. The agent produced excellent enhancement for the first 30 minutes post-injection, and had a unique characteristic of enhancing the myocardium, which may prove useful in studies evaluating wall motion.

The effect of x-ray dose delivered during a longitudinal micro-CT study was also evaluated. C57BL/6 mice were scanned weekly for six weeks; the total entrance dose delivered over the study was 5.04 Gy. No significant changes to the heart or lungs were detectable on the micro-CT images at six weeks, and the histology performed on myocardial and pulmonary tissue showed no indication of early inflammation at a cellular level. Micro-CT can therefore be used in longitudinal studies without concern of adverse effects.

Cardiac micro-CT was used to evaluate conductance catheters, and found that the catheter volumes were drastically underestimated compared to the micro-CT volumes. It was also determined that catheterization has the potential for causing cardiac enlargement; 40% of the mice demonstrated enlarged hearts following the catheterization

procedure. Overall, cardiac-gated micro-CT is a rapid and reproducible imaging technique, and is proving to be valuable tool in cardiovascular disease research.

Key Words: cardiac micro-CT, micro-computed tomography, retrospective gating, contrast agent, conductance catheter, x-ray dose, mouse model, left ventricle, ejection fraction, cardiovascular disease

Co-authorship

Chapter 2 was published in *Investigative Radiology* as: SA Detombe, NL Ford, F Xiang, X Lu, Q Feng, and M Drangova, "Longitudinal follow-up of cardiac structure and functional changes in an infarct mouse model using retrospectively gated micro-computed tomography," *Invest Radiol* 43, 2008. All authors contributed to the editing of the paper. Fuli Xiang and Xiangru Lu were responsible for surgically creating the infarcts in the MI mouse group, as well as acquiring and analyzing the hemodynamic measurements. Nancy Ford was responsible for scanning half of the mice, and I was responsible for scanning the other half. I reconstructed and analyzed the micro-CT images, analyzed the resulting data, and performed the statistical analyses. Nancy and I worked under the supervision of Maria Drangova, and Fuli Xiang and Xiangru Lu worked under the supervision of Qingping Feng.

Chapter 3 was published in *Contrast Media and Molecular Imaging* as: SA Detombe, J Dunmore-Buyze, and M Drangova, "Evaluation of eXIA 160 Cardiac-related Enhancement in C57BL/6 and BALB/c mice using Micro-CT", *Contrast Media Mol Imaging* 7, 2012. All authors contributed to the editing of this paper. Joy Dunmore-Buyze helped with scanning the mice, and was responsible for their care during the study. I acquired the scans, reconstructed the images, performed the image analysis and analyzed the resulting data, and carried out the statistical analyses. All work was carried out under the supervision of Maria Drangova.

Chapter 4 is in preparation to be submitted with the authors: SA Detombe, J Dunmore-Buyze, IE Petrov, and M Drangova. Joy Dunmore-Buyze helped with the scans, mainly responsible for animal handling and care both during, and in between, scan sessions. Ivailo Petrov reconstructed the scans with respiratory gating. I acquired all the scans, reconstructed the cardic-gated images, analyzed the images and resulting data, and performed the statistical analyses. All work was carried out under the supervision of Maria Drangova.

Chapter 5 is in press with the *Journal of Applied Physiology* as: SA Detombe, F Xiang, J Dunmore-Buyze, JA White, Q Feng, and M Drangova, "Rapid micro-computed tomography suggests cardiac enlargement occurs during conductance catheter

measurements in mice", 2012. All authors contributed to the editing of the paper. Fuli Xiang was responsible for surgically creating the infarcts in the MI mice, and she also participated in the scan sessions, during which she catheterized the mice and collected the hemodynamic data. She is also responsible for analyzing the hemodynamic data. Joy Dunmore-Buyze was responsible for animal handling, and helped during the scan sessions. I acquired all the scans, reconstructed the images, analyzed the images and the resulting data, including the comparison to the hemodynamic data. I also performed the statistical analyses. James White helped with the interpretation of the data as it related to cardiovascular physiology. I worked under the supervision of Maria Drangova, and Fuli Xiang worked under the supervision of Qingping Feng.

Acknowledgements

First and foremost, this thesis would not have been possible without the dedication, advice, and unwavering patience of my supervisor, Dr. Maria Drangova. She supported and encouraged me through all my ups and downs, and her contributions and advice on everything from experimental design to conference presentations has been invaluable. She is both a mentor and a friend, and I am sincerely grateful for her generosity and input during my graduate studies.

Thank you to my committee members, Dr. David Holdsworth, and Dr. Qingping Feng, for their interest in both my research and my progress. Our conversations were always edifying, and often entertaining.

Thank you also to Joy Dunmore-Buyze, for her never-ending patience as I rambled on about my projects (and anything else), as well as for being willing to forgo an evening with her daughter to come and scan with me instead – she made those long scan sessions not just bearable, but enjoyable (well, almost!). I truly appreciate all her suggestions and help over the years.

I was lucky to work with Dr. Fuli Xiang, a wonderful collaborator, on several of my projects. She is a skilled surgeon who managed to make catheterizing mice look easy. I'm thankful for her willingness to come scan again and again as we worked out the logistics, as well as for showing a genuine interest in the imaging aspects of the project.

I also want to thank a number of individuals who have helped me over the years. Dr. Nancy Ford first taught me the ropes, and was patient with a very green new student. Thank you also to Steve Pollman, Chris Norley, and Hristo Nikolov for their technical support, whether it was rebooting a stubborn computer, or fixing malfunctioning equipment on the fly (because things always break when there's a mouse asleep in the scanner); my thesis went smoother because of their help. And a great big thank you to Jennifer Hadway, whose skill with tail vein injections made these projects possible.

I would like to acknowledge my funding sources over the years. I was funded by a Heart and Stroke Master's Studentship from 2005 to 2007, Ontario Graduate Scholarships from 2007 to 2009, and a CIHR Frederick Banting and Charles Best Canada

Graduate Scholarship from 2009 to 2010. I would also like to acknowledge support from the CIHR Vascular Research Fellowship, the Western Graduate Research Scholarships, and the Schulich Graduate Scholarships.

And finally, I am forever grateful to my family. My parents, John and Cindy, have provided love and support no matter what I chose to do. They are ever encouraging and always interested in my work, celebrating my successes, and commiserating my setbacks. They are also the rock I cling to during the stormy times of my life. They instilled all of their children with a love of learning, and I am where I am today because of them. And my brothers, Jon and Andrew: although being scattered across the country means we don't often meet face-to-face, their support from afar means a lot, and their phone calls always manage to make me laugh, even on my toughest days. My Ph.D. would not have been possible without the encouragement of my entire family, and to them I dedicate this thesis.

Table of Contents

List of Tables

List of Figures

List of Symbols

α	Baan's constant
G	Total conductance
G_p	Parallel conductance
L	Length between the electrodes
ρ	Resistivity constant
μ_{tissue}	Mean attenuation coefficient of tissue within a voxel
μ_{water}	Mean attenuation coefficient of water
V	Volume

List of Acronyms & Abbreviations

2D	Two-dimensional
3D	Three-dimensional
ANOVA	Analysis of variance
BAT	Brown adipose tissue
CC	Conductance catheter
CO	Cardiac output
CT	Computed tomography
CVD	Cardiovascular disease
dP/dt_{max}	Maximal rate of LV pressure increase
dP/dt_{min}	Maximal rate of LV pressure decline
ECG	Electrocardiogram
EDV	End-diastolic volume
EF	Ejection fraction
ESV	End-systolic volume
Gy	Gray
HR	Heart rate
HU	Hounsfield unit
IP	Intraperitoneal
ITG	Iodinated triglyceride
kVp	Kilovolt peak
LD_{50}	Dose that is lethal to 50% of the subjects in 30 days
LV	Left ventricle
mA	Milliampere
MI	Myocardial infarction
micro-CT	Micro-computed tomography
MR/MRI	Magnetic resonance imaging
PEG	Polyethylene glycol
PET	Positron-emitted tomography
PV	Pressure-volume

RES	Reticuloendothelial system
ROI	Region of interest
RV	Right ventricle
RVU	Relative volume units
s.c.	Sub-cutaneous
SD	Standard deviation
SEM	Standard error of measurement
SNR	Signal to noise ratio
SPECT	Single positron-emitted computed tomography
SV	Stroke volume

1 Introduction

1.1 Overview

Cardiovascular diseases (CVD) are the leading cause of mortality worldwide, responsible for over 17.3 million deaths per year.[1] In Canada, 29% of all deaths annually are attributed to CVD,[2] and it is estimated to cost the Canadian economy $20.9 billion every year.[3] But on a positive note, the country has also seen a steady decline in deaths related to CVD over the past forty years, which can be partly attributed to the research investigating treatment strategies and prevention. An abundance of this research is performed in mouse models, a necessary step in translating basic science research to implementation in human patients; given the importance of preclinical investigations, the development of techniques specifically designed to assess cardiac function in small animals is an essential area of research. Cardiac micro-computed tomography (micro-CT) is one such technique, which offers a rapid, non-invasive imaging method to monitor changes in cardiac structure and function over time, providing quantitative information on both ventricular volume and function.

The goal of this thesis is to demonstrate the role of micro-CT in cardiac studies involving mouse models. A method for retrospectively gating cardiac micro-CT scans had been recently developed (fully detailed in Appendix A), and the next step was to assess the ability of this technique to measure quantitative changes in both ventricular volume and cardiac function over time. Several key aspects of micro-CT imaging were also investigated: the use of a contrast agent is important for differentiating the blood pool from the myocardium, and a new agent had shown some unique properties that were investigated for their applicability to cardiac studies. Additionally, a frequent concern associated with micro-CT imaging is the x-ray dose delivered to the animal, which becomes more relevant in longitudinal studies where an animal is imaged multiple times. Therefore, the effects of dose on cardiac and pulmonary tissue, delivered during a longitudinal study, were evaluated. Finally, cardiac gated micro-CT was used to

determine if another frequently used measurement technique, conductance catheterization, had any detrimental effect on the mouse heart.

In order to provide some context for the subsequent chapters, this chapter first discusses the advantages of using mouse models, as well as some of the cardiovascular diseases that can be modeled. Methods used to evaluate the cardiovascular system in mice are briefly outlined, as well as the advantages of employing imaging techniques. Options for cardiovascular imaging are presented, followed by a more detailed discussion of computed tomography in general, and of cardiac micro-CT more specifically. Some of the key elements associated with micro-CT, including use of a contrast agent and the radiation dose delivered to the animal, are explored, and finally, some potential applications of cardiac micro-CT are presented, followed by a more detailed outline of the thesis chapters.

1.2 Preclinical Cardiovascular Research

Clinical investigation of cardiovascular diseases is an important approach for trying to understand etiology and the impact of therapies, but animal models are essential tools for determining the mechanism of pathogenesis, as well as investigating interventions. With animal models it is possible to investigate a risk factor as a single independent variable, given the well-known genetic characteristics, as well as the absence of any abnormalities. New diagnostics, treatments, and preventative procedures are also best performed in animals, given ethical and practical considerations.

Large animal models are often used as a final step before beginning clinical investigations.[4] Dogs, sheep, and pigs are common species, and the decision of which animal to use is based on the disease or disorder being modeled, as each species best reflects different aspects of human cardiac physiology.[5] Small animal models have greater differences in physiology compared to humans, but much of the insight into the molecular and cellular basis of cardiovascular biology is a result of using these smaller species, particularly mice.[6]

1.2.1 Advantages of Mouse Models

One of the major advantages of using the mouse as a small animal model of cardiovascular disease is the availability of well-defined genetics. Highly standardized mouse strains have been created, whose genetic characteristics are precisely known,[7] and the use of these inbred strains has offered the ability to investigate disease at the genomic level; the genetic background of a mouse can be manipulated very precisely and with relative ease, which can then be correlated to the phenotype of a living animal. Use of transgenic mouse models enables specific characteristics of cardiovascular disease to be investigated,[6] and it also offers the opportunity to define new therapeutic strategies that may one day be of use to the human population. In addition, use of the mouse to model diseases is also popular due to the economic and practical benefits of working with small animals.

The size of the mouse, and consequently the heart, is the main challenge of working with the species; the small size and rapid heart rate can act as an impediment to investigations.[8] However, advances in technology have led to the availability of increasingly diminutive tools and more sophisticated measurement techniques, making it easier for researchers to benefit from the advantages of using mouse models.

1.2.2 Cardiovascular Disease Models

Many cardiovascular diseases can be modeled in mice, through genetic manipulation, surgical interventions, pharmacological agents, or through changes in external factors such as diet modifications. For example, atherosclerosis is modeled in mice by the generation of plaques caused by hyperlipidemia. Hyperlipidemia can be induced by using a genetically modified mouse model that lacks ApoE, or a model deficient in LDL receptors,[9, 10] both of which result in increased cholesterol levels in the bloodstream. Hyperlipidemia can also be induced by dietary modifications, changing the mouse's normal chow to one high in saturated fat and cholesterol;[9] a combination of the two methods is also used.[11]

Pharmacological agents can also be used to induce a cardiovascular disease state. Angiotensin II is a peptide hormone that is responsible for constricting blood vessels and

increasing blood pressure, but it has also been discovered that chronic subcutaneous infusion leads to the development of abdominal aortic aneurysms through direct inflammatory effects.[12]

A mouse model of myocardial infarction, on the other hand, is created through surgical intervention.[13] The thorax of the mouse is opened and, commonly, the left anterior descending coronary artery is ligated to create an infarct in the apex region of the left ventricle. This model could either represent a chronic infarction, where the ligation is left in place,[14, 15] or a reperfusion model, where the ligation is removed after a certain period of time.[16, 17]

1.2.3 Methods of Evaluation

There are a number of techniques used to evaluate and quantify the disease process in mice. They are often terminal in nature, requiring that the heart be removed for evaluation. For example, histological evaluation of the aortic root,[18] or cross-sections of fixed aortas, is used to quantify atherosclerotic lesions, as well providing the opportunity for morphological analysis. Evaluation of the weight and diameter of the heart can also provide useful information in cases of cardiac hypertrophy. Myocardial infarctions are often quantified through histology;[19] blood markers (*i.e.* cardiac proteins) can also provide useful data.[20]

Catheterization is also often used in cardiac analysis. Electrophysiological catheters can be inserted into the right ventricle (RV) and changes to the conduction system of the heart investigated.[21, 22] Conductance catheters are a frequently-used method of monitoring cardiac function. This is accomplished by inserting a pressure-conductance catheter, measuring 1.4F in diameter, into the left ventricle (LV). The catheter contains a pressure sensor, which measures the pressure of the LV, and four electrodes, which create an electric field and measure the conductance of the blood within the LV. Conductance measurements are converted to volume measurements using the equation $V = \rho L^2 (G - Gp)/\alpha$ where ρ is the resistivity constant, L is the length between the electrodes, α is Baan's constant, G is the total conductance measured, and G_p is the parallel conductance of the surrounding tissue. When combined with the pressure measurements, real-time pressure-volume loops are created that give information about

heart function and myocardial health.[23, 24] Both types catheters are often inserted into the heart retrograde through the aortic valves, and although in theory they can be removed without requiring the animal be sacrificed, that is not usually the case.

As technology continues to improve, non-invasive methods are becoming increasingly available. Imaging techniques can be used to quantify atherosclerotic plaques[25, 26] and myocardial infarcts,[13, 27] and measure the size and mass of the heart,[28, 29] without sacrificing the animal. Echocardiography is especially useful for non-invasive hemodynamic measurements.[28] Several imaging modalities used in CVD research are detailed in the next section.

1.3 In vivo Micro Imaging

One of the key advantages of *in vivo* imaging of mouse models is the non-invasive nature of the technology. The ability to evaluate the heart *in vivo* may provide information about morphology that would be lost by the removal of the organ. Individual animals can also be followed throughout the study, rather than sacrificing a group of mice at each time point; this may decrease the number of animals required for a study to reach statistical significance, with the added advantage of tracking disease progression or treatment process in the same animal.

1.3.1 Echocardiography

Echocardiography is a rapid and portable imaging technique, making it easy to integrate into active physiology research labs. Its value in investigations employing mouse models has increased since the availability of high-frequency small-animal ultrasound devices, which have a resolution range of approximately 65 μm – 200 μm, making it easier to evaluate the small anatomy of the mouse.[30] Even more significant to the field of cardiovascular imaging has been the introduction of linear array transducers, which, along with a high resolution, have an increased frame rate that enables the ability to evaluate individual phases of the cardiac cycle with sufficient temporal resolution.[30]

Although 3D echocardiography has been demonstrated,[31] left ventricular volume is typically measured using M-mode or 2D images. This necessitates the translation of 2D measurements to 3D volumes, which requires geometric approximations; although these approximations may produce reasonably accurate volumes of a healthy, regular-shaped heart, if the organ is misshapen or distorted, as it would be in models of myocardial infarction, for example, it would be more difficult to obtain accurate measurements. Additionally, since measurements are taken from only one longitudinal plane, foreshortening may occur, where the ultrasound beam is not passing directly through the centre of the chamber, creating artificially smaller chamber dimensions, and resulting in a smaller LV volume.

One of the key advantages of echocardiography is the ability to measure hemodynamic function non-invasively;[28] for example, flow velocity in arteries or through cardiac valves can be quantified using Doppler imaging. This imaging technique may also be used to evaluate myocardial strain, through the use of tissue Doppler imaging.

1.3.2 MRI

Magnetic resonance imaging (MR/MRI) enables the acquisition of high-resolution images, with high soft tissue contrast. MR images are typically anisotropic, with an in-plane resolution between 50 μm and 120 μm, and slice thicknesses of approximately 1 mm. Although 3D cine MRI with isotropic resolution has been demonstrated,[32] time constraints may be a limiting factor, as one scan with sufficient SNR typically takes more than one hour to acquire.

Cine MRI can be used to evaluate both cardiac structure and, with the use of gating techniques, cardiac function.[33] MRI has the advantage of not requiring a contrast agent to evaluate the heart. Bright blood imaging methods are typically used, but black blood cine imaging can also be performed,[34] which provides more accurate measurements of LV mass and volume; the acquisition time, however, more than doubles. The definitive myocardial boundaries enable the measurement of wall mass, which can be used to track cardiac hypertrophy in mouse models displaying cardiomyopathy.[34, 35] The high resolution of soft tissue also enables wall motion measurements to be acquired, for example with the use of tagged cine MRI.[36]

MRI typically has long exam times, made longer still with the use of gating to capture individual phases of the cardiac cycle. This has implications on the health of the animals being scanned – the longer they are under anesthetic, the greater the risk of developing complications; the risk is more significant with mouse models that are likely already in compromised health.

1.3.3 Nuclear Medicine Imaging

Molecular imaging is a growing field that includes single photon emission computed tomography (SPECT) and positron emission tomography (PET), both of which are imaging modalities that use radionuclides as tracers. One of the main advantages of this type of imaging is the ability to study dynamic biologic processes within *in vivo* mouse models. For example, areas of myocardial ischemia can be detected by changes in perfusion, measured via SPECT imaging after injection of ^{99m}Tc-sestamibi.[37]

Micro-SPECT imaging probes are labeled with gamma-emitting radionuclides that are detected using SPECT cameras with lead collimators. Micro-PET probes are labeled with positron-emitting radionuclides, which produce gamma rays through annihilation events. Both imaging techniques are highly sensitive to trace amount of radioactivity, enabling small amounts of an individual probe to be used. However, both technique have a relatively low resolution (micro-SPECT has a resolution of 0.5 mm – 2mm; micro-PET has a resolution of 1 mm – 2 mm), and require a generator/cyclotron to produce the necessary radionuclides.[38] There is also a lack of anatomic information available in SPECT and PET images; this, however, has been improved by using combined SPECT/CT and PET/CT images, where the CT provides the necessary anatomical boundaries (for example, the myocardial border) to properly interpret the SPECT/PET information.[38]

1.3.4 Micro-CT

Micro-CT is a rapid imaging method with a high isotropic resolution of 150 μm or better.[39] Micro-CT is faster and more economical than MRI, and has a higher SNR than echocardiography. However, the inherent low soft tissue contrast of micro-CT

requires the use of a contrast agent in cardiac studies,[40-42] and it also prevents any evaluation of myocardial strain or function. Also, as micro-CT uses x-rays, another concern is the effect of the radiation dose on the animal being scanned, which places an upper limit on image quality in an *in vivo* application. A more detailed description of cardiac micro-CT follows in Section 1.5.

1.4 Overview of Computed Tomography

Computed tomography (CT) was first introduced by Sir Godfrey Hounsfield in the early 1970's as an imaging technique that uses a series of x-ray projection images to generate cross-sectional images, or slices, of an object.[43] The images essentially represent a map of the linear attenuation coefficients of the object scanned, expressed in a matrix of volume elements (voxels). The intensity of each voxel is proportional to the attenuation coefficient and is expressed in Hounsfield units, calculated as:

$$CT\# = \frac{\left(\mu_{tissue} - \mu_{water}\right)}{\mu_{water}} \times 1000 HU, \qquad (1.1)$$

where μ_{tissue} is the mean attenuation coefficient of the tissue within that voxel. X-ray attenuation is primarily a function of x-ray energy and the density and composition of the material being scanned.

The fundamental components of a CT scanner include an x-ray source and a detector, which rotate about the object being scanned. Collimators are used to help reduce the dose delivered to the patient, as well as to prevent scattered photons from hitting the detector; filters are used remove the low-energy x-rays from an emitted beam before they reach the object, in an effort to reduce beam hardening. The tube's voltage and current values are chosen based on the composition and size of the object being scanned. The acquired projection data are typically reconstructed using filtered back-projection,[44] which has traditionally been computationally faster than Fourier transform[45] and algebraic reconstruction techniques,[46] although algebraic reconstruction techniques are gaining popularity.

There have been a number of advancements in scanner geometries over the past forty years.[47] The earliest systems used a translate/rotate method, during which the pencil beam x-ray source and detector moved laterally, then rotated around the object and repeated the process; this system required approximately 4.5 minutes to image a single slice. Second generation scanners used a fan-beam x-ray source and an array of detectors, thereby improving the speed and efficiency of data collection during the translation process. With this improvement, imaging times were reduced to 2.5 minutes per slice. Third generation scanners employed larger detector arrays, and wider fan-beam angles, preventing the need for translation and relying solely on source/detector rotation around the object; scan time was further reduced to 18 seconds. Fourth generation scanners replaced the moving detector array with a fixed detector ring; however, because these scanners tend to be more expensive and suffer from higher levels of Compton scatter artifacts, most of the commercial CT scanners available today are third generation. The improvement in scan times enabled the CT scanner to become widely used in whole-body imaging, and was capable of imaging fairly static cardiac structures such as the pericardium, the contracting heart was not well visualized. A further problem existed in the form of scanner cabling restricting the tube movement; this was solved in the early 1990's with the introduction of slip-ring technology,[48] enabling continuous acquisition of data over multiple rotations. Combined with increasingly fast scanners, decreases in detector element size, and the introduction of multislice detector CT scanners, imaging of dynamic processes such as the beating heart are now possible, when combined with gating techniques.[49]

The spatial resolution of clinical scanners (*i.e.* 1 mm^3 voxel elements) prevented their use in investigations using small animals, but technical advances in computing speed and detector technology made it possible to obtain images of small-specimens and -animals with a resolution measured in micrometers.[50]

1.5 Micro-computed tomography

Micro-CT was first developed in the early 1980's[51, 52] for use in applications with very fine structures that required a high resolution to visualize. However, in order to

provide CT image signal-to-noise ratio (SNR) comparable to clinical CT scanners, the x-ray exposure of the animal or specimen needed to be increased by an amount proportional to at least the inverse of the voxel volume.[53] X-ray tubes with a larger focal spot can achieve higher fluence rates and therefore an increase in exposure, however this would also introduce blurring. Therefore the only way to increase dose is by using longer scan times. Specimen scanners typically use a micro-focus x-ray tube and variable geometric magnification; as x-ray exposure is not an issue with tissue samples, projection data may be acquired over a few hours, resulting in high-resolution images with isotropic voxels ranging from 15-50 μm over a field of view (FOV) of 15-50 mm.[50, 54] In *in vivo* imaging, a compromise between voxel size and shorter scan times is required, both to limit the dose delivered to the live animal, as well as to minimize the length of time the animal is under anesthetic. Another difference between specimen and *in vivo* scanners is that the specimen is rotated while the x-ray tube/detector assembly remains stationary, whereas with commercial *in vivo* scanners, the x-ray tube/detector assembly is rotated around a stationary animal.[50]

1.5.1 *In vivo* micro-CT

As mentioned in the previous section, *in vivo* imaging necessitates a decrease in resolution in order to limit the x-ray dose delivered to the animal. The decrease in resolution requirements enables the use of lower geometric magnifications and larger x-ray tube focal spot size, facilitating higher tube current and shorter acquisition times, typically 5-10 minutes.[50] The resolution of these scanners ranges from 25-100 μm, with a FOV of 45-55 mm.

Traditional micro-CT scanners use a step-and-shoot mode, where the gantry moves in a stepwise motion around the animal, and projection data are acquired at each position. The development of a continuous rotation mode, where data are collected constantly during a continuous gantry rotation, has decreased acquisition times; with the implementation of slip ring technology, commercial scanners such as the GE Locus Ultra are capable of rapid multiple continuous rotations, enabling capture of dynamic processes in a living animal, such as in cardiac and lung imaging.[42, 55]

In addition to the faster acquisition times, cardiac and lung imaging also require a gating method to "freeze" the motion of the organ, necessary for both structural and functional evaluation. A physiological monitoring and triggering system is required, such as the BioVet system available from m2m Imaging, to monitor and record the ECG and/or respiratory signal of the animal, and to send triggers to the scanner at the appropriate time point in the physiological waveforms. These triggers act as a signal for x-ray activation during prospective gating, and are used to identify the appropriate projection data when reconstructing images during retrospective gating. Further information regarding these gating protocols is detailed in section 1.5.2.

Other considerations when imaging live animals is the method of anesthesia used, as well as the maintenance of physiological homeostasis while anesthetized. An anesthetic is required to keep the animal motionless during the scans, and to minimize stress. Typical anesthetics used include inhalational anesthetics, such as isoflurane,[56] and injectable anesthetics such as a ketamine/xylazine combination.[57] The most appropriate anesthetic depends on the type of study; for example, during cardiac studies isoflurane is the best choice, as it has minimal effects on heart rate and cardiac function, and will therefore not dramatically interfere with interpretation of the results.[56] Body temperature maintenance is also an important factor during *in vivo* imaging, as an animal cannot properly maintain its own temperature while anesthetized. When scanning mice, the temperature should remain between 36-37°C to sustain proper physiologic function. This is especially important during cardiac imaging, where body temperature has a significant impact on heart rate, and ultimately cardiac function.[58] The recent introduction of an animal management system,[59] capable of maintaining the animal's body temperature and anesthesia level within an enclosed tube, while also monitoring ECG and respiratory signals, offers a solution for simplifying the physiological monitoring process during micro-CT scans.

Micro-CT images are based on linear attenuation coefficients, so a contrast agent is required when interested in imaging soft tissues.[40, 42] For example, during cardiac scans, a contrast agent is required to differentiate the blood pool in the heart chamber from the myocardium, which is necessary when measuring chamber volumes, or evaluating structural changes. One objective of this thesis has been to evaluate a new

blood pool contrast agent and its applicability for use in cardiac studies. This is further discussed below.

1.5.2 Cardiac-gated micro-CT

In order to evaluate cardiac structure and function, selected phases of the cardiac cycle need to be reconstructed. The challenge of imaging the mouse heart is its small size and rapid heart rate, but the development of fast, high-resolution micro-CT scanners has helped to address these challenges. A gating technique is also required to "freeze" the motion of the heart; either prospective or retrospective gating can be used. Both gating techniques can also be used to image the lungs: the high contrast between pulmonary tissue and the rest of the body makes micro-CT images particularly appropriate for evaluating lung function, but a gating method is required to generate images in both inspiration and expiration phases.[55, 60]

Prospective cardiac gating during a micro-CT scan was first described by Badea *et al.*[40, 61] During prospective gating, projection data are only acquired during a selected phase of the cardiac cycle, e.g. diastole, with a temporal resolution (*i.e.* window size) of 10-15 ms. In other words, the ECG of the mouse is monitored continuously, and the x-rays are only triggered when a specific phase is reached.[40] The main advantage associated with prospective gating is the lower dose delivered to the mouse compared to retrospective gating. The main disadvantage of using prospective gating is length of time required: it can take up to 15 minutes to acquire data for only one cardiac phase, making it a challenge to carry out high throughput experiments, although recently Guo *et al.* has introduced a fast prospective gating technique that acquires a scan in less than 5 minutes.[62] Additionally, it may be challenging to maintain a consistent heart rate during the longer scan, depending on experimental setup; a change in heart rate may alter the placement of the desired cardiac phase within the ECG, leading to the x-rays being triggered at the incorrect phase.

Retrospective gating is carried out by continuous acquisition of projection data for the duration of the scan. ECG is monitored and recorded during the scan; following data collection, projections occurring at the selected phase of the cardiac cycle are then used to reconstruct an image. This enables reconstruction of multiple images of the heart

spanning the entire cardiac cycle from one scan. Retrospective cardiac gating in micro-CT scans was first described by Drangova *et al.*;[42] using a scanner with a slip-ring gantry, projection data were continuously acquired over 10 rotations in a 50-second scan time (this scanning and reconstruction technique is fully described in Appendix A). This technique, employed in the study described in Chapter 2, uses a 12 ms fixed window size, enabling between nine to twelve images to be reconstructed throughout the cardiac cycle. Retrospective gating is also possible with a step-and-shoot scanner, but the acquisition times and doses are much larger.[63] The advantage of the retrospective gating technique is the rapid scan times and large amount of data acquired in that short time, making it ideal for high throughput studies. One drawback associated with retrospective gating is the inevitable irregular angular distribution of the collected projections, which can lead to streaking in the reconstructed image; however, reconstruction algorithms have been proposed that minimize streaking in the final image.[63, 64] One such method, described by Armitage *et al.*,[64] uses a least-error sorting technique, where the projections closest to the phase of interest in the cardiac cycle are used to fill the view angles. Approximately 80% of the angles can be filled at a fixed window size (*i.e.* 12 ms), the window is then incrementally expanded to fill in the missing views with projections acquired at a slightly different phase. Using the scanning protocol outlined in Appendix A, this results in an effective window size of 27 ms. In Chapters 4 and 5, a variation of the least-error technique is used – the images are reconstructed with only the first 80% of view angles filled, resulting in a window size close to the 12 ms described in Appendix A, but without the streaking artifacts.

Another potential drawback associated with retrospective gating is the dose; the x-rays are on continuously during the scan, leading to a higher delivered dose than during prospective gating. One of the objectives of this work has been to determine the effects of x-ray dose during a longitudinal retrospectively gated study on the mouse, and will be discussed further below.

1.5.3 Contrast agents

As was mentioned previously, a contrast agent of radio-opaque material is required to enable soft tissue differentiation in a micro-CT image. Specifically,

evaluating cardiovascular function requires a contrast agent to differentiate between the blood in the heart chambers and the myocardium.

Clinical contrast agents in use, such as iohexol, a nonionic iodinated contrast agent, provide excellent contrast between blood and tissue, but are quickly cleared via glomerular filtration; this is useful for perfusion studies, but scans measuring cardiac function in small animal models require longer scan times with consistent contrast, and an optimal protocol using iohexol can be challenging to develop. A contrast agent was therefore required that remained within the blood-pool for an extended period of time. Fenestra VC, an iodinated triglyceride (ITG) emulsion containing polyethylene glycol (PEG) molecules, was the first to be developed.[65] The PEG molecules prevent rapid uptake of the ITG by the liver, providing contrast in the blood for over four hours.[66] Other blood-pool agents have since been developed. For example, Exitron nano 12000 is an alkaline earth-based nanoparticulate contrast agent with a delayed uptake by the reticuloendothelial system, resulting in sufficient vascular contrast for over two hours.[67] eXIA 160 is another example; it is described as an aqueous colloidal polydispersed contrast agent with a delayed diffusion from the vasculature. But although the liver- and spleen-enhancing properties of this contrast agent have been investigated,[68] there has not yet been an evaluation of its suitability for use in cardiac studies.

The blood volume of a 25 g mouse is 1.5 – 2 mL, and so contrast agents with a higher iodine concentration are more beneficial, as they require a lower injected volume to achieve sufficient enhancement and are less likely to disrupt the hemodynamics of the mouse. Fenestra VC has the lowest iodine concentration: at 50 mg/mL, a recommended dose is 500 µl for a 25 g mouse, a significant fraction of the animal's blood volume.[40] By comparison, in order to achieve the same enhancement, Exitron nano 12000, with an equivalent iodine concentration of 300 mg/mL,[67] would require an injected volume of 83 µl, and eXIA 160, with a iodine concentration of 160 mg/mL, would require an injected volume of 156 µl.

1.5.4 Radiation Dose

One of the main perceived drawbacks of micro-CT is a concern over the x-ray dose delivered during the scans. A typical ungated micro-CT scan delivers a dose of 10

cGy,[69] which, although much smaller than the LD_{50} of the mouse,[70] is larger than the dose delivered during a clinical cardiac CT (2-5 cGy).[71] This is particularly relevant in longitudinal studies, where more than one scan is performed per animal. Additionally, studies requiring cardiac or pulmonary gating deliver a larger dose.[42]

In cardiac studies, the main tissue of interest is the myocardium; x-ray damage can result in necrotic and fibrotic areas developing in the tissue, contributing to radiation-induced cardiac hypertrophy.[72] However, cardiac tissue is not particularly radiosensitive, and therefore not the best choice for determining dose effects in mice. Pulmonary tissue, on the other hand, is one of the most radiosensitive in the body; the lungs will therefore be the first to display the effects of x-ray dose, making it the ideal organ to use for evaluation. X-ray damage in the lungs generally presents in two phases, an early inflammatory phase, often called radiation pneumonitis, and a later chronic fibrosis phase.[73] For the purposes of most micro-CT studies the early inflammatory phase is the most relevant; it results in an increase in inflammatory cells building up in the alveoli and pulmonary ducts of the lungs, resulting in a decrease in lung volume, and an increase in lung density.

There have been a number of studies looking at the effect of dose on pulmonary tissue in mice;[74, 75] however, they have focused mainly on investigating radiotherapy doses of 10-20 Gy delivered in a single session at the beginning of the study. Additionally, evaluation of dose effects typically does not begin for 8-12 weeks following delivery. This creates some difficulties in trying to apply the results of these studies to a typical micro-CT study, where the doses are smaller, often by a factor of 100, delivered multiple times over a period of weeks, in a study less than 8 weeks in length. The effect of dose during a longitudinal micro-CT study has not yet been investigated.

1.5.5 Potential Applications of Cardiac micro-CT

Cardiac micro-CT offers numerous advantages for investigating cardiovascular diseases. For example, the fast acquisition time facilitates high throughput studies; high-resolution isotropic voxels enable direct volume measurements without the need for estimations or approximations, increasing the accuracy of the measurements; and from these scans both qualitative, structural information and quantitative data can be acquired.

And ultimately, the non-invasive nature makes longitudinal evaluations possible. The benefits of micro-CT suggest a number of potential applications: the high throughput ability would be especially beneficial when identifying phenotypes of various mouse strains; technique can also be used to evaluate longitudinally the progression of diseases, or the evaluation of various therapies, that affect the structure or function of the heart. Additionally, cardiac micro-CT can also be used to evaluate other methods of measuring cardiac function, to determine if there are ways to improve the commonly used methodologies.

1.6 Hypothesis

I hypothesize that cardiac-gated micro-CT can be used to accurately and reproducibly evaluate, both quantitatively and qualitatively, cardiac structure and function in mouse models. I further hypothesize that this technique can be safely employed in longitudinal studies, to monitor disease progression, and also be used to evaluate other methods of measuring cardiac function in mice. In order to test these hypotheses, several objectives were set:

1. To evaluate the ability of micro-CT to evaluate disease progression longitudinally in a mouse model of myocardial infarction, and to evaluate inter- and intra-observer variability;
2. To determine the suitability of a new blood-pool contrast agent for use in cardiac imaging;
3. To determine the x-ray dose effects of a typical longitudinal cardiac micro-CT study on the pulmonary and cardiac tissue in mice;
4. And finally, to apply this cardiac micro-CT technique in an evaluation of conductance catheter effects on the mouse heart.

1.7 Thesis Outline

This thesis examines the use of rapid cardiac micro-CT to both quantitatively and qualitatively evaluate cardiac structure and function in mouse models. In particular, each of the objectives outlined above is addressed in one of the following chapters.

1.7.1 Chapter 2

Chapter 2 demonstrates the ability of micro-CT to evaluate cardiac disease progression over a 4-week period. A mouse model of myocardial infarction (MI) was chosen, and was scanned at baseline, prior to the ligation of the coronary artery that produced the MI, as well as weekly following the surgery. These results were compared to a sham group, as well as to hemodynamic data obtained using a conductance catheter. The inter- and intra-observer variability of micro-CT measurements was also evaluated. Cardiac micro-CT was effective in quantitatively measuring changes in both LV volume and ejection fraction in the MI mice; these trends were mirrored in the hemodynamic measurements, however the absolute values obtained with the conductance catheter were quite different from the micro-CT values, suggesting that the catheter was not the most appropriate methodology for evaluating volume. This formed the basis for the study presented in Chapter 5.

1.7.2 Chapter 3

An important element of cardiac micro-CT is the use of a contrast agent, necessary for visualizing the heart. A new blood-pool contrast agent had become available with a higher iodine concentration than previous products, which offered the possibility of using a smaller injected volume and therefore less risk of disrupting the hemodynamics of the mouse. Chapter 3 examines the new agent from the perspective of its use in cardiac studies; overall, the contrast agent provided excellent enhancement, and seemed easier for the mouse to clear than previous agents. It also displayed a unique property: enhancement of the myocardium several hours after injection. Given the

inherent low soft tissue contrast of micro-CT, the enhancement witnessed offers intriguing possibilities in the evaluation of myocardial function.

1.7.3 Chapter 4

Chapter 4 investigates a frequent concern of using micro-CT, especially in longitudinal studies: the x-ray dose delivered to the mice, and the potentially adverse effects on cardiac and pulmonary tissue. A typical cardiac micro-CT study was modeled, with the mice being scanned weekly over a period of six weeks. At the end of the study, both the heart and lungs were evaluated on the CT images for any changes indicating adverse effects, and more importantly cardiac and pulmonary tissue were histologically evaluated for evidence of early radiation damage at a cellular level. Overall, there were no indications of x-ray damage induced during the micro-CT study in either the images or the histology slides, indicating that micro-CT can be safely used in longitudinal studies without concerns of any negative consequences related to the radiation dose.

1.7.4 Chapter 5

Finally, in Chapter 5, cardiac micro-CT was employed to evaluate the conductance catheter methodology first introduced in Chapter 2. Other studies have been performed indicating that conductance catheter volume measurements can be grossly underestimated; this study sought to confirm this, but also to determine if the invasive nature of catheterizing the heart is causing any unintended damage to the cardiac tissue, possibly affecting the functional measurements. The rapid nature of the cardiac micro-CT technique of this thesis enabled scans to be performed simultaneously with conductance catheter measurements, allowing direct comparison of volume measurements between the two techniques to be carried out, as well as high-resolution visualization of the catheter in place in the LV. This study confirmed that the volume measurements of the catheter were underestimated, and more interestingly that the catheterization caused LV enlargement in almost half the mice of the study. Although not enough to create a statistical significance of 0.05, the results suggest that the catheter is causing some damage to the heart, which should be further explored.

References

1. Global Atlas on cardiovascular disease prevention and control. World Health Organization, 2011.

2. Mortality, summary of list of causes. Statistics Canada, 2008.

3. The Canadian heart health strategy: risk factors and future cost implications. Conference Board of Canada, 2010.

4. Dixon JA, and Spinale FG. Large animal models of heart failure: a critical link in the translation of basic science to clinical practice. *Circ Heart Fail* 2: 262-271, 2009.

5. Gandolfi F, Vanelli A, Pennarossa G, et al. Large animal models for cardiac stem cell therapies. *Theriogenology* 75: 1416-1425, 2011.

6. James JF, Hewett TE, and Robbins J. Cardiac physiology in transgenic mice. *Circ Res* 82: 407-415, 1998.

7. Eppig JT, Blake JA, Bult CJ, et al. The Mouse Genome Database (MGD): comprehensive resource for genetics and genomics of the laboratory mouse. *Nucleic Acids Res* 40: D881-886, 2012.

8. Tsui BM, and Kraitchman DL. Recent advances in small-animal cardiovascular imaging. *J Nucl Med* 50: 667-670, 2009.

9. Jawien J. The role of an experimental model of atherosclerosis: apoE-knockout mice in developing new drugs against atherogenesis. *Curr Pharm Biotechnol* 2012.

10. Zhang SH, Reddick RL, Piedrahita JA, et al. Spontaneous hypercholesterolemia and arterial lesions in mice lacking apolipoprotein E. *Science* 258: 468-471, 1992.

11. Mulvihill EE, Assini JM, Sutherland BG, et al. Naringenin decreases progression of atherosclerosis by improving dyslipidemia in high-fat-fed low-density lipoprotein receptor-null mice. *Arterioscler Thromb Vasc Biol* 30: 742-748, 2010.

12. Daugherty A, Manning MW, and Cassis LA. Angiotensin II promotes atherosclerotic lesions and aneurysms in apolipoprotein E-deficient mice. *J Clin Invest* 105: 1605-1612, 2000.

13. Borst O, Ochmann C, Schonberger T, et al. Methods employed for induction and analysis of experimental myocardial infarction in mice. *Cell Physiol Biochem* 28: 1-12, 2011.

14. Alves GD, Pazzine M, Gomes de Macedo Braga LM, et al. Molecular mapping of the regenerative niche in a murine model of myocardial infarction. *Int J Mol Med* 29: 479-484, 2012.

15. Greco A, Petretta MP, Larobina M, et al. Reproducibility and accuracy of non-invasive measurement of infarct size in mice with high-resolution PET/CT. *J Nucl Cardiol* 2012.

16. Aragon JP, Condit ME, Bhushan S, et al. Beta3-adrenoreceptor stimulation ameliorates myocardial ischemia-reperfusion injury via endothelial nitric oxide synthase and neuronal nitric oxide synthase activation. *J Am Coll Cardiol* 58: 2683-2691, 2012.

17. Tekabe Y, Luma J, Li Q, et al. Imaging of receptors for advanced glycation end products in experimental myocardial ischemia and reperfusion injury. *JACC Cardiovasc Imaging* 5: 59-67, 2012.

18. Paigen B, Morrow A, Holmes PA, et al. Quantitative assessment of atherosclerotic lesions in mice. *Atherosclerosis* 68: 231-240, 1987.

19. Michael LH, Entman ML, Hartley CJ, et al. Myocardial ischemia and reperfusion: a murine model. *Am J Physiol* 269: H2147-2154, 1995.

20. Metzler B, Hammerer-Lercher A, Jehle J, et al. Plasma cardiac troponin T closely correlates with infarct size in a mouse model of acute myocardial infarction. *Clin Chim Acta* 325: 87-90, 2002.

21. Roell W, Lewalter T, Sasse P, et al. Engraftment of connexin 43-expressing cells prevents post-infarct arrhythmia. *Nature* 450: 819-824, 2007.

22. Tuomi JM, Chidiac P, and Jones DL. Evidence for enhanced M3 muscarinic receptor function and sensitivity to atrial arrhythmia in the RGS2-deficient mouse. *Am J Physiol Heart Circ Physiol* 298: H554-561, 2010.

23. Chen J, Wu J, Li L, et al. Effect of an acute mechanical stimulus on aortic structure in the transverse aortic constriction mouse model. *Clin Exp Pharmacol Physiol* 38: 570-576, 2011.

24. Fraccarollo D, Berger S, Galuppo P, et al. Deletion of cardiomyocyte mineralocorticoid receptor ameliorates adverse remodeling after myocardial infarction. *Circulation* 123: 400-408, 2011.

25. Awan Z, Denis M, Bailey D, et al. The LDLR deficient mouse as a model for aortic calcification and quantification by micro-computed tomography. *Atherosclerosis* 219: 455-462, 2011.

26. Klug G, Herold V, and Hiller KH. Plaque imaging in murine models of cardiovascular disease. *Methods Mol Biol* 771: 407-420, 2011.

27. Yuan LJ, Wang T, Kahn ML, et al. High-resolution echocardiographic assessment of infarct size and cardiac function in mice with myocardial infarction. *J Am Soc Echocardiogr* 24: 219-226, 2011.

28. Liu J, and Rigel DF. Echocardiographic examination in rats and mice. *Methods Mol Biol* 573: 139-155, 2009.

29. Schneider JE. Assessment of global cardiac function. *Methods Mol Biol* 771: 387-405, 2011.

30. Foster FS, Mehi J, Lukacs M, et al. A new 15-50 MHz array-based micro-ultrasound scanner for preclinical imaging. *Ultrasound Med Biol* 35: 1700-1708, 2009.

31. Dawson D, Lygate CA, Saunders J, et al. Quantitative 3-dimensional echocardiography for accurate and rapid cardiac phenotype characterization in mice. *Circulation* 110: 1632-1637, 2004.

32. Feintuch A, Zhu Y, Bishop J, et al. 4D cardiac MRI in the mouse. *NMR Biomed* 20: 360-365, 2007.

33. Ruff J, Wiesmann F, Hiller KH, et al. Magnetic resonance microimaging for noninvasive quantification of myocardial function and mass in the mouse. *Magn Reson Med* 40: 43-48, 1998.

34. Berr SS, Roy RJ, French BA, et al. Black blood gradient echo cine magnetic resonance imaging of the mouse heart. *Magn Reson Med* 53: 1074-1079, 2005.

35. Slawson SE, Roman BB, Williams DS, et al. Cardiac MRI of the normal and hypertrophied mouse heart. *Magn Reson Med* 39: 980-987, 1998.

36. Young AA, French BA, Yang Z, et al. Reperfused myocardial infarction in mice: 3D mapping of late gadolinium enhancement and strain. *J Cardiovasc Magn Reson* 8: 685-692, 2006.

37. Liu Z, Kastis GA, Stevenson GD, et al. Quantitative analysis of acute myocardial infarct in rat hearts with ischemia-reperfusion using a high-resolution stationary SPECT system. *J Nucl Med* 43: 933-939, 2002.

38. Chen IY, and Wu JC. Cardiovascular molecular imaging: focus on clinical translation. *Circulation* 123: 425-443, 2011.

39. Ross W, Cody DD, and Hazle JD. Design and performance characteristics of a digital flat-panel computed tomography system. *Med Phys* 33: 1888-1901, 2006.

40. Badea CT, Fubara B, Hedlund LW, et al. 4-D micro-CT of the mouse heart. *Mol Imaging* 4: 110-116, 2005.

41. Bartling SH, Stiller W, Grasruck M, et al. Retrospective motion gating in small animal CT of mice and rats. *Invest Radiol* 42: 704-714, 2007.

42. Drangova M, Ford NL, Detombe SA, et al. Fast retrospectively gated quantitative four-dimensional (4D) cardiac micro computed tomography imaging of free-breathing mice. *Invest Radiol* 42: 85-94, 2007.

43. Hounsfield GN. Historical notes on computerized axial tomography. *J Can Assoc Radiol* 27: 135-142, 1976.

44. Noo F, Defrise M, and Clackdoyle R. Single-slice rebinning method for helical cone-beam CT. *Phys Med Biol* 44: 561-570, 1999.

45. La Riviere PJ, and Pan X. Anti-aliasing weighting functions for single-slice helical CT. *IEEE Trans Med Imaging* 21: 978-990, 2002.

46. Nielsen T, Manzke R, Proksa R, et al. Cardiac cone-beam CT volume reconstruction using ART. *Med Phys* 32: 851-860, 2005.

47. Stanford W. CT of the heart: past, present, and future. In: *CT of the heart: principles and applications*, edited by Schoepf UJ. Totowa, NJ: Humana Press, 2005, p. 3-12.

48. Kalendar WA, Seissler W, Klotz E, et al. Spiral volumetric CT with single breath-hold technique: continuous transport and continuous scanner rotation. *Radiology* 176: 181-183, 1990.

49. Hurlock GS, Higashino H, and Mochizuki T. History of cardiac computed tomography: single to 320-detector row multislice computed tomography. *Int J Cardiovasc Imaging* 25 Suppl 1: 31-42, 2009.

50. Holdsworth DW, and Thorton MM. Micro-CT in small animal and specimen imaging. *Trends in Biotechnology* 8: S34-S39, 2002.

51. Elliott JC, and Dover SD. X-ray microtomography. *J Microsc* 126: 211-213, 1982.

52. Flannery BP, Deckman HW, Roberge WG, et al. Three-Dimensional X-ray Microtomography. *Science* 237: 1439-1444, 1987.

53. Ford NL, Thornton MM, and Holdsworth DW. Fundamental image quality limits for microcomputed tomography in small animals. *Med Phys* 30: 2869-2877, 2003.

54. Paulus MJ, Gleason SS, Easterly ME, et al. A review of high-resolution X-ray computed tomography and other imaging modalities for small animal research. *Lab Anim (NY)* 30: 36-45, 2001.

55. Ford NL, Martin EL, Lewis JF, et al. Quantifying lung morphology with respiratory-gated micro-CT in a murine model of emphysema. *Phys Med Biol* 54: 2121-2130, 2009.

56. Constantinides C, Mean R, and Janssen BJ. Effects of isoflurane anesthesia on the cardiovascular function of the C57BL/6 mouse. *ILAR J* 52: e21-31, 2011.

57. Kawahara Y, Tanonaka K, Daicho T, et al. Preferable anesthetic conditions for echocardiographic determination of murine cardiac function. *J Pharmacol Sci* 99: 95-104, 2005.

58. Hartley CJ, Taffet GE, Reddy AK, et al. Noninvasive cardiovascular phenotyping in mice. *ILAR J* 43: 147-158, 2002.

59. Holdsworth DW, Detombe SA, Chiodo C, et al. Implementation and assessment of an animal management system for small-animal micro-CT / micro-SPECT imaging. In: *SPIE Medical Imaging 2011: Biomedical Applications in Molecular, Structural, and Functional Imaging*, edited by Weaver JB, and Molthen RC. Orlando, Florida: 2011.

60. Ford NL, Nikolov HN, Norley CJ, et al. Prospective respiratory-gated micro-CT of free breathing rodents. *Med Phys* 32: 2888-2898, 2005.

61. Badea C, Hedlund LW, and Johnson GA. Micro-CT with respiratory and cardiac gating. *Med Phys* 31: 3324-3329, 2004.

62. Guo X, Johnston SM, Qi Y, et al. 4D micro-CT using fast prospective gating. *Phys Med Biol* 57: 257-271, 2012.

63. Song J, Liu QH, Johnson GA, et al. Sparseness prior based iterative image reconstruction for retrospectively gated cardiac micro-CT. *Med Phys* 34: 4476-4483, 2007.

64. Armitage SE, Pollmann SI, Detombe SA, et al. Least-error projection sorting to optimize retrospectively gated cardiac micro-CT of free-breathing mice. *Med Phys* 39: 1452-1461, 2012.

65. Weichert JP, Lee FT, Jr., Longino MA, et al. Lipid-based blood-pool CT imaging of the liver. *Acad Radiol* 5 Suppl 1: S16-19; discussion S28-30, 1998.

66. Ford NL, Graham KC, Groom AC, et al. Time-course characterization of the computed tomography contrast enhancement of an iodinated blood-pool contrast agent in mice using a volumetric flat-panel equipped computed tomography scanner. *Invest Radiol* 41: 384-390, 2006.

67. Boll H, Nittka S, Doyon F, et al. Micro-CT based experimental liver imaging using a nanoparticulate contrast agent: a longitudinal study in mice. *PLoS One* 6: e25692, 2011.

68. Willekens I, Lahoutte T, Buls N, et al. Time-course of contrast enhancement in spleen and liver with Exia 160, Fenestra LC, and VC. *Mol Imaging Biol* 11: 128-135, 2009.

69. Du LY, Umoh J, Nikolov HN, et al. A quality assurance phantom for the performance evaluation of volumetric micro-CT systems. *Phys Med Biol* 52: 7087-7108, 2007.

70. Sato F, Sasaki S, Kawashima N, et al. Late effects of whole or partial body x-irradiation on mice: life shortening. *Int J Radiat Biol Relat Stud Phys Chem Med* 39: 607-615, 1981.

71. Campbell J, Kalra MK, Rizzo S, et al. Scanning beyond anatomic limits of the thorax in chest CT: findings, radiation dose, and automatic tube current modulation. *AJR Am J Roentgenol* 185: 1525-1530, 2005.

72. Monceau V, Pasinetti N, Schupp C, et al. Modulation of the Rho/ROCK pathway in heart and lung after thorax irradiation reveals targets to improve normal tissue toxicity. *Curr Drug Targets* 11: 1395-1404, 2010.

73. Morgan GW, and Breit SN. Radiation and the lung: a reevaluation of the mechanisms mediating pulmonary injury. *Int J Radiat Oncol Biol Phys* 31: 361-369, 1995.

74. Jackson IL, Vujaskovic Z, and Down JD. Revisiting strain-related differences in radiation sensitivity of the mouse lung: recognizing and avoiding the confounding effects of pleural effusions. *Radiat Res* 173: 10-20, 2010.

75. Johnston CJ, Manning C, Hernady E, et al. Effect of total body irradiation on late lung effects: hidden dangers. *Int J Radiat Biol* 87: 902-913, 2011.

2 Longitudinal Follow-up of Cardiac Structure and Functional Changes in an Infarct Mouse Model using Retrospectively Gated Micro-computed Tomography

The content of this chapter is adapted from "Longitudinal follow-up of cardiac structure and functional changes in an infarct mouse model using retrospectively gated micro-computed tomography", published in Investigative Radiology, vol 43 (7) July 2008, by Sarah A. Detombe, Nancy L. Ford, Fuli Xiang, Xiangru Lu, Qingping Feng, and Maria Drangova.

2.1 Introduction

Mouse models have become increasingly important in the study of cardiovascular diseases. Detailed information about the genome has allowed models to be developed that either overexpress or underexpress specific genes to study their contribution to the pathophysiology of a given cardiovascular disease process.

The established method for studying cardiac function in mouse models involves the analysis of pressure-volume relationships measured using a pressure-conductance catheter. By inserting a catheter into the left ventricle (LV) and recording both pressure and volume readouts, heart function can be determined, most notably by detecting small alterations in myocardial contractility.[1] However, due to the inability of pressure-volume conductance devices to continuously measure parallel conductance, LV volume is often underestimated.[2, 3] The procedure is also invasive, resulting in a terminal experiment, and requires an individual with specialized surgical skill to produce consistent data.

Multiple imaging modalities have been developed that have the capability of measuring cardiac structure and function in the mouse; these are non-invasive procedures that allow individual animals to be tracked over the entire study. Commonly used

techniques are magnetic resonance imaging (MRI)[4-10] and echocardiography,[11-16] both of which have been used to successfully measure LV function. MR images typically require long scan times and are usually acquired with large slice thicknesses (approximately 1 mm). Accurate heart function measurements also require that the scans be acquired in the short axis orientation, which can be difficult to define in diseased hearts,[5] although a recent study[17] has described a method of acquiring three-dimensional (3D) MR images with 200-μm isotropic voxels, which may alleviate this limitation.

Echocardiography is frequently used because it is easy to operate, can provide real-time images, and can measure velocity. Although two-dimensional (2D) imaging is available (and 3D imaging has been demonstrated[18]), cardiac function is most frequently measured from M-mode images.[12, 19-21] Estimating cardiac function from M-mode and 2D images relies on geometrical assumptions and is highly user-dependent.

In recent years, micro-computed tomography (micro-CT) techniques have emerged, capable of overcoming the challenges of imaging the mouse heart such as the fast heart rate (about 500 beats per minute under anesthetic) and the small size (5 mm across the short axis of the ventricle). Badea *et al.*[22] demonstrated a prospectively gated micro-CT technique that acquires 3D images with 90-μm isotropic voxels, and a scan time of approximately 10 minutes for each cardiac phase, which has recently been applied to an infarct mouse model.[23] This technique, however, requires that the animals be intubated, and mice are scanned in a vertical position, which may disrupt cardiac function.[24]

Retrospectively gated micro-CT imaging techniques have been recently developed that enable the acquisition of 3D images throughout the cardiac cycle in free-breathing mice.[25, 26] The methodology outlined by Drangova *et al.*[25] has multiple advantages, including a short scan time (<1 minute), and high resolution (150-μm isotropic voxel spacing). Retrospectively gated micro-CT can provide both quantitative and qualitative assessment of cardiac function that, as a result of the minimal anesthetic required and the short scan times, offers nominal disruption to the animal. In this study, we follow heart failure progression in an infarct mouse model over four weeks to demonstrate the utility of this technique when investigating a mouse model of cardiovascular disease. To the best of our knowledge, this is the first study using

retrospectively gated micro-CT to follow cardiac remodeling in each individual mouse over time following the induction of an infarct.

2.2 Methods

All studies performed were approved by the Animal Use Subcommittee of the University Council on Animal Care at The University of Western Ontario. Fourteen male C57BL/6 mice, approximately 25 weeks old and weighing 32 ± 3 g, were split into two groups; one group underwent ligation of the left coronary artery, and the other group underwent sham surgery. Mice were scanned at baseline (before surgery), and weeks 1, 2, 3, and 4 post-surgery; 3 of the sham mice and 3 of the myocardial infarction (MI) mice did not receive a scan at baseline and week 2 post-surgery.

2.2.1 Induction of Myocardial Infarction

Surgery was performed as previously described.[27] Animals were anesthetized with ketamine (50 mg/kg) and xylazine (12.5 mg/kg) delivered intraperitoneally. The mice were then intubated and artificially ventilated. A left thoracotomy was performed, exposing the LV wall; the left coronary artery was ligated by positioning a suture between the pulmonary artery out-flow tract and the left atrium. Sham-operated animals underwent the same surgical procedure, including positioning of the suture, but it was not tightened to ligate the artery. To decrease acute mortality after ligation, atropine (0.05 mg s.c.) was administered before surgery to decrease airway excretion. Following surgery, mice were treated with antibiotic agent (oxytetracycline, 200 mg/L) via drinking water for 3 days; analgesic (0.03 mg/kg burprenorphine s.c.) was administered to relieve pain.

2.2.2 Animal Preparation for Scanning

Mice were anesthetized with 1.5% isoflurane in O_2. Approximately 5 minutes prior to scanning, the animals were injected intravenously with 0.01 mL/g Fenestra VC

(50 mg I/mL; Advanced Research Technologies, Inc., St. Laurent, Quebec, Canada), an iodinated blood-pool contrast agent that enhances the vasculature for several hours.[28] The dose given in this study was half the dose administered by Drangova *et al*.[25] and Badea *et al.*[22] This dose of contrast agent was selected to reduce the volume injected into the mouse, and pilot experiments demonstrated that sufficient contrast was achieved at this dose level.[28] Three neonatal ECG electrodes (2269T, 3M Health Care, St. Paul, MN) were attached to the paws, and the animal was placed prone on a respiratory monitoring bed connected to a pressure transducer, which translates diaphragm motion to a recording of a respiratory wave signal.[29] Physiological signals were recorded using a physiological monitoring and triggering system (BioVet, m2m Imaging Corp., Newark, NJ, USA). Temperature was monitored and maintained between 36°C and 37°C for all scans. The mice were not intubated and remained free-breathing during the experiment.

2.2.3 Image Acquisition and Retrospective Gating

Images were acquired using a volumetric cone-beam micro-CT scanner (Locus Ultra, General Electric Healthcare, London, ON, Canada), equipped with a flat-panel detector and clinical x-ray tube mounted on a slip-ring gantry, which enables continuous dynamic acquisition of x-ray projections. Projection images were acquired at 80 kVp and 50 mA over a field of view measuring 14 cm (transaxial) x 5.4 cm (longitudinal). To enable retrospective gating, projections were acquired over 10 rotations (5 seconds per rotation, 416 projection images per rotation at a rate of 12 milliseconds/projection) for a total scan time of 50 seconds. Entrance dose for a 50 second scan was previously calculated to be 0.28 Gy.[25]

Retrospective gating and reconstruction of acquired projection images is described in detail by Drangova *et al.*[25] Briefly, for each phase of the cardiac cycle projections were selected, from those acquired, based on the recorded respiratory and ECG signals; only projections occurring during end expiration and a predetermined cardiac window (12 ms) were used to reconstruct the 3D image for the selected cardiac phase. For this study 9-13 3D images were reconstructed per cardiac cycle, depending on

the heart rate. All images were reconstructed on a 256 x 256 x 360 matrix with isotropic voxel spacing of 150 μm x 150 μm x 150 μm.[30]

2.2.4 Image Analysis

Image analysis was performed using MicroView software (version ABA 2.2, General Electric Healthcare, London, ON, Canada). Images were reoriented to align with the long and short axes of the heart. To calculate LV volume, an automated seeded region-growing algorithm was used. First, a threshold level that separated the blood from the myocardium in the images was identified automatically[31] by drawing small regions of interest containing equal parts of tissue and blood. Because of small differences in the concentration of contrast agent in each mouse at scan time, a separate threshold value was defined for each animal at each time point. Automatic region growing was then used to segment the LV chamber from the myocardium; the region growing was terminated at the aortic valve, with manually drawn contours limiting the segmentation near the valve where the wall of the ventricle became too thin to constrain the region-growing algorithm. The aortic valve was visually located in the short axis plane and the anatomical location was confirmed in the coronal view. LV volume was calculated based on the segmented region and the known voxel size. Systolic and diastolic images were identified by calculating LV volume throughout the cardiac cycle to determine the frames that had minimum and maximum volumes. Once the end-systolic volume (ESV) and the end-diastolic volume (EDV) were determined, stroke volume (SV = EDV – ESV), ejection fraction (EF = SV / EDV), and cardiac output (CO = SV * heart rate) were calculated.

2.2.5 LV Mass Measurements

LV mass was determined from the CT images for all mice in weeks 1 and 4. A contour was manually drawn around the outer edge of the LV, using the aortic valve as an upper boundary, and the LV wall was automatically segmented within the contoured region using the threshold previously calculated for LV chamber volume determination.

The resulting myocardium volumes were multiplied by the density of myocardium (1.05 g/ml) in order to calculate LV mass.

2.2.6 Reproducibility

The reproducibility of the technique was determined in terms of inter-observer, intra-observer, and intra-subject variability. For inter-observer variability, the systolic and diastolic images of 13 mice (7 sham and 6 MI), acquired at weeks 1 and 4 post-surgery, were analyzed by three independent operators. Intra-observer variability was determined by one individual analyzing these same images three times. For intra-subject variability determination, two sham and three MI mice were each scanned three times, following repositioning, at the final scan time-point (4 weeks).

2.2.7 Hemodynamic Measurements

Hemodynamic measurements were performed as previously described:[27] following scanning at the 4-week time-point, mice were anesthetized with sodium pentobarbital (50 mg/kg IP), and a Millar pressure conductance catheter (model SPR-839, 1.4 F) was inserted into the LV via the right carotid artery to measure LV pressures, volumes, and heart rate. Data were recorded by a PowerLab Chart program (ADInstruments Inc, Colorado Springs, CO). All hemodynamic parameters were analyzed by a PVAN software (Millar Instruments, Houston, TX). Following hemodynamic analysis, hearts were excised, fixed with 10% formalin, then sliced and stained with hematoxylin and eosin.

2.2.8 Statistical Analysis

Data are presented as mean ± SD for continuous variables. Two-way ANOVA was performed, using Prism 4 (GraphPad Software, Inc., San Diego, CA), to compare differences between sham and MI groups over time for each of the cardiac functional parameters (ESV, EDV, SV, EF, CO); Bonferroni post-tests were also performed. Variabilities were calculated as the standard deviations of the means of multiple

measurements. Power tests were performed using StatMate 2 (GraphPad Software, Inc., San Diego, CA). Results were considered statistically significant at $p<0.05$.

2.3 Results

Retrospectively gated micro-CT images were successfully acquired in all 14 mice; one mouse was excluded from analysis retrospectively due to unsuccessful ligation of the coronary artery, which failed to create an infarct. On average, the contrast agent increased the attenuation of the blood pool to 331 ± 57 HU, compared to the myocardial tissue (76 ± 27 HU); the average threshold that separated the blood pool in the LV from the myocardium was 255 ± 54 HU. Out of 416 possible projections, an average of 325 ± 42 projections were available to reconstruct an image at each point in the cardiac cycle. The average noise in the myocardium was previously measured to be 36 ± 4.6 HU.[25]

Figure 2.1 shows representative long- and short-axis images acquired at week 4 post-surgery in a sham-operated (Fig. 2.1 a, c) and a MI (Fig. 2.1 b, d) mouse. The images were extracted from the 3D images reconstructed at the selected phase of the cardiac cycle. The infarcted heart (Fig. 2.1b) is distended, with a thinning of the wall in the apex of the ventricle, representing the infarct (noted with arrows). Note the entire heart of the MI mouse appears to be enlarged. Figure 2.2 shows the histology of the LV from an MI (a) and a sham (b) mouse at week 4 post-surgery. The enlarged LV from the MI mouse, and the area of infarction, are clearly demonstrated.

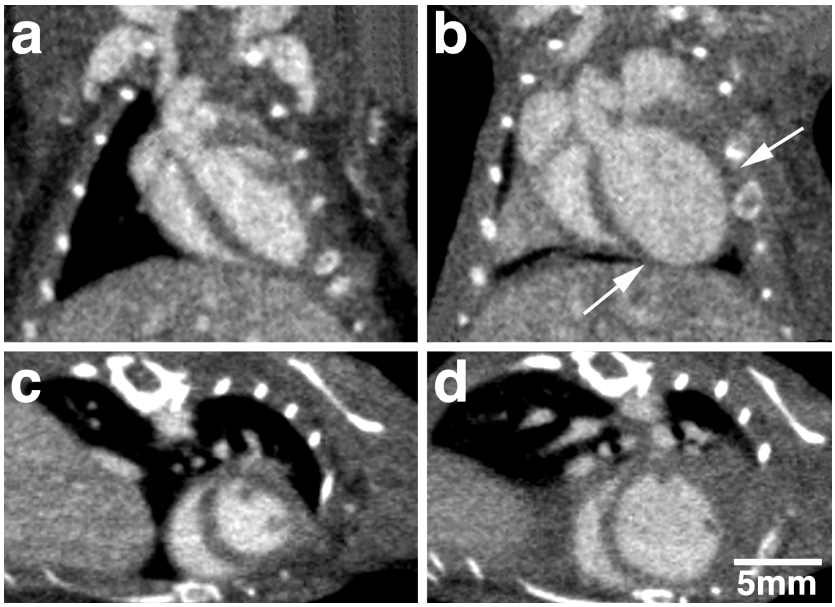

Figure 2.1: Long (a, b) and short (c, d) axis images of the mouse heart in diastole of a sham-operated (a, c) and MI (b, d) mouse. These images represent 150-μm sections taken from the reconstructed 3D volumes. The in-plane voxel spacing is also 150 μm. Note that the entire heart of the MI mouse is enlarged, indicating the global effects of the infarct. The infarct is evident in the thinned wall in the apex of the LV, below the arrows.

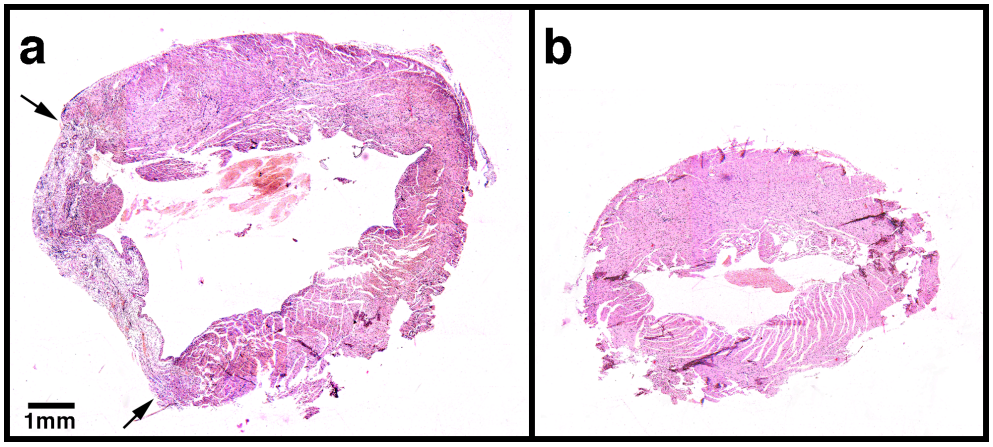

Figure 2.2: Histological slides of the LV from an MI (a) and a sham (b) mouse, stained with hematoxylin and eosin. The infarct is identified by arrows in (a).

Figures 2.3a (sham-operated) and 2.3b (infarct model) represent long- and short-axis views of an individual mouse heart in diastole (i, iii) and systole (ii, iv). Apparent from these images are the differences in size between diastole and systole when comparing sham and MI animals.

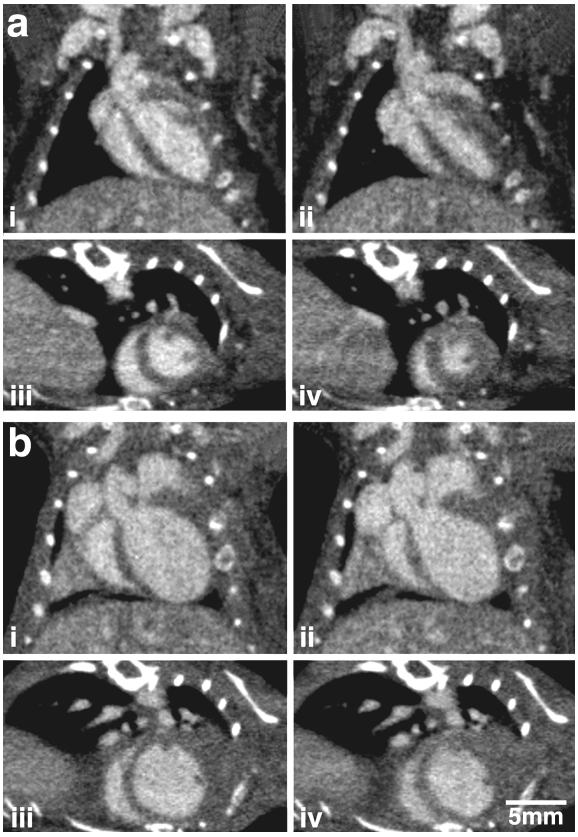

Figure 2.3: Long and short axis images of a sham-operated mouse heart (a) and a MI mouse heart (b) in diastole (i, iii) and systole (ii, iv). The images were acquired 4 weeks post surgery. Note the obvious reduction in contraction of the infarcted heart (b) compared to the sham-operated heart (a).

Figures 2.4 and 2.5 illustrate differences in cardiac morphology of a heart in diastole in a sham-operated and MI mouse, respectively, over the course of experiment. The size and shape difference between baseline and the final time point is also

demonstrated in the 3D representation of the LV chambers of a MI mouse shown in Figure 2.6.

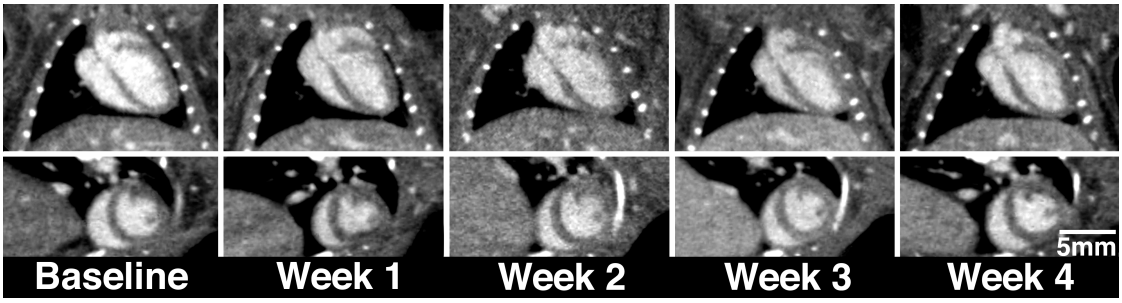

Figure 2.4: A series of long and short axis images showing weekly changes in a sham-operated mouse heart in diastole. Time points represented are: baseline, 1 week post-surgery, 2 weeks post-surgery, 3 weeks post-surgery, and 4 weeks post-surgery.

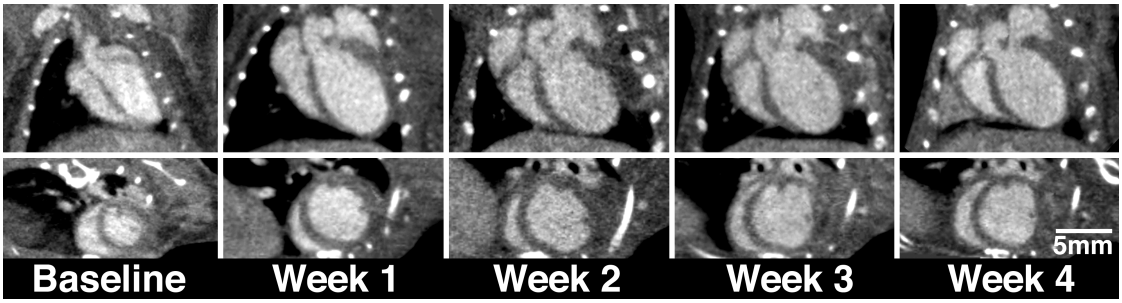

Figure 2.5: A series of long and short axis images showing weekly changes in a MI mouse heart in diastole. Time points represented are: baseline, 1 week post-surgery, 2 weeks post-surgery, 3 weeks post-surgery, and 4 weeks post-surgery.

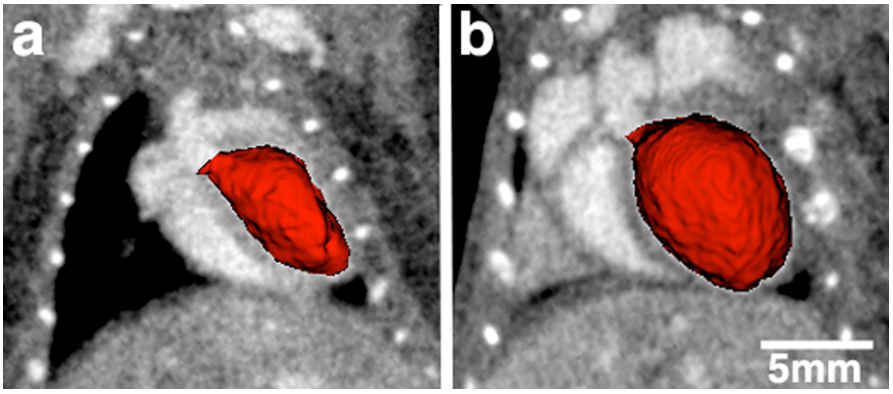

Figure 2.6: 3D representation (isosurface) of the LV overlaid on images of an infarcted heart at baseline (a) and week-4 post infarction (b). The isosurface models were generated from wire-frame meshes created following an intensity-based region growing operation.

One of the main advantages of using a non-invasive imaging technique includes the ability to quantify changes in cardiac function in individual animals over time. Figure 2.7(a-e) illustrate the functional parameters calculated for individual mice and Fig. 2.7f tracks the measured heart rates. Note the small weekly changes observed in individual mice in ESV (Fig. 2.7a) and EDV, (Fig. 2.7b), as well as in the functional parameters calculated from the volumes.

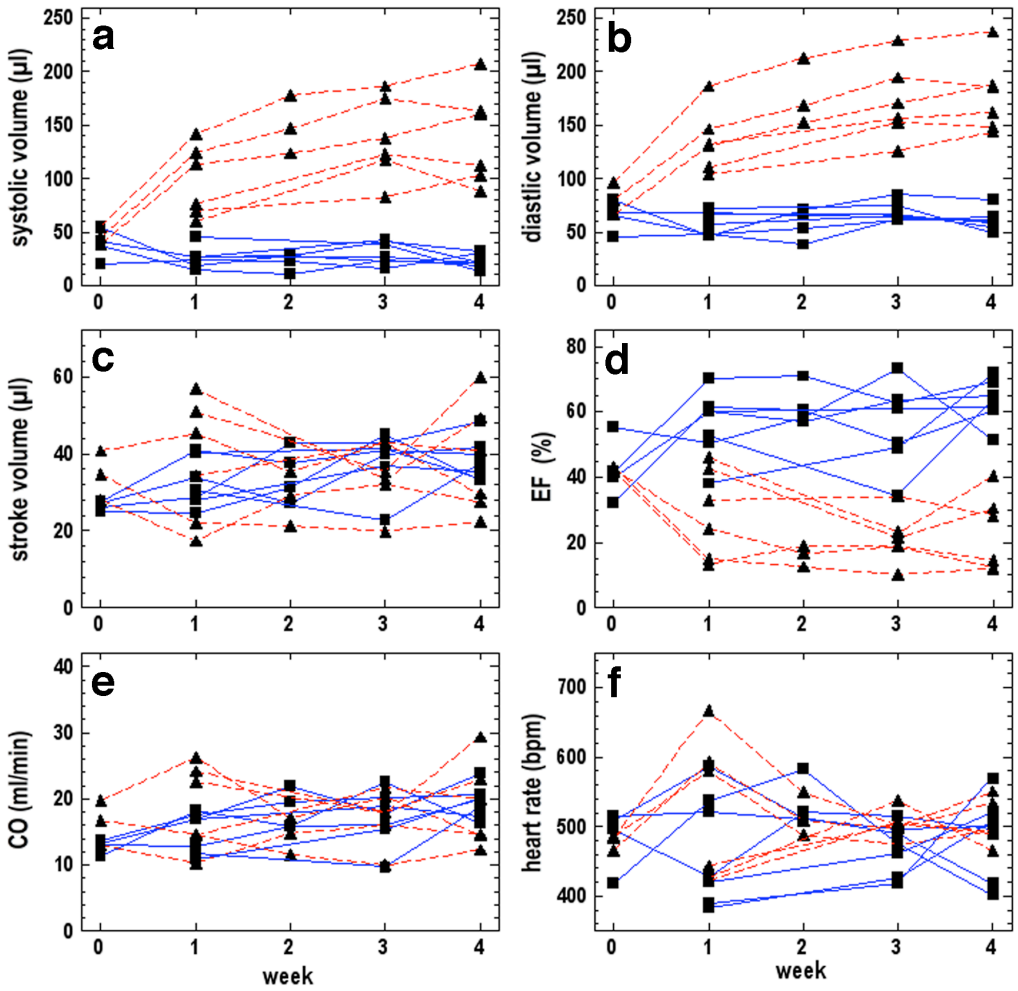

Figure 2.7: Measured cardiac functional parameters tracking individual mice over the 5-week experiment. Graphs represent systolic volume (a), diastolic volume (b), stroke volume (c), ejection fraction (d), cardiac output (e), and heart rate (f). Sham-operated mice are represented by blue solid lines and squares; MI mice are represented by red dashed lines and triangles. Note that each symbol represents the measurements of an individual mouse at each time point.

Average values of the functional parameters for each week were also calculated and are listed in Table 2.1.

Table 2.1. Weekly Average Functional Parameters of Sham-operated and MI Groups

	Functional Parameter				
	ESV (μl)	*EDV (μl)*	*SV (μl)*	*EF (%)*	*CO (ml/min)*
Baseline					
Sham (4)	38.5 ± 14.1	65.1 ± 14.7	26.5 ± 1.1	42.4 ± 9.5	12.9 ± 1.0
MI (3)	46.5 ± 8.2	81.0 ± 14.7	34.5 ± 6.5	42.5 ± 1.0	16.5 ± 3.4
p-value	ns	ns	ns	ns	ns
Week 1					
Sham (7)	26.1 ± 9.7	58.6 ± 10.9	32.4 ± 6.3	56.2 ± 10.2	15.0 ± 3.1
MI (6)	97.5 ± 33.3	135.2 ± 29.6	37.8 ± 15.9	29.0 ± 13.8	18.8 ± 6.4
p-value	0.0002	<0.0001	ns	0.0018	ns
Week 2					
Sham (4)	22.3 ± 7.9	57.1 ± 14.5	34.7 ± 7.0	61.8 ± 6.2	18.3 ± 3.0
MI (3)	149.4 ± 27.1	177.9 ± 31.2	28.5 ± 7.1	16.1 ± 3.3	14.5 ± 2.8
p-value	0.0003	0.0009	ns	<0.0001	ns
Week 3					
Sham (7)	30.5 ± 10.5	68.9 ± 8.3	38.4 ± 7.4	56.3 ± 12.7	17.3 ± 4.1
MI (6)	137.0 ± 38.4	171.5 ± 36.2	34.4 ± 8.5	21.1 ± 7.8	17.3 ± 4.1
p-value	<0.0001	< 0.0001	ns	0.0001	ns
Week 4					
Sham (7)	22.7 ± 6.5	61.3 ± 9.7	38.5 ± 5.5	63.3 ± 6.6	19.6 ± 2.4
MI (6)	139.3 ± 45.4	177.5 ± 34.6	38.2 ± 14.5	23.1 ± 11.7	19.0 ± 6.5
p-value	<0.0001	< 0.0001	ns	< 0.0001	ns

Values are means ± SD; ESV, end-systolic volume; EDV, end-diastolic volume; SV, stroke volume; EF, ejection fraction; CO, cardiac output; numbers in brackets represent no. of animals

Significant differences ($p<0.0001$) were observed between the sham and MI groups for ESV, EDV, and EF, as demonstrated by 2-way ANOVA; also, ESV and EDV showed significant differences over time ($p<0.0001$). Bonferroni post-tests confirmed that significant differences occurred between each group at each time point. SV and CO did not show significant differences either between the surgery groups or over time ($p>0.1$ for all tests). Power tests determined there was sufficient power (>80%) to detect

expected differences[18, 23, 32] in ESV, EDV, and EF. Power calculations for SV and CO showed insufficient power to detect differences of 20%, which have been previously observed between sham and MI mice.[33]

LV mass measurements calculated from the CT images are listed in Table 2.2. Significant differences were seen between the sham and MI groups in both weeks 1 and 4 (p=0.012 and 0.008, respectively); changes in LV mass between weeks 1 and 4 were insignificant for both the sham (p=0.60) and MI (p=0.08) groups.

Table 2.2. Average LV mass measurements for Sham and MI groups in Weeks 1 and 4 Post-Surgery

	LV mass (mg)		
Group	**Week 1**	**Week 4**	
Sham mice *(n=7)*	91 ± 14	101 ± 14	*p=ns*
MI mice *(n=6)*	122 ± 23	136 ± 24	*p=ns*
	p=0.012	*p=0.008*	

Values are means ± SD; *n*, no. of animals

Variability studies showed excellent reproducibility of measurements between individuals, and by the same individual (Table 2.3). Intrasubject measurements also show good reproducibility, with variation in volumes of infarcted hearts being slightly higher than variations in sham-operated hearts (Table 2.3). Overall, the variability due to image analysis by the same or different observers was low (on average, less than ±0.85 and ±1.8 µl, respectively) and was lower than the intra-subject variability in LV volumes (±2.8 µl on average).

Hemodynamic measurements made in week 4 (Table 2.4) were compared to measurements made from CT images. Comparison of the ejection fractions measured using the two techniques showed no significant differences for either the sham or the MI groups ($p > 0.1$).

Table 2.3. Average Inter-observer, Intra-observer, and Intra-subject Variabilities of Systolic and Diastolic Volumes

	Sham mice		**MI mice**	
	Systole (µl)	*Diastole (µl)*	*Systole (µl)*	*Diastole (µl)*
Inter-observer	*(n=7)*	*(n=7)*	*(n=6)*	*(n=6)*
Week 1	1.9 ± 1.6	1.6 ± 1.0	1.8 ± 2.2	2.6 ± 1.6
Week 4	1.0 ± 0.6	1.3 ± 0.5	1.7 ± 1.4	1.7 ± 1.1
Intra-observer	*(n=7)*	*(n=7)*	*(n=6)*	*(n=6)*
Week 1	0.9 ± 0.8	0.6 ± 0.3	0.8 ± 0.7	0.9 ± 0.7
Week 4	0.5 ± 0.5	0.8 ± 0.8	0.8 ± 0.5	1.4 ± 0.9
Intra-subject	*(n=2)*	*(n=2)*	*(n=3)*	*(n=3)*
Week 4	0.19; 1.32	1.24; 1.73	3.6 ± 0.2	5.5 ± 0.8

Values are means ± SD, excepting Intra-subject group where exact values are listed for each sham mouse; *n*, no. of animals.

Table 2.4. Comparison of CT-based Measurements and Hemodynamic Measurements at Four Weeks Post Surgery

Functional Measurements	**CT Measurements**		**Hemodynamic Measurements**	
	Sham (n=7)	*MI (n=6)*	*Sham (n=7)*	*MI (n=6)*
EDV (µl)	61 ± 10	178 ± 35	26 ± 8	29 ± 10
ESV (µl)	23 ± 7	139 ± 45	12 ± 6	21 ± 7
SV (µl)	39 ± 6	38 ± 15	14 ± 7	7 ± 5
EF (%)	63 ± 7	23 ± 12	54 ± 20	26 ± 15
CO (ml/min)	20 ± 2	19 ± 7	5 ± 3	2 ± 1
$+dP/dt_{max}$(mmHg.s)	-	-	7321 ± 948	3456 ± 1032
$-dP/dt_{min}$(mmHg.s)	-	-	5969 ± 1070	3102 ± 861
Heart rate (bpm)	511 ± 30	505 ± 32	360 ± 80	281 ± 48

Values are means ± SD; *n*, no. of animals; ESV, end-systolic volume; EDV, end-diastolic volume; SV, stroke volume; EF, ejection fraction; CO, cardiac output; $+dP/dt_{max}$, maximal rate of LV pressure increase; $-dP/dt_{min}$, maximal rate of LV pressure decline.

2.4 Discussion

This study is the first to demonstrate longitudinal tracking of quantitative cardiac functional parameters in individual mice using a dynamic micro-CT scanner. Recently published data demonstrated, in healthy mice, that retrospectively gated micro-CT rapidly

and reproducibly acquires images that can be used to quantify cardiac function.[25] Retrospectively gated micro-CT takes advantage of the scanning capabilities of a volumetric CT scanner equipped with a 2D detector mounted on a slip-ring gantry, making continuous image acquisition possible. Contrast between blood and myocardium is provided by a tri-iodinated blood-pool contrast agent, which provides excellent contrast for several hours.[28] The entrance dose of 0.28 Gy per scan, although higher than the dose reported for clinical diagnostic CT thorax exams,[34, 35] is not anticipated to have a detrimental effect on cardiovascular physiology in the mouse.[25, 36, 37] The advantages of this micro-CT scanning method include: 1) scan times of less than one minute to characterize cardiac function over the entire cycle, by generating a series of high-resolution (150 μm isotropic voxels) 3D images; 2) the capability of scanning free-breathing animals in a prone position and; 3) the ability to scan animals under very light anesthesia (typically provided by isoflurane, which has little effect on cardiac function when compared to injectable anesthetics[38-41]).

This current study endeavored to demonstrate that retrospectively gated micro-CT precisely identifies the differences in heart function between infarcted and control mice and can follow these differences longitudinally in individual mice. Differences in cardiac structure were clearly identifiable in the 3D images (Fig. 2.1), where infarcted mice demonstrated drastically enlarged hearts and thinned walls in the apical 40% of the LV (arrows Fig. 2.1b); the enlarged right ventricle and atria illustrate the widespread effect of the infarct. Histological slides of the LV from an MI mouse and a sham mouse (Fig. 2.2) confirm the enlarged size and the area of infarction identified on the CT images. Quantitative differences in LV size and function were also observed between the sham and MI groups at all time points in the study (Table 2.1). Significant differences were observed for systolic and diastolic LV volumes, and for ejection fraction between the two groups at all time points post surgery. Significant increases in LV size with time over the course of the experiment were also observed in the MI mice (Fig. 2.7 a, b).

Baseline EF values were lower than expected for healthy mice.[17, 23, 32] It was necessary to transport the mice between facilities for the baseline scans, whereas for weeks 1-4, the animals were housed in the same building as the scanner; at the time, this was an unavoidable complication of the study. The transportation may have caused a low

level of stress in the mice, resulting in abnormally low ejection fractions.[42, 43] The unexpected results highlight an advantage of this micro-CT technique – the ability to closely track perturbations in the animal's health during a study that would have otherwise been undetected. These results also suggest that transportation of mice prior to imaging, or other study that measures physiological function, should be avoided on the day of the procedure.

On average, the measured values for CO agreed with previously reported results at the experimental end point.[32, 33] The lack of significant differences in SV and CO between the sham and MI groups is potentially attributable to the limited time frame over which the experiment was carried out; although the EF was clearly reduced in the MI mice, the compensatory increase in heart size may be responsible for the maintenance of a relatively constant stroke volume, and therefore, cardiac output. Had the study continued past week four, decreases in stroke volume and cardiac output are likely to have been measured. Additionally, it's possible that a decrease in stroke volume may occur early in the first week, before compensatory LV dilation takes place, however no scans were performed during that time period in this study. Any future studies evaluating MI disease progression in mice should take this into account. Regarding the measurements recorded during the time frame of this study, similar increases in cardiac dimension were reported by Yang *et al*.[44] who used echocardiography to measure LV diastolic shortening in different groups of infarcted mice, which were sacrificed at each experimental time point.

An important advantage of tracking the same animal over the entire course of an experiment using a non-invasive imaging technique is that small changes in individual animals are not lost in the averaging process of a population of mice; a baseline scan can act as the ideal control for the animal at later time points, and paired statistical analyses can be performed. This advantage is seen qualitatively in the series of images in Fig. 2.5, which depict the gradual cardiac remodeling as it occurs over the 4 weeks, and quantitatively in Fig. 2.7.

LV mass measurements are an important element of tracking changes to the myocardium. In this study we determined LV mass in both groups of mice at week 1 and week 4 (Table 2.2). A significant difference in mass between the sham and MI groups

was observed, confirming that hypertrophy had occurred following the induction of the infarct; there was no significant difference between the weeks, indicating that the observed hypertrophy took place during the first week after surgery.

The variability studies demonstrated that overall the quantitative measurements were highly reproducible. Because most of the analysis was automatic, both inter- and intra-observer variability depended mostly on the variability of contour placement in the regions near the base of the LV. The excellent intra-subject variability (repeated scans on the same mouse in the same scanning session) provided further support that the low EF measurements made at baseline reflect true physiological changes. The intra-subject variability was slightly higher for the MI mice than the sham-operated mice; this difference was attributed to the rounded shape of the LV in infarcted mice making the identification of the base of the heart more subjective. The ability to reorient the high-resolution 3D isotropic images to align with the long and short axis of the hearts improves the ease of identifying the base of the heart, where manually drawn contours were required. This is in contrast to most MRI and echocardiography experiments, where the images must be acquired in the short axis of the heart, which can be difficult, especially in remodeled hearts.[5] Note that retrospective reorientation of MR or echocardiographic images acquired with thicker slices (approximately 1 mm) or large inter-slice spacing (in the case of 3D echo) is typically not possible; the voxels are not isotropic and reorienting would introduce interpolation effects.

2.4.1 Limitations

One of the limitations of this study was the inability to directly compare CT-derived measurements with the catheter-derived LV volume measurements, due to the accepted underestimation and large variability of volume measurements made invasively by pressure-conductance catheters.[2, 3] The use of different anesthetics when comparing micro-CT to catheterization was not ideal, however our aim in using inhalation anesthetics during CT scanning was to emphasize the low invasiveness of the CT approach. Using an injectable anesthetic would have made controlling the depth of anesthesia difficult, as well as increasing the invasiveness of the procedure. In addition,

the hemodynamic measurements were made on the same day as the scanning occurred, but following the administration of a second (injectable) anesthetic agent, which resulted in further lowering the heart rates during the procedure. The number of animals in the study was small, but important functional parameters could be followed over time with sufficient statistical power, indicating the effectiveness of the technique to follow cardiac remodeling.

2.4.2 Conclusion

The present work demonstrates that retrospectively gated micro-CT precisely defines the differences in heart function and volume between sham and MI animals. This methodology has the ability of following individual animals over the entire study, enabling the tracking of small changes in cardiac remodeling that may be not be evident when averaging a group of mice. Reproducibility studies show low variability during analysis (inter- and intra- observer). The rapid acquisition of dynamic 3D images also makes the technique highly suitable for large throughput phenotyping studies. Furthermore, the retrospectively gated micro-CT technique can be combined with the injection of a conventional contrast agent, as suggested by Nahrendorf *et al*.,[23] to identify areas of infarction, where the contrast agent extravasates over time. Ultimately, retrospectively gated micro-CT has the potential to become an important tool for following disease progression and disease regression, following the administration of various experimental therapeutic agents.

References

1. Lips DJ, van der Nagel T, Steendijk P, et al. Left ventricular pressure-volume measurements in mice: comparison of closed-chest versus open-chest approach. *Basic Res Cardiol* 99: 351-359, 2004.

2. Jacoby C, Molojavyi A, Flogel U, et al. Direct comparison of magnetic resonance imaging and conductance microcatheter in the evaluation of left ventricular function in mice. *Basic Res Cardiol* 101: 87-95, 2006.

3. Nielsen JM, Kristiansen SB, Ringgaard S, et al. Left ventricular volume measurement in mice by conductance catheter. Evaluation and optimization of calibration. *Am J Physiol Heart Circ Physiol* 2007.

4. Schneider JE, Cassidy PJ, Lygate C, et al. Fast, high-resolution in vivo cine magnetic resonance imaging in normal and failing mouse hearts on a vertical 11.7 T system. *J Magn Reson Imaging* 18: 691-701, 2003.

5. Schneider JE, Wiesmann F, Lygate CA, et al. How to perform an accurate assessment of cardiac function in mice using high-resolution magnetic resonance imaging. *J Cardiovasc Magn Reson* 8: 693-701, 2006.

6. Gilson WD, Yang Z, French BA, et al. Measurement of myocardial mechanics in mice before and after infarction using multislice displacement-encoded MRI with 3D motion encoding. *Am J Physiol Heart Circ Physiol* 288: H1491-1497, 2005.

7. Liu W, Ashford MW, Chen J, et al. MR tagging demonstrates quantitative differences in regional ventricular wall motion in mice, rats, and men. *Am J Physiol Heart Circ Physiol* 291: H2515-2521, 2006.

8. Zhou R, Pickup S, Glickson JD, et al. Assessment of global and regional myocardial function in the mouse using cine and tagged MRI. *Magn Reson Med* 49: 760-764, 2003.

9. Bishop J, Feintuch A, Bock NA, et al. Retrospective gating for mouse cardiac MRI. *Magn Reson Med* 55: 472-477, 2006.

10. Hiba B, Richard N, Janier M, et al. Cardiac and respiratory double self-gated cine MRI in the mouse at 7 T. *Magn Reson Med* 55: 506-513, 2006.

11. Zhou YQ, Foster FS, Nieman BJ, et al. Comprehensive transthoracic cardiac imaging in mice using ultrasound biomicroscopy with anatomical confirmation by magnetic resonance imaging. *Physiol Genomics* 18: 232-244, 2004.

12. Costandi PN, Frank LR, McCulloch AD, et al. Role of diastolic properties in the transition to failure in a mouse model of the cardiac dilatation. *Am J Physiol Heart Circ Physiol* 291: H2971-2979, 2006.

13. Saraste A, Kyto V, Saraste M, et al. Coronary flow reserve and heart failure in experimental coxsackievirus myocarditis. A transthoracic Doppler echocardiography study. *Am J Physiol Heart Circ Physiol* 291: H871-875, 2006.

14. Neilan TG, Jassal DS, Perez-Sanz TM, et al. Tissue Doppler imaging predicts left ventricular dysfunction and mortality in a murine model of cardiac injury. *Eur Heart J* 27: 1868-1875, 2006.

15. Sebag IA, Handschumacher MD, Ichinose F, et al. Quantitative assessment of regional myocardial function in mice by tissue Doppler imaging: comparison with hemodynamics and sonomicrometry. *Circulation* 111: 2611-2616, 2005.

16. Cherin E, Williams R, Needles A, et al. Ultrahigh frame rate retrospective ultrasound microimaging and blood flow visualization in mice in vivo. *Ultrasound Med Biol* 32: 683-691, 2006.

17. Feintuch A, Zhu Y, Bishop J, et al. 4D cardiac MRI in the mouse. *NMR Biomed* 20: 360-365, 2007.

18. Dawson D, Lygate CA, Saunders J, et al. Quantitative 3-dimensional echocardiography for accurate and rapid cardiac phenotype characterization in mice. *Circulation* 110: 1632-1637, 2004.

19. Xu M, Uemura R, Dai Y, et al. In vitro and in vivo effects of bone marrow stem cells on cardiac structure and function. *J Mol Cell Cardiol* 42: 441-448, 2007.

20. Semsarian C, Ahmad I, Giewat M, et al. The L-type calcium channel inhibitor diltiazem prevents cardiomyopathy in a mouse model. *J Clin Invest* 109: 1013-1020, 2002.

21. Alvarez BV, Kieller DM, Quon AL, et al. Cardiac hypertrophy in anion exchanger 1-null mutant mice with severe hemolytic anemia. *Am J Physiol Heart Circ Physiol* 292: H1301-1312, 2007.

22. Badea CT, Fubara B, Hedlund LW, et al. 4-D micro-CT of the mouse heart. *Mol Imaging* 4: 110-116, 2005.

23. Nahrendorf M, Badea C, Hedlund LW, et al. High-resolution imaging of murine myocardial infarction with delayed-enhancement cine micro-CT. *Am J Physiol Heart Circ Physiol* 292: H3172-3178, 2007.

24. Schneider JE, Hulbert KJ, Lygate CA, et al. Long-term stability of cardiac function in normal and chronically failing mouse hearts in a vertical-bore MR system. *Magma* 17: 162-169, 2004.

25. Drangova M, Ford NL, Detombe SA, et al. Fast retrospectively gated quantitative four-dimensional (4D) cardiac micro computed tomography imaging of free-breathing mice. *Invest Radiol* 42: 85-94, 2007.

26. Bartling SH, Stiller W, Grasruck M, et al. Retrospective motion gating in small animal CT of mice and rats. *Invest Radiol* 42: 704-714, 2007.

27. Feng Q, Lu X, Jones DL, et al. Increased inducible nitric oxide synthase expression contributes to myocardial dysfunction and higher mortality after myocardial infarction in mice. *Circulation* 104: 700-704, 2001.

28. Ford NL, Graham KC, Groom AC, et al. Time-course characterization of the computed tomography contrast enhancement of an iodinated blood-pool contrast agent in mice using a volumetric flat-panel equipped computed tomography scanner. *Invest Radiol* 41: 384-390, 2006.

29. Ford NL, Nikolov HN, Norley CJ, et al. Prospective respiratory-gated micro-CT of free breathing rodents. *Med Phys* 32: 2888-2898, 2005.

30. Du LY, Umoh J, Nikolov HN, et al. A quality assurance phantom for the performance evaluation of volumetric micro-CT systems. *Phys Med Biol* 52: 7087-7108, 2007.

31. Otsu N. A threshold selection method from gray-level histograms. *IEEE Trans Syst Man Cybern (USA)* SMC-9: 62-66, 1979.

32. Wiesmann F, Ruff J, Engelhardt S, et al. Dobutamine-stress magnetic resonance microimaging in mice : acute changes of cardiac geometry and function in normal and failing murine hearts. *Circ Res* 88: 563-569, 2001.

33. Janssen B, Debets J, Leenders P, et al. Chronic measurement of cardiac output in conscious mice. *Am J Physiol Regul Integr Comp Physiol* 282: R928-935, 2002.

34. Mayo JR, Aldrich J, and Muller NL. Radiation exposure at chest CT: a statement of the Fleischner Society. *Radiology* 228: 15-21, 2003.

35. Campbell J, Kalra MK, Rizzo S, et al. Scanning beyond anatomic limits of the thorax in chest CT: findings, radiation dose, and automatic tube current modulation. *AJR Am J Roentgenol* 185: 1525-1530, 2005.

36. van Rongen E, Travis EL, and Thames HD, Jr. Repair rate in mouse lung after clinically relevant radiation doses per fraction. *Radiat Res* 141: 74-78, 1995.

37. Vegesna V, Withers HR, and Taylor JM. Repair kinetics of mouse lung. *Radiother Oncol* 15: 115-123, 1989.

38. Takuma S, Suehiro K, Cardinale C, et al. Anesthetic inhibition in ischemic and nonischemic murine heart: comparison with conscious echocardiographic approach. *Am J Physiol Heart Circ Physiol* 280: H2364-2370, 2001.

39. Tan TP, Gao XM, Krawczyszyn M, et al. Assessment of cardiac function by echocardiography in conscious and anesthetized mice: importance of the autonomic nervous system and disease state. *J Cardiovasc Pharmacol* 42: 182-190, 2003.

40. Ishizaka S, Sievers RE, Zhu BQ, et al. New technique for measurement of left ventricular pressure in conscious mice. *Am J Physiol Heart Circ Physiol* 286: H1208-1215, 2004.

41. Roth DM, Swaney JS, Dalton ND, et al. Impact of anesthesia on cardiac function during echocardiography in mice. *Am J Physiol Heart Circ Physiol* 282: H2134-2140, 2002.

42. Bairey CN, de Yang L, Berman DS, et al. Comparison of physiologic ejection fraction responses to activities of daily living: implications for clinical testing. *J Am Coll Cardiol* 16: 847-854, 1990.

43. Becker LC, Pepine CJ, Bonsall R, et al. Left ventricular, peripheral vascular, and neurohumoral responses to mental stress in normal middle-aged men and women. Reference Group for the Psychophysiological Investigations of Myocardial Ischemia (PIMI) Study. *Circulation* 94: 2768-2777, 1996.

44. Yang F, Liu YH, Yang XP, et al. Myocardial infarction and cardiac remodelling in mice. *Exp Physiol* 87: 547-555, 2002.

3 Evaluation of eXIA 160 Cardiac-related Enhancement in C57BL/6 and BALB/c mice using Micro-CT

The content of this chapter has been adapted from "Evaluation of eXIA 160 cardiac-related enhancement in C57BL/6 and BALB/c mice using micro-CT", published in Contrast Media and Molecular Imaging vol 7 (2) March 2012, by Sarah A. Detombe, Joy Dunmore-Buyze, and Maria Drangova.

3.1 Introduction

The use of small animal models to study a variety of diseases has driven the development of imaging devices capable of studying structural and functional changes in organ systems on a small scale. Micro-computed tomography (micro-CT), a non-invasive imaging technique capable of producing images with high-resolution isotropic voxels, measures the attenuation of x-rays passing through the subject. It is adept at providing excellent information regarding skeletal structure, but soft tissues in the body are very similar in density and require a contrast agent of radio-opaque material to enable soft tissue differentiation. Specifically, evaluating cardiovascular function requires a contrast agent to distinguish the blood in the heart chambers from the myocardium.

Clinical contrast agents in use, such as iohexol and iopamidol, have high concentrations of organically-bound iodine that provide excellent contrast between blood and tissue, but are quickly cleared via glomerular filtration.[1] Scans measuring cardiac function in small animal models require longer scan times with consistent contrast, and an optimal protocol using these clinical agents can be challenging to develop.

An iodinated triglyceride emulsion (ITG) was designed and developed specifically to visualize liver tumors;[2,3] as the ITG is preferentially taken up by the

hepatocytes tumors are visualized as hypodense regions. However, this contrast was also rapidly cleared from the bloodstream. In 1998, Weichert *et al.* reported the development of an ITG that also contained polyethylene glycol (ITG-PEG).[4] The PEG molecules prevented rapid uptake of the ITG by the liver, due to steric hindrance, and as a result, the contrast agent remained in the blood-pool and provided vascular enhancement for several hours. Marketed as Fenestra VC, this contrast agent was subsequently used in multiple studies reporting the development and use of cardiac-gated micro-CT to measure cardiac function in mice,[5-9] vascular micro-imaging,[10] as well as for characterizing liver tumor size.[11, 12]

Recently, a new preclinical blood-pool contrast agent has been developed: eXIA 160 is an aqueous colloidal poly-disperse contrast agent with a high concentration of iodine (160 mg I/mL) compared to Fenestra VC (50 mg I/mL), creating strong contrast between blood and tissue with a low injection volume. This is especially beneficial when monitoring cardiac function in mice, as their small blood volume limits the volume that can be safely injected without adverse hemodynamic effects. Although enhancement of the liver and spleen using eXIA 160 has been reported,[13] and eXIA 160 was recently used in a study investigating vessel imaging,[14] a blood-pool enhancement time-course and the related implications for measuring cardiac function have not yet been characterized.

Transgenic mice have been used extensively in cardiovascular research to investigate a variety of cardiovascular diseases, but the genetic strain of the mice used is rarely considered in physiological studies.[15] However, several recent studies have highlighted the importance of considering genetic strain when investigating disease models, as similar procedures can provoke opposite responses in different strains.[16, 17] It will therefore be useful to determine if any strain-related differences in contrast agent uptake and elimination occur between the C57BL/6 and BALB/c strains, two of the most commonly used strains in cardiac research.[15]

In this study, a high-resolution volumetric micro-CT scanner was used to evaluate whole-body tissue enhancement of eXIA 160 in both C57BL/6 and BALB/c strains over a 48-hour period. Our objective was to determine the optimal use of this contrast agent during cardiac function studies in mice and if strain-related differences in enhancement are occurring against different genetic backgrounds.

3.2 Methods

3.2.1 Animal Preparation

All animal studies were carried out in accordance with the regulations set out by The University of Western Ontario's Council on Animal Care. Six C57BL/6 male mice, 22-24 g, and six BALB/c male mice, 22-24 g (Jackson Laboratories, Bar Harbor, ME), were anesthetized with 1.5% isoflurane in O_2 via a nose cone placed on the snout of the animals, which allowed them to freely breathe the isoflurane; a respirator was not utilized and intubation was not necessary. Mice were placed prone on the scanner bed and kept warm with infrared lamps, previously shown to maintain body temperature near 37°.[8, 9] Following a control scan, acquired prior to contrast administration, 5 μL/g body weight of eXIA 160 (Binitio Biomedical Inc, Ottawa, ON, Canada) was slowly injected into the anesthetized animals over a 2-minute period via tail vein. In addition to the precontrast scan, animals were also scanned at 5, 15, 30, 45, 60 min, and 2, 4, 8, 12, 24, and 48 hr post injection. Numerous scans were performed in the first hour post-injection, as previous studies indicated rapid elimination from the blood-pool within the first hour.[13] Mice were kept anesthetized for the first hour of scanning, then re-anesthetized for each subsequent scan. Saline (0.5 ml) was administered subcutaneously following the 60 min. scan to aid in recovery.

3.2.2 Scan Acquisition and Reconstruction

Scans were performed using the GE Locus Ultra (GE Healthcare, London, ON, Canada), a scanner comprised of a clinical x-ray tube and a 1024 x 1024 flat-panel detector mounted on a slip-ring gantry. Anatomical scans were acquired at 80 kVp and 110 mA over a 14 cm transaxial and 5.7 cm longitudinal field of view during an 8-second acquisition; as functional information was not being collected, gating scans were not performed. The approximate entrance dose delivered during one scan was 10.1 cGy. Images were reconstructed using a cone-beam reconstruction algorithm[18] with an isotropic voxel spacing of 150 μm.[19]

3.2.3 Image Analysis

Image analysis was performed using MicroView (v ABA 2.2, GE Healthcare, London, ON, Canada). All images were first rescaled into Hounsfield units (HU), by using water and air calibrators. Regions of interest (ROI) 0.45 mm x 0.45 mm x 0.15 mm in size were chosen to correctly measure the organs of interest without intersecting other tissues or vasculature; they were generated in the left ventricle (LV) to measure blood-pool contrast, as well as in the liver, spleen, myocardium, renal cortex, bladder, and brown adipose tissue (BAT), located suprascapularly (Fig. 3.1). In each tissue of interest, the ROI was drawn in 3 different coronal slices, with care taken to avoid the major arteries, as that would artificially increase the CT number. The CT number from each of the 3 ROIs was averaged together, to obtain a mean CT number for each tissue at each time point, for each mouse.

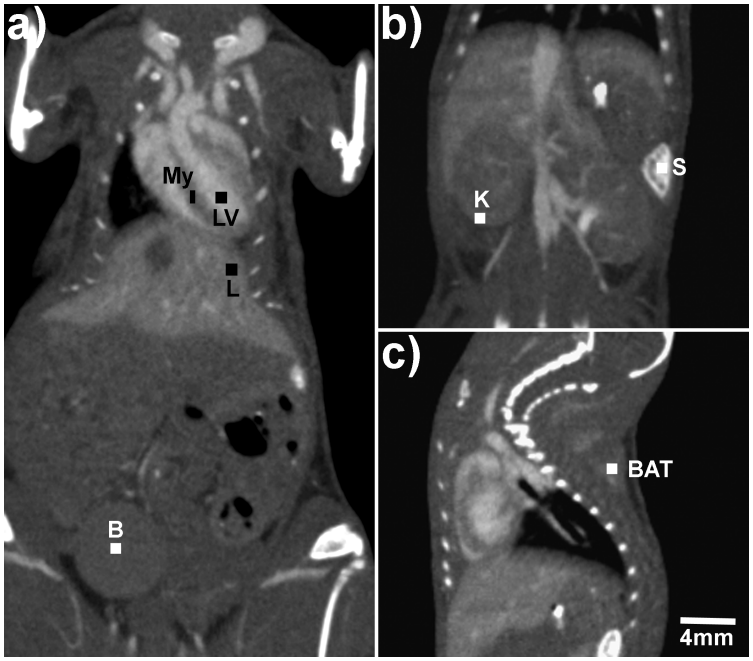

Figure 3.1: Coronal (a, b) and sagittal (c) images of a C57BL/6 mouse 30 minutes post-administration of the contrast agent, displaying the ROIs drawn in each tissue to determine enhancement. LV, left ventricle; My, myocardium; L, liver; B, bladder; K, kidney (renal cortex); S, spleen; BAT, brown adipose tissue.

For each strain, enhancement time curves were generated for all tissues by averaging the CT values measured at each time point for all mice within the respective groups.

3.2.4 Statistical Analysis

All values are reported as mean ± SD for continous variables. Analysis was performed using Prism 4 (GraphPad Software, Inc., San Diego, CA). Repeated measures 2-way ANOVA and Bonfferoni post-tests were performed for each tissue type to measure enhancement differences between strains over time. Results were considered statistically significant at $p<0.05$.

3.3 Results

Scans were successfully acquired and images reconstructed for each animal at each time point. The contrast agent was well tolerated by the mice in this study, with only minor lethargy witnessed in between scans – possibly a consequence of the animal metabolizing the contrast agent, or perhaps due to the repeated anesthesia sessions.

The enhancement values measured for each mouse were averaged together by strain, and the resulting enhancement-time curves were plotted by tissue type in Figure 3.2. The LV showed immediate enhancement upon injection, with the peak enhancement occurring at the 5-minute scan and measuring 687 HU ± 86 HU above the precontrast value in the C57BL/6 group and 666 HU ± 53 HU above the precontrast value in the BALB/c group. The high contrast in the blood-pool dropped rapidly in both strains during the first 2 hours and reached baseline values by the 8-hour time point.

The myocardium showed a continual increase in contrast over the first 2 hours, peaking in enhancement at the 4-hour time point (278 ± 13 HU and 272 ± 27 HU above precontrast in the C57BL/6 and BALB/c groups, respectively). Figure 3.3 visually illustrates the time-course of eXIA 160 enhancement in the LV and myocardium; note that by one hour post contrast agent administration, the myocardium was sufficiently enhanced to inhibit accurate LV segmentation, which relies on adequate differentiation between the blood in the LV chamber and the myocardium.

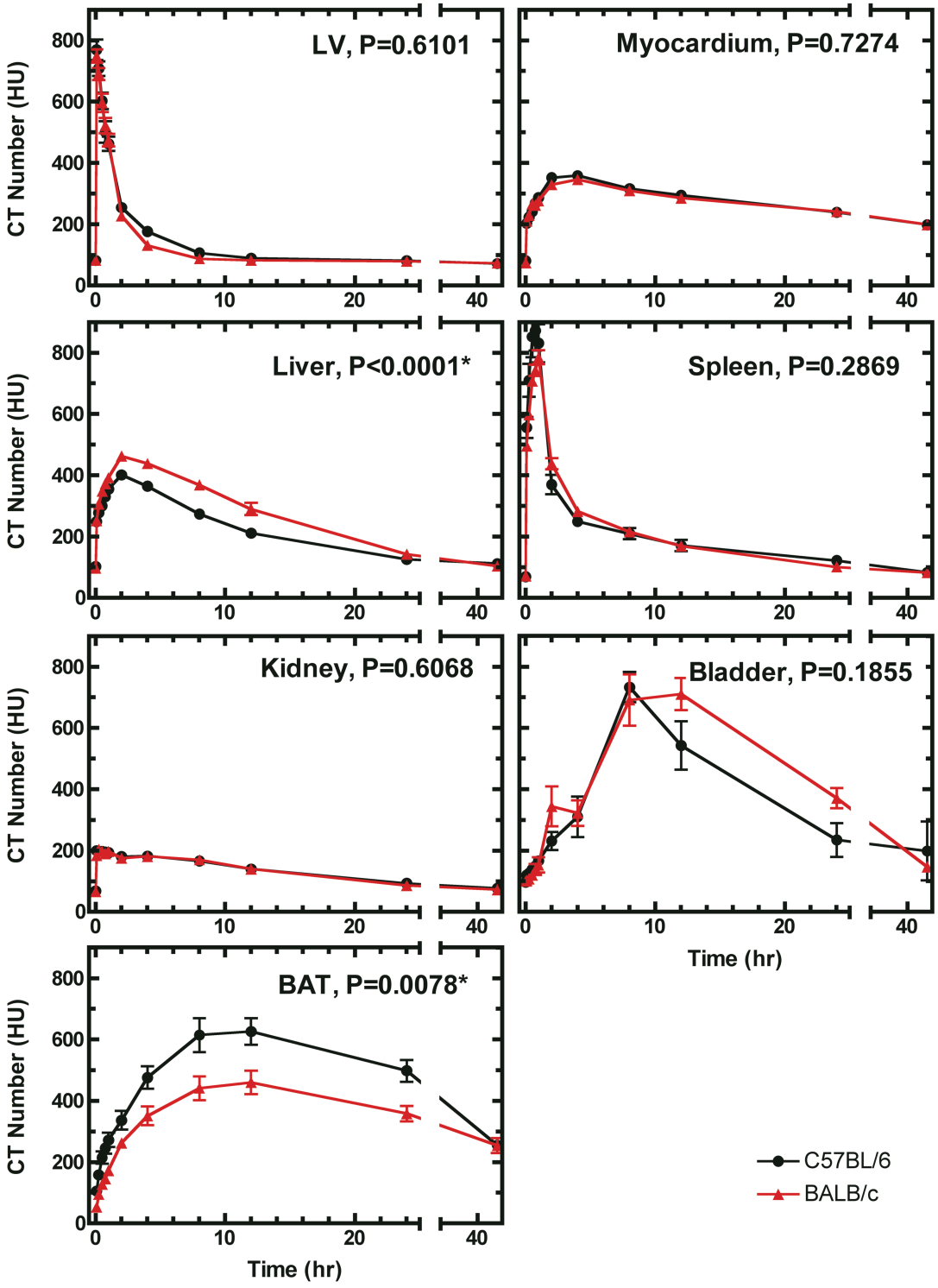

Figure 3.2: Enhancement-time curves of the tissues measured. Black line represents C57BL/6 group, red line represents BALB/c group. P-values listed on each plot represent the results of a repeated-measures 2-way ANOVA comparing the strains. *represents significant differences.

As LV segmentation is required to measure cardiac function, it was therefore important to determine the optimal timeframe during which cardiac-related scans should be acquired. This was accomplished by plotting the LV and myocardium enhancement-time curves together (Fig. 3.4a). The times post injection corresponding to the highest contrast between LV blood and myocardium can be determined from Fig. 3.4b, which is a plot of the difference between the myocardial and LV values over time.

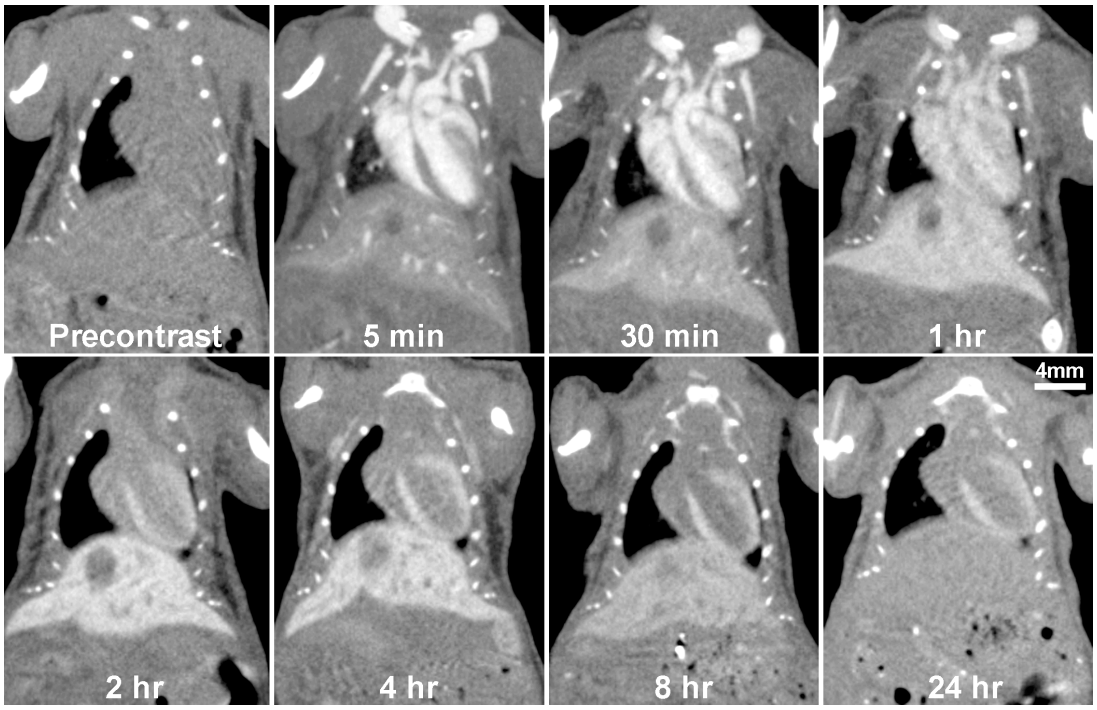

Figure 3.3: Coronal slices from 3D images of the same C57BL/6 mouse scanned at different time points. Note that at the one-hour time point, the myocardial enhancement is beginning to obscure the LV chamber, and that by the four-hour time point, the myocardial enhancement is sufficient to enable LV wall segmentation.

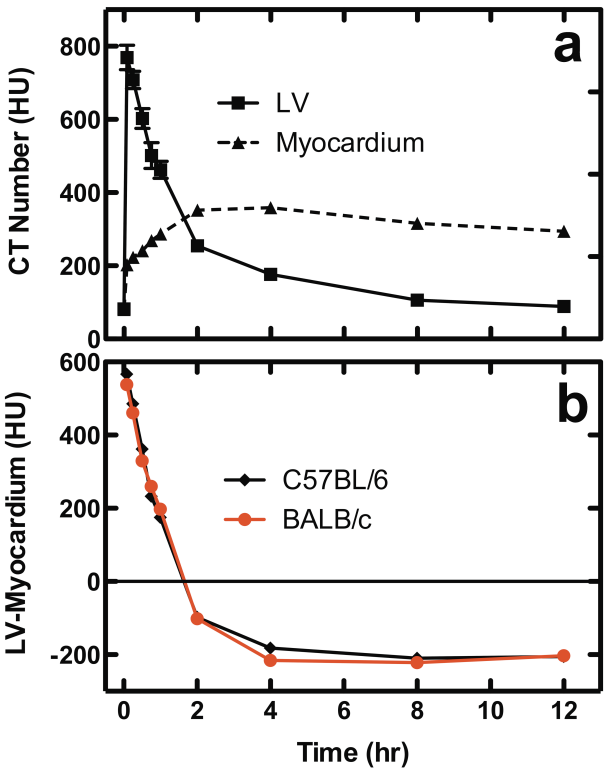

Figure 3.4: (a) Enhancement-time curves for the left ventricle (LV) and myocardium for the C57BL6 group. (b) Value of the difference between LV blood pool and myocardium for both strains studied.

eXIA 160 also provided enhancement in the liver and spleen (Fig. 3.5). In both strains, peak liver enhancement occurred 2 hours post-injection (299 HU ± 26 HU and 365 HU ± 23 HU above the precontrast value for the C57BL/6 and BALB/c groups, respectively) and dropped close to baseline values by 24 hours. Likewise, the spleen displayed peak enhancement early in the study (45 minutes for C57BL/6 group and 1 hour for BALB/c group) with values of 802 HU ± 165 HU and 714 HU ± 60 HU, respectively; precontrast levels were reached within 24 hours.

The renal cortex of the kidneys showed average enhancement immediately following injection of the contrast agent (Fig. 3.5), and maintained a steady contrast (an enhancement over baseline of approximately 130 HU) for the first several hours, with a slow decline towards precontrast values by 24 hours (Fig. 3.2). Bladder enhancement was consistent with the production of urine as the contrast agent was filtered through the kidneys (Fig. 3.2).

Another unique elimination pathway was reflected in the enhancement of the brown adipose tissue (BAT), which was most noticeable in the suprascapular BAT deposit (Fig. 3.5). Enhancement values peaked at 12 hours, with values of 639 ± 105 HU

for the C57BL/6 group and 497 ± 87 HU for the BALB/c group; contrast remained strong in this tissue at 48 hours (270 HU above precontrast values).

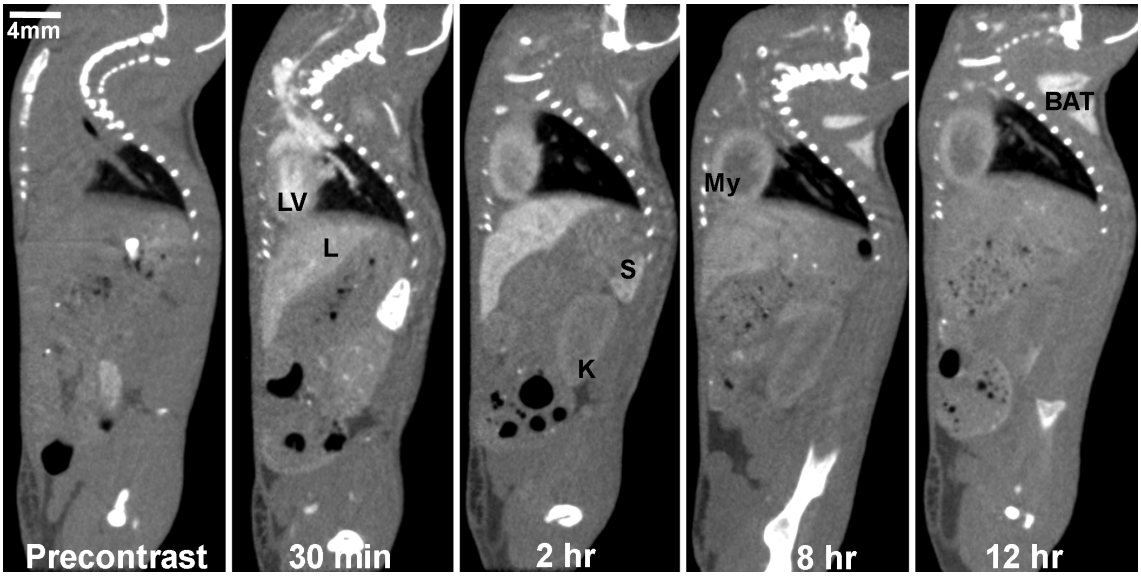

Figure 3.5: Sagittal slices from 3D images of the same C57BL/6 mouse scanned at different time points. The sagittal view was chosen to display a wider range of measured tissues. LV, left ventricle; My, myocardium; L, liver; S, spleen; K, kidney; BAT, brown adipose tissue.

A repeated-measures 2-way ANOVA performed on each tissue type indicated there were no significant differences between the C57BL/6 and the BALB/c groups, with the exception of the liver and BAT, which showed statistically significant differences ($P < 0.0001$ for liver and $P < 0.01$ for BAT) between the strains.

3.4 Discussion

Enhancement of over 650 HU, over precontrast values, was measured in the blood pool of all mice at 5 minutes following the injection of only 0.1ml of eXIA 160 (in a 20 g mouse). To achieve similar blood-pool enhancement with Fenestra VC, injection volumes of 0.4 ml (per 20 g) were required.[5] This difference in enhancement is consistent with the difference in Iodine loading of the two agents – eXIA 160, contains 3.2 times more iodine per mL than Fenestra VC. The present study also demonstrates

that eXIA 160 is eliminated from the blood-pool at a faster rate than previously reported for Fenestra VC: rather than maintaining a relatively stable enhancement for several hours post-injection (half-life of approximately 8 hr),[5,20] eXIA 160 enhancement dropped 40% within the first hour (Fig. 3.2). However, enhancement values remained above 500 HU during the first 30 minutes post-injection, thereby providing excellent contrast for a period of time sufficient to perform several prospectively gated cardiac micro-CT scans.

A unique – and unexpected – quality of eXIA 160 was the contrast uptake into the myocardium, which may represent one of the ways in which the contrast agent is metabolized in the mouse. Enhancement began immediately following injection of the contrast agent, and continued to increase until peak enhancement occurred at 4 hours post-administration for both the C57BL/6 (278 HU) and the BALB/c groups (272 HU). The increasing enhancement of the myocardium during the first hour did decrease the length of time during which scans measuring cardiac function could be acquired, as sufficient difference between the LV blood-pool and the myocardium is required for proper segmentation of the LV (Fig. 3.3). In fact, Fig 3.4 demonstrates that between 1 and 2 hrs post-injection contrast between the blood-pool and myocardium reverses, implying that at around 1.75 hr, the contrast is equal to zero. Therefore, the optimal timeframe for acquiring cardiac functional scans is within the first 30 minutes post-injection (Fig. 3.4); during this time the contrast between the blood and myocardium remained above 360 HU.

Although myocardial enhancement limits the time during which cardiac functional studies can be optimally performed, it also offers a number of possibilities for further study: for example, an accurate measurement of myocardial mass that is not dependent on manual tracing but rather on automatic segmentation; and the ability to study wall motion and wall function, normally not feasible with micro-CT, given the low soft tissue contrast inherent in the imaging technique. Therefore, eXIA 160 may be advantageously used as a dual-phase cardiac contrast agent, capable of providing contrast for LV function soon after injection, then enhancing the myocardium for wall motion studies at a further time-point in the experiment in the same animal. Referring again to Fig. 3.4, the cardiac function scans could optimally be acquired in the first 30 minutes post-injection, and the LV wall-related scans acquired between 4 to 8 hours post-

injection. Additionally, the potential use of eXIA 160 to evaluate myocardial wall structure and function may also prove to be of use in multi-modality imaging studies; an injection of a molecular imaging contrast agent, in addition to eXIA 160, would enable monitoring of metabolic activity during SPECT/CT and PET/CT experiments.[21]

In addition to providing blood-pool contrast for an extended period of time, eXIA 160 also enhanced a number of other tissues as it was eliminated from the body. The liver and spleen appear to be major clearance pathways; this is similar to Fenestra VC, which was developed specifically to be eliminated by the hepatobiliary system.[4] However, given that the spleen has a central role in the reticuloendothelial system (RES), it is likely that Fenestra is also eliminated at least partly by the RES. The similar enhancement pattern of eXIA 160 therefore suggests that the contrast agent was eliminated by one or both of these systems. Peak enhancement of eXIA 160 in the spleen occurred 45-60 minutes post-injection and in the liver 2 hours post-injection, in contrast to Fenestra VC, which has a peak enhancement at 24 hours post-injection in both organs.[20] This suggests that, although eXIA 160 may have a similar elimination pathway to Fenestra VC, it is metabolized more quickly. In addition, eXIA 160 administration produced kidney and bladder enhancement; kidney enhancement began in both strains immediately following injection, signifying the contrast agent was not metabolized but rather filtered unaltered through the glomeruli and eliminated in the urine. Unlike the enhancement time-course of Fenestra VC, which does not lead to kidney/bladder enhancement, eXIA 160 appears to partly mimic the main elimination pathway of clinical contrast agents.[1] The multiple elimination pathways observed in this study are consistent with, and likely a result of, the poly-disperse nature of the eXIA contrast agent.

Enhancement of the BAT was witnessed, which peaked at 12 hours for both strains, and measured 639 HU (C57BL/6) and 497 HU (BALB/c) above baseline. The mechanism of this uptake is as unclear, but contrast was still present at the 48-hour time-point, indicating eXIA 160 is metabolized slowly in this tissue. BAT is responsible for non-shivering thermogenesis, and low body temperature has been shown to increase uptake of glucose-based tracers used in nuclear imaging.[22] Although eXIA 160 would not enter the BAT via glucose receptors, it is possible that the body temperature of the

mouse may likewise have an effect on contrast agent uptake. Further studies are required to explore this effect.

Earlier work by Willekens *et al.* also reported enhancement curves for eXIA 160 in the liver and spleen;[13] however, the values reported were dramatically lower than observed in this study. Willekens *et al.* presented their results as "percent contrast," rather than in HU, making direct comparison difficult. However, converting the data in our study using the equation provided by Willekens (difference between pixel value at a given time point and the unenhanced pixel value of the same region, normalized by the unenhanced pixel value and expressed as a percentage) the enhancement values we achieved ranged from 181% in the renal cortex to 1135% in the spleen. The largest value reported by Willekens was 38% in the spleen, which was particularly surprising given that a 50 kVp x-ray spectrum was used; this should have generated images with a larger "percent contrast" than those generated with the 80 kVp spectrum used in our study. Willekens' study also measured enhancement-time curves for Fenestra VC that were much lower than the enhancement values reported previously.[20] A potential explanation may lie in the challenge of performing tail vein injections: it is possible that in Willekens' study, a portion of the contrast agent accumulated in the tail space rather than entering the vein, artificially lowering the observed enhancement values. Another difference between the two studies is the more rapid decrease in blood pool enhancement observed by Willekens' study, which can also be attributed to a smaller amount of contrast entering the blood stream during injection.

The present study is the first to compare the uptake and elimination of eXIA contrast in two different strains of mice. Both the C57BL/6 and BALB/C mice studied displayed excellent contrast in the vasculature and very similar elimination times, indicating that cardiac functional measurements can be performed using micro-CT on either strain without the need to adjust the protocol or times reported in this study. There did appear to be some difference in the way the strains metabolized the contrast agent, evidenced by the significantly different enhancement-time curves for liver and BAT; when the liver and BAT measurements were compared, the C57Bl/6 group showed lower liver values, but higher BAT values, than the BALB/c group. Although it is not clear why this disparity between strains is occurring, the significant differences seen in BAT

enhancement suggest there may be variations in the way the two strains regulate body temperature. It is interesting to note that for both strains the enhancement curves (Fig. 3.2) for all tissues (other than bladder and BAT) had very tight standard deviations of the mean values for the 6 mice in each group (on the order of 20 HU, except for the blood pool during the first hour, where the SD was approximately 60 HU). This result suggests that all 20-24 g mice of the two strains studied metabolize the contrast agent with similar a time course. The larger SDs observed in the bladder are related to the continuous elimination of urine; since the contrast agent is denser and settles during the scans, the measurement is highly sensitive to the position of the ROI. The high standard deviation of the values obtained in the BAT can be explained by possible variations in body temperature, or to ROI position sensitivity (BAT is highly vascularized).

eXIA 160 was well-tolerated by the mice in this study. All mice returned to normal behavior soon after being removed from anesthesia; except for a slight lethargy around the 4-hour time point, all mice recovered all normal activity within the first 8 hours. However, in other experiments (unpublished) performed on larger mice (~35-40 g), the same dose (5 μL/g body weight) had adverse effects, with a mortality rate of approximately 50% occurring between 24 and 48 hours. Post mortems performed on the affected animals showed necrotic areas in the kidneys and liver, organs responsible for metabolizing and eliminating the contrast agent. This may indicate that higher doses cause liver and/or renal toxicity, although the cause of death was ultimately determined inconclusive. Mortality following higher doses was also seen in previously reported data (Willekens *et al.*)[23], where administration of twice the dose (10 μL/g body weight) to mice ~25 g in size resulted in a 100% mortality rate within 48 hours. These combined results suggest there is an upper tolerance limit on the total amount of eXIA 160 a mouse can adequately process and eliminate, and that a dosage based on body weight is not appropriate for larger animals. We suggest that for mice larger than 30 g, no more than 0.15 mL eXIA 160 be administered, in order to prevent adverse effects.

3.4.1 Conclusion

eXIA 160 is a blood-pool contrast agent with a high iodine concentration, making it possible to administer a low volume of contrast to the mice, and reduce potential

negative hemodynamic effects. Excellent, strain independent, contrast was observed between myocardium and blood (ranging between 560 and 330 HU) during the first 30 minutes post contrast administration. Myocardial enhancement peaked at 4 hours (contrast between blood and myocardium of approximately 200 HU), enabling dual-phase cardiac imaging, where both function and myocardial mass and motion can be studied in the same animal.

References

1. Bourin M, Jolliet P, and Ballereau F. An overview of the clinical pharmacokinetics of x-ray contrast media. *Clin Pharmacokinet* 32: 180-193, 1997.

2. Bakan DA, Doerr-Stevens JK, Weichert JP, et al. Imaging efficacy of a hepatocyte-selective polyiodinated triglyceride for contrast-enhanced computed tomography. *Am J Ther* 8: 359-365, 2001.

3. Bakan DA, Lee FT, Jr., Weichert JP, et al. Hepatobiliary imaging using a novel hepatocyte-selective CT contrast agent. *Acad Radiol* 9 Suppl 1: S194-199, 2002.
4. Weichert JP, Lee FT, Jr., Longino MA, et al. Lipid-based blood-pool CT imaging of the liver. *Acad Radiol* 5 Suppl 1: S16-19; discussion S28-30, 1998.

5. Badea CT, Fubara B, Hedlund LW, et al. 4-D micro-CT of the mouse heart. *Mol Imaging* 4: 110-116, 2005.

6. Badea CT, Hedlund LW, Mackel JF, et al. Cardiac micro-computed tomography for morphological and functional phenotyping of muscle LIM protein null mice. *Mol Imaging* 6: 261-268, 2007.

7. Cao G, Burk LM, Lee YZ, et al. Prospective-gated cardiac micro-CT imaging of free-breathing mice using carbon nanotube field emission x-ray. *Med Phys* 37: 5306-5312, 2010.

8. Detombe SA, Ford NL, Xiang F, et al. Longitudinal follow-up of cardiac structure and functional changes in an infarct mouse model using retrospectively gated micro-computed tomography. *Invest Radiol* 43: 520-529, 2008.

9. Drangova M, Ford NL, Detombe SA, et al. Fast retrospectively gated quantitative four-dimensional (4D) cardiac micro computed tomography imaging of free-breathing mice. *Invest Radiol* 42: 85-94, 2007.

10. Badea CT, Drangova M, Holdsworth DW, et al. In vivo small-animal imaging using micro-CT and digital subtraction angiography. *Phys Med Biol* 53: R319-350, 2008.

11. Graham KC, Detombe SA, MacKenzie LT, et al. Contrast-enhanced microcomputed tomography using intraperitoneal contrast injection for the assessment of tumor-burden in liver metastasis models. *Invest Radiol* 43: 488-495, 2008.

12. Graham KC, Ford NL, MacKenzie LT, et al. Noninvasive quantification of tumor volume in preclinical liver metastasis models using contrast-enhanced x-ray computed tomography. *Invest Radiol* 43: 92-99, 2008.

13. Willekens I, Lahoutte T, Buls N, et al. Time-course of contrast enhancement in spleen and liver with Exia 160, Fenestra LC, and VC. *Mol Imaging Biol* 11: 128-135, 2009.

14. Prajapati SI, and Keller C. Contrast enhanced vessel imaging using microCT. *J Vis Exp* 2011.

15. Shah AP, Siedlecka U, Gandhi A, et al. Genetic background affects function and intracellular calcium regulation of mouse hearts. *Cardiovasc Res* 87: 683-693, 2010.

16. Barrick CJ, Roberts RB, Rojas M, et al. Reduced EGFR causes abnormal valvular differentiation leading to calcific aortic stenosis and left ventricular hypertrophy in C57BL/6J but not 129S1/SvImJ mice. *Am J Physiol Heart Circ Physiol* 297: H65-75, 2009.

17. Barrick CJ, Rojas M, Schoonhoven R, et al. Cardiac response to pressure overload in 129S1/SvImJ and C57BL/6J mice: temporal- and background-dependent development of concentric left ventricular hypertrophy. *Am J Physiol Heart Circ Physiol* 292: H2119-2130, 2007.

18. Feldkamp LA, Davis LC, and Kress JW. Practical cone-beam algorithm. *J Opt Soc Am A* 1: 612-619, 1984.

19. Du LY, Umoh J, Nikolov HN, et al. A quality assurance phantom for the performance evaluation of volumetric micro-CT systems. *Phys Med Biol* 52: 7087-7108, 2007.

20. Ford NL, Graham KC, Groom AC, et al. Time-course characterization of the computed tomography contrast enhancement of an iodinated blood-pool contrast agent in mice using a volumetric flat-panel equipped computed tomography scanner. *Invest Radiol* 41: 384-390, 2006.

21. Pysz MA, Gambhir SS, and Willmann JK. Molecular imaging: current status and emerging strategies. *Clin Radiol* 65: 500-516.

22. Nedergaard J, Bengtsson T, and Cannon B. Three years with adult human brown adipose tissue. *Ann N Y Acad Sci* 1212: E20-36, 2011.

23. Willekens I, Lahoutte T, Caveliers V, et al. Contrast-enhanced in vivo micro-CT imaging. *Mol Imaging Biol* 12: S227-S228, 2009.

4 X-ray dose delivered during a longitudinal micro-CT study has no adverse effects on cardiac and pulmonary tissue in C57BL/6 mice

The contents of this chapter are in preparation to be submitted as a paper with the author list Sarah A. Detombe, Joy Dunmore-Buyze, Ivailo E. Petrov, and Maria Drangova.

4.1 Introduction

Mouse models have become a critical element of preclinical research; at least 80% of the genes in the mouse genome represent an analogous gene in the human genome, and diseases can often be modeled that behave in ways similar to diseases in humans.[1,2] Specifically, mouse models have become popular for modeling cardiovascular disease. As a result, technological advances have led to the development of imaging techniques capable of visualizing small animal cardiovascular systems with sufficient detail. In particular, micro-computed tomography (micro-CT) offers numerous advantages for small animal imaging: rapid scan times ranging from seconds to minutes, and the acquisition of high-resolution images with isotropic voxels enables evaluation of the mouse with minimal impact on the animal's physiology.[3] Additionally, dynamic acquisition of images using gating techniques enables functional measurements of the cardiovascular system in free breathing mice, with scans that are both rapid and reproducible.[4-7] As a result, micro-CT can be particularly useful for detecting the onset of, and monitoring the progression of, cardiac diseases, and phenotype characterization can be performed with the addition of a contrast agent, facilitating measurement of changes in heart size and myocardial structure.[8]

The non-invasive quality of micro-CT enables its use in longitudinal studies,[6] where the same animal can be scanned multiple times over the course of the study.

Disease progression can therefore be tracked in an individual animal, allowing it to act as its own control, and potentially reducing the number of animals required to produce statistical significance in a study.

One of the main drawbacks of micro-CT often stated is a concern over the x-ray dose delivered during the scans. A typical ungated micro-CT scan delivers a dose of 10 cGy[9] which, although much smaller than the LD_{50} of the mouse,[10] is larger than the dose delivered during a clinical cardiac CT (2-5 cGy).[11] This is particularly relevant in longitudinal studies, where more than one scan is performed per animal. Additionally, the cardiac-gated scans required for cardiovascular studies deliver a larger dose.[7]

Radiation damage has been shown to cause cardiac hypertrophy and decrease left ventricular systolic function in the form of a lowered ejection fraction,[12] although a fairly high x-ray dose (16 Gy) is required to cause this damage. Pulmonary tissue is more sensitive to radiation-induced damage than myocardial tissue, and in a cardiovascular study the lungs will be exposed to the same amount of radiation as the heart. As the lungs are more likely to display evidence of radiation exposure before the heart, it would be beneficial to evaluate the pulmonary tissue, in addition to the myocardial tissue, for adverse effects related to the delivered dose of a cardiac micro-CT study.

There have been a number of studies looking at the effect of dose on pulmonary tissue in mice;[13, 14] however, they have focused mainly on investigating radiotherapy doses of 10-20 Gy delivered in a single session at the beginning of the study. Additionally, evaluation of dose effects typically does not begin for 8-12 weeks following exposure. This creates some difficulties in trying to apply the results to a typical micro-CT study, where the doses are smaller, often by a factor of 100, delivered multiple times over a period of weeks, and often less than eight weeks in length.

The objective of this study was to reproduce a longitudinal cardiac micro-CT study and evaluate the effects of dose on pulmonary and myocardial tissue. We scanned C57BL/6 mice multiple times per week for six weeks, and evaluated micro-CT images for any anatomic or functional changes to the lungs and heart, and performed histology to determine if any effects were seen at a cellular level.

4.2 Methods

4.2.1 Animal Groups and Delivered Dose

Twenty C57BL/6 male mice (24 ± 1 g) were split into two groups: the first was the Irradiated Group, which was scanned weekly for six weeks; each weekly session was comprised of three scans (thereby providing three times the dose of a typical micro-CT study). The second group was a Control Group, which was not scanned until week six. In an effort to assess both the pulmonary and cardiac systems, in the final week both groups were first scanned using respiratory gating to evaluate the lungs; a contrast agent (5 µl/g body weight eXIA 160 (Binitio Biomedical Inc, Ottawa, Canada) was then administered via the tail vein and a cardiac-gated scan was acquired to evaluate the heart.

Each scan delivered an entrance dose of 0.28 Gy;[7] as a result, the Irradiated Group received a weekly dose of 0.84 Gy, and a total entrance dose of 5.04 Gy by the end of the study. All studies performed were approved by the Animal Use Subcommittee of the University Council on Animal Care at The University of Western Ontario.

4.2.2 Scan Protocol

Prior to scanning, mice were anesthetized with 1.5% isoflurane in O_2, and placed prone on the micro-CT bed. When required for respiratory gating, a pneumatic pillow was placed beneath the diaphragm to measure breathing signals; likewise, when required for cardiac gating, neonatal electrodes (2269T, 3M Health Care, St. Paul, MN) were affixed to the paws to measure ECG. These physiological signals were recorded using a monitoring and triggering system (BioVet; m2m Imaging Corp., Newark, NJ). Temperature was maintained between 36°C and 37°C during the entire experiment.

Weekly scans were performed using a volumetric cone-beam micro-CT scanner (Locus Ultra, General Electric Healthcare, London, ON, Canada), equipped with a flat-panel detector mounted on a slip-ring gantry, enabling continuous acquisition of x-ray projections. Projection images were acquired at 80 kVp and 50 mA over 10 rotations (5 seconds per rotation, 416 projection images per rotation at a rate of 12 milliseconds/projection) for a total acquisition time of 50 seconds per scan.

4.2.3 Retrospectively-gated reconstruction

All gated reconstructions performed in this study were done using the technique described by Armitage *et al.*[15] and were reconstructed with 150 μm isotropic voxels.[9]

Respiratory Gating: Respiratory-gated reconstructions were performed on week six scans for mice in both groups. Projection images were sorted based on the phase of the respiratory cycle during which they were acquired; images at both peak-inspiration and end-expiration phases were reconstructed. The average window sizes of the two phases were 63 ms and 140 ms, respectively.

Cardiac Gating: Cardiac-gated reconstructions were performed on week six scans acquired following the injection of the contrast agent. Projection images were sorted based on the phase within the cardiac cycle during which they were acquired, enabling subsequent reconstruction of 3D images at 12-ms intervals. For this study, between 9 and 12 3D images were reconstructed per cardiac cycle, depending on the heart rate.

4.2.4 Image analysis

Image analysis was performed using MicroView software (version ABA 2.2, General Electric Healthcare, London, ON, Canada). Images were initially converted to Hounsfield units (HU) using water and air samples in the reconstructed image as a reference.

Respiratory analysis: To calculate lung volume, an upper threshold was first identified for segmenting the lung from the surrounding thoracic tissue; this was performed by generating a region of interest (ROI) that contained 50% lung tissue, and 50% surrounding tissue. The threshold was then automatically determined[16] as -220 HU. A lower threshold was chosen as -750 HU, which effectively segmented the lung parenchyma from the major airways (trachea, bronchi). An ROI was generated around both lungs, and a segmented region-growing algorithm segmented the lung tissue using the upper and lower thresholds previously determined. Thresholds were the same for both inspiration and expiration. The volume was determined for both inspiration and

expiration phases; the density for both phases was determined by finding the mean CT number of the segmented lung tissue.

Cardiac analysis: To calculate LV volume, a threshold level that separated the myocardium from the blood pool was identified automatically;[16] this was done separately for each scan, as contrast level in the blood changed over the course of the study. As described in prior studies,[6, 7] automatic segmentation of the LV chamber from the myocardium was achieved using a region-growing approach. LV volume was calculated for each image throughout the cardiac cycle, and the minimum and maximum were used as end-systolic volume (ESV) and end-diastolic volume (EDV), respectively. Knowledge of the ESV and EDV enabled ejection fraction (EF) to be calculated.

4.2.5 Histology

Following the final scan on week six, the mice were euthanized and the lungs and heart were extracted. Lungs were inflated with 10% formalin, and both the lungs and heart were fixed in the formalin solution. The tissue was then embedded in paraffin and sliced 4 μm thick. Slices were stained with hematoxylin and eosin and evaluated for evidence of dose-related damage (*i.e.* early inflammation in the form of inflammatory cells and edema).

4.2.6 Statistical analysis

Data are presented as mean ± SD for continuous variables; all analysis was performed using Prism 4 (GraphPad Software, Inc., San Diego, CA). Unpaired t-tests were used to evaluate changes in lung volume and lung density between the Irradiated Group and the Control Group, for both the inspiration and expiration phases. Unpaired t-tests were also used to assess differences in cardiac function between the two groups; systolic and diastolic volume, and EF were evaluated. Results were considered statistically significant at $p<0.05$.

4.3 Results

Scans from all animals acquired in the final week were successfully reconstructed and analyzed. Overall, the x-ray dose delivered during the longitudinal study had no significant effect on mouse pulmonary and cardiac tissue.

Qualitatively, the lungs displayed no visual differences between the two groups (Fig. 4.1). This was reflected quantitatively both in lung volume (Fig. 4.2) and lung density (Fig. 4.3).

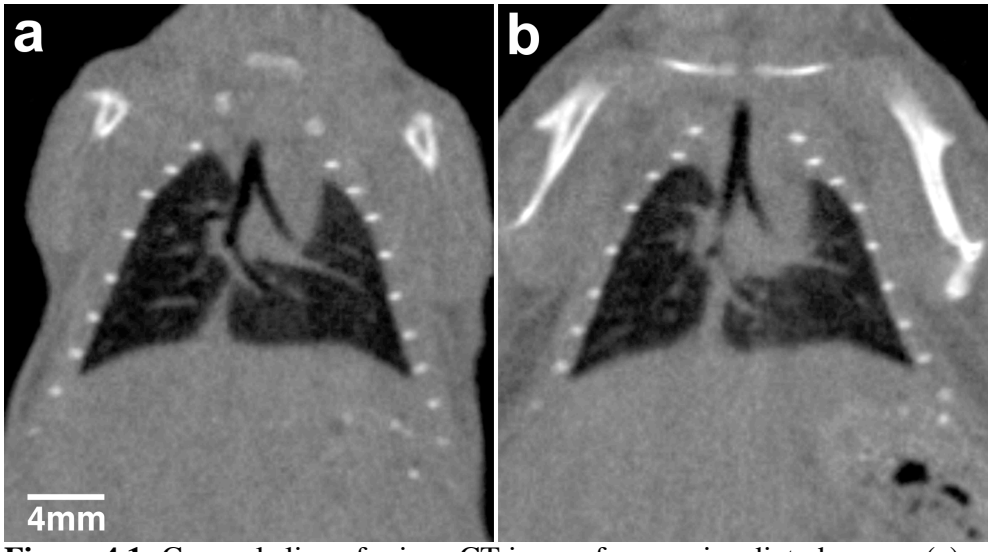

Figure 4.1: Coronal slice of micro-CT image from an irradiated mouse (a) and a control mouse (b) during inspiration. Note the apparent lack of density and volume changes in (a) compared to (b).

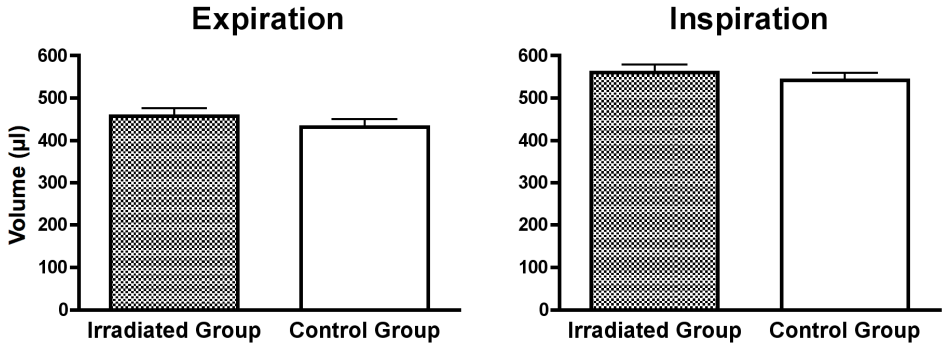

Figure 4.2: A comparison of lung volume between the Irradiated and the Control Group, for both expiration and inspiration phases. No significant differences were measured between groups for either phase.

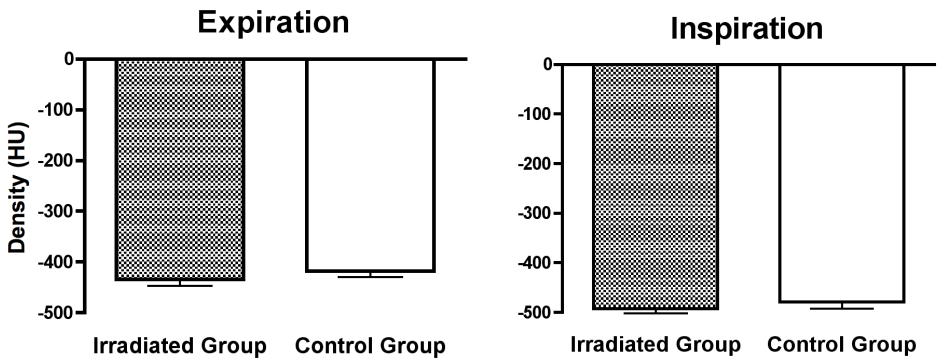

Figure 4.3: A comparison of lung density between the Irradiated and the Control Group, for both expiration and inspiration phases. Differences between groups was not significant for either phase.

T-tests comparing lung volume between the Irradiated and Control groups indicated no significant differences in either expiration ($p=0.3492$) or inspiration ($p=0.4841$) phases. Similarly, t-tests comparing lung density showed no significant differences in either expiration ($p=0.3566$) or inspiration ($p=0.4432$).

More importantly, histological samples of pulmonary tissue showed no early damage in the Irradiated Group as compared to the Control Group (Fig. 4.4). This early damage would show up in the form of inflammatory cells filling up the air spaces, but no evidence of this is present.

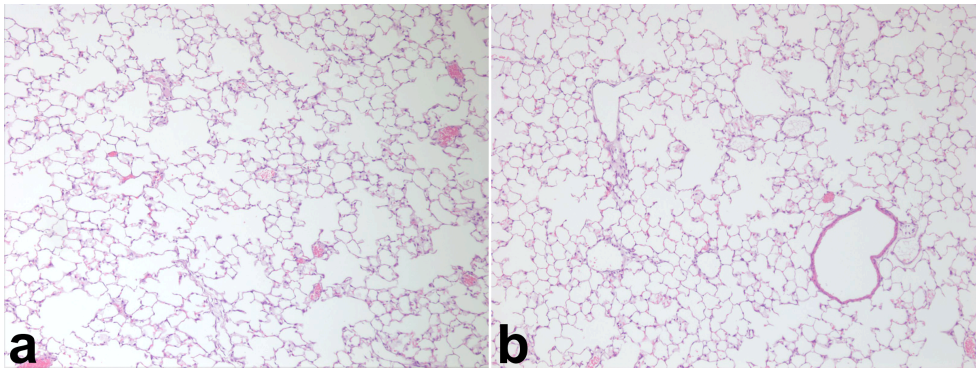

Figure 4.4: Histological slides of pulmonary tissue taken from an irradiated mouse (a) and a control mouse (b). Magnification at x100. No evidence of early inflammation is present in the irradiated mouse, which would be identified by the occurrence of inflammatory cells and edema within the alveoli.

Cardiac function was also evaluated; qualitatively, no changes to the myocardium are evident (Fig. 4.5), which is also reflected quantitatively in the evaluation of LV volume and ejection fraction. No significant differences between the Irradiated and Control groups were witnessed in LV systolic (p=0.1953) and diastolic (p=0.0807) volumes (Fig. 4.6), nor were there any changes in ejection fraction (p=0.9263) (Fig. 4.7).

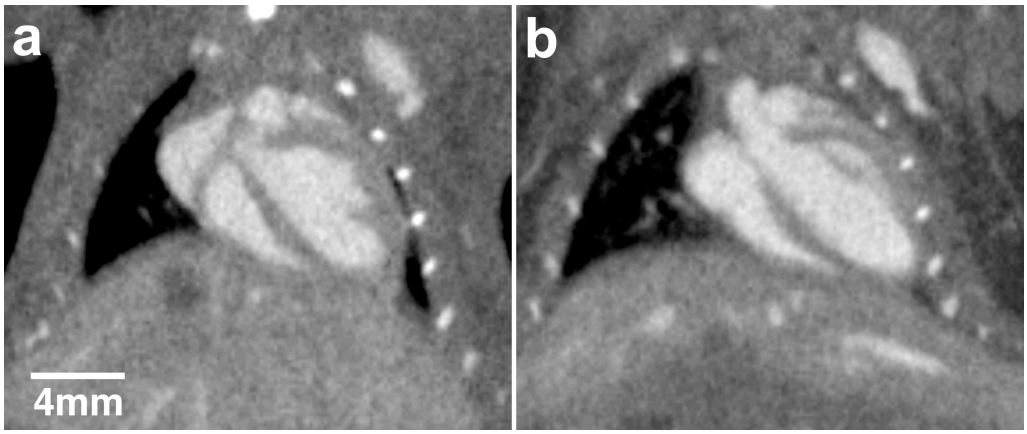

Figure 4.5: Coronal slices of a micro-CT image of an irradiated mouse (a) and a control mouse (b), displaying the heart in diastole. Note the similarity in LV volume and myocardial thickness between the two mice, indicating that no adverse dose effects have occurred.

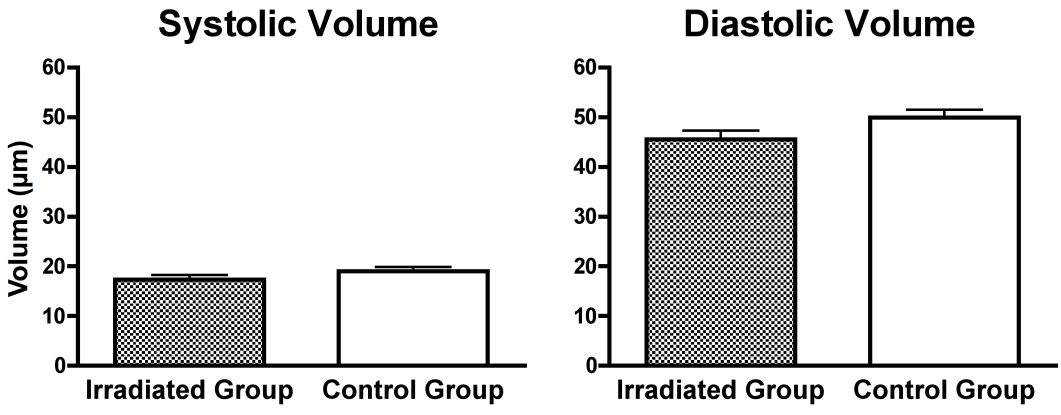

Figure 4.6: A comparison of systolic and diastolic LV volumes between the Irradiated Group and the Control Group. Differences between the groups was not significant for either phase.

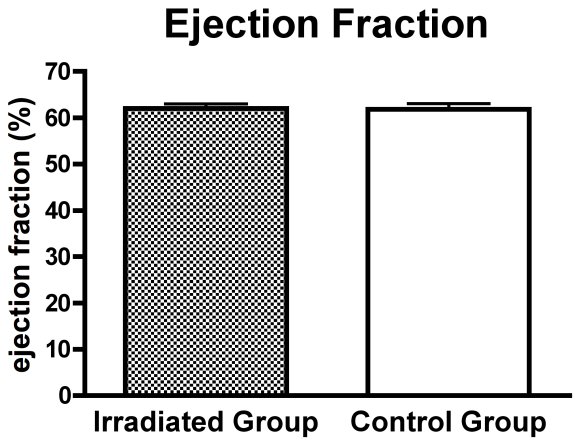

Figure 4.7: A comparison of cardiac function between the Irradiated Group and the Control Group, measured using ejection fraction. No significant differences in function were measured between groups.

Similar to the evaluation of pulmonary tissue, histological samples of the myocardium were evaluated, and no signs of early dose-related damage were present (Fig. 4.8).

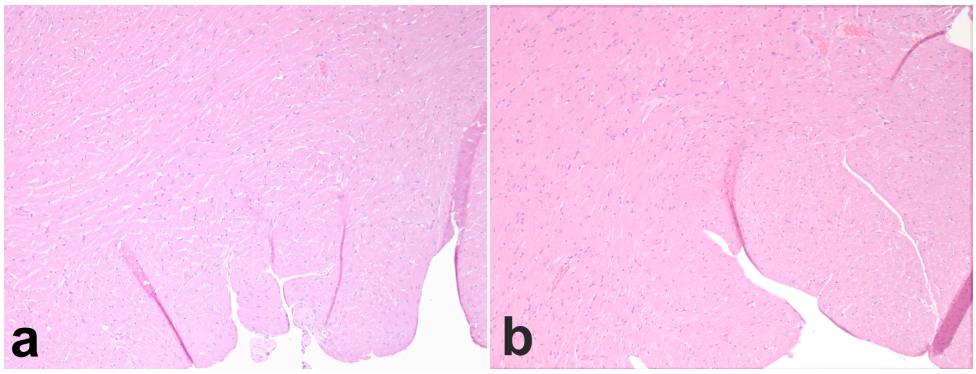

Figure 4.8: Histological slides of myocardial tissue taken from an irradiated mouse (a) and a control mouse (b). Magnification at x100. No evidence of fibrotic tissue is present in the irradiated mouse, indicating that x-ray dose had no adverse effects.

4.4 Discussion

The goal of this study was to determine the effects, if any, of x-ray dose delivered during a typical longitudinal cardiac micro-CT study on the myocardial and pulmonary tissue in C57BL/6 mice. Both pulmonary and cardiac tissue were evaluated because, during a cardiac scan, the field of view is centered on the heart and the lungs are inevitably irradiated, even with a narrow FOV. This is significant because pulmonary tissue has a higher radiosensitivity than myocardial tissue; any early indications of radiation-induced damage will present in the lungs.

Radiation-induced lung damage is generally split into two phases: an early acute inflammatory phase, often called radiation pneumonitis, and a later chronic fibrosis phase.[17] As fibrosis typically develops 4-6 months following radiation exposure, an early inflammatory reaction would be the most likely to occur if a micro-CT study caused damage. Signs of an inflammatory reaction are marked by an increase in inflammatory cells and edema within the air spaces of pulmonary tissue, which can be seen histologically. On a micro-CT image, these changes would result in a decrease in lung volume, and an increase in lung density.

Referring to Figs. 4.2 and 4.3, there were no significant changes to either lung volume or lung density in the Irradiated Group compared to the Control Group, indicating that a cumulative entrance dose of 5.04 Gy caused no significant damage apparent at an anatomic level. More importantly, histology of the pulmonary tissue (Fig. 4.4) showed no early signs of inflammation at a cellular level – there were no inflammatory cells accumulating in the air spaces, no edema was present, and no vascular dilation of the capillaries surrounding the alveoli. This is strong evidence that the dose delivered during a longitudinal micro-CT study does not have an adverse effect on the mouse.

The results presented are consistent with other studies that have evaluated radiation damage to the lungs in mice. In general, a dose threshold of 12 Gy needs to be exceeded in order for radiation pneumonitis to occur in mouse models.[18-21] This is confirmed more recently by Jackson *et al.,*[13] which showed that C57BL/6 mice irradiated with a single 15 Gy dose delivered to the thorax displayed no changes to lung volume or lung density at 16 weeks following exposure, and that changes at a cellular level were

detectable histologically at 28-32 weeks. Interestingly, Johnston *et al.* has recently indicated that doses of 10 Gy delivered full-body may have an effect beyond 12 months;[14] however, these effects, detectable histologically as the onset of fibrosis, with increased levels of collagen in areas of tissue remodeling and inflammation, did not result in changes to lung function, as measured by changes in breathing rate.

The myocardial tissue was also evaluated for evidence of dose effects. The most significant type of radiation-induced heart disease is myocardium damage,[22, 23] which would result in evidence of degenerative morphological changes of cardiomyopathy such as myocyte degeneration/necrosis, increase in the amount of interstitial fibrous connective tissue, mineralization, and/or presence of mononuclear cells in histological analysis.[24] On a micro-CT image, this would present as cardiac hypertrophy (a thickening of the LV wall and an enlargement of the heart), with a decrease in ejection fraction.

As Figures 4.6 and 4.7 indicate, there were no significant changes to either the LV volume, or the ejection fraction in the Irradiated Group, although the p-value of the diastolic volume (0.0807) is very close to significance, suggesting that there may be some difference between the Control and the Irradiated Groups. However, given that there was no evidence of radiation damage present in the pulmonary tissue, it is likely that the potential differences in volume between groups are due to biological variability, rather than dose effects. This is further supported by Figure 4.5, which shows no changes to wall thickness, and Figure 4.8, which confirms no evidence of myocyte degeneration, or presence of inflammatory cells occurring interstitially. Although not unexpected, these results are consistent with other studies evaluating radiation damage to the heart, which in general show that larger doses and a longer period of time are required to cause measurable damage. For example, Monceau *et al.* delivered a dose of 16 Gy to the thorax of C57Bl/6 mice and witnessed radiation-induced cardiac hypertrophy 15 weeks following irradiation;[12] however a significant decrease in ejection fraction did not occur until 30 weeks. Qian *et al.*[25] evaluated short-term effects of 7 Gy delivered to the heart, and found that a mild myocyte degeneration was not witnessed until 100 days following treatment. A study which may have more relevance to micro-CT experiments was described by Baker *et al.*:[26] performed in rats, they found that 10 Gy delivered full-body

had the potential for indirectly contributing to heart disease development, compared to 10 Gy delivered to the thorax alone, which had no significant effect on the myocardium. It was proposed that full-body exposure had effects on non-thoracic organs that contributed to coronary sclerosis and ventricular dysfunction through changes in blood lipid profiles. However, it is important to note that these effects were not witnessed until 120 days following exposure, and that the animals were irradiated in a single dose much larger than would be delivered during a longitudinal micro-CT study.

The results presented in this study have relevance beyond the applicability to other cardiac micro-CT experiments. A scan protocol for retrospective gating was used, which means that these results can be applied to any micro-CT study that employs prosepective gating, or ungated scans, which deliver a lower dose than presented here. Additionally, the dose was purposely tripled beyond a typical dose, widening the variety of studies to which these results can be applied. Finally, studies in which micro-CT is not used longitudinally can also benefit from the results presented, which indicate that the small dose delivered will have no adverse effects on the health of the animal.

The C57BL/6 mouse strain was used, as it is one of the most common strains used in biomedical applications.[13] However, variations in radiation-induced damage between patients in a clinical setting indicate that the damage has a genetic component. This is further supported by studies that present differences in radiation-induced lung damage between mouse strains.[13, 20] But from these studies we can also infer that, given the lower doses (below 12 Gy) of a longitudinal micro-CT study, and the short time frame involved (less than 8 weeks), it is highly unlikely that strain-related differences in radiation effects would occur.

Not addressed in this study is the possibility that cardiac sensitivity to stress may be affected by dose, ultimately resulting in a change in function. A future study may address this by incorporating a cardiac stress test (using, for example, a dobutamine injection); however, given that the x-ray dose presented here had no apparent effects on the more radiosensitive pulmonary tissue, it is unlikely that the dose delivered during the relatively short time-frame of a micro-CT study would result in an abnormal stress test.

Also not covered by this study is the effect of dose delivered during a micro-CT experiment on cancer mouse models. Longitudinal evaluation of tumor growth,

regression, or metastasis is useful for evaluating new therapeutic approaches.[27, 28] Although the dose delivered during micro-CT scans has no negative effect on the health of the animal, it is uncertain how the radiation dose may influence the fast-growing tumor-cells, potentially confounding the investigation of treatment therapies. Future studies should address this area of research.

4.4.1 Conclusion

The x-ray dose delivered during a longitudinal cardiac micro-CT study had no significant effects on the pulmonary and myocardial tissue in mice. Due to the artificially high dose delivered during this study, the results presented can be applied to a wide variety of micro-CT experiments; therefore the benefits of using micro-CT, including rapid scan times that produce high-resolution isotropic images, can be safely taken advantage of without concern that the dose delivered will have an adverse effect on the animal or the study.

References

1. Rosenthal N, and Brown S. The mouse ascending: perspectives for human-disease models. *Nat Cell Biol* 9: 993-999, 2007.

2. Waterston RH, Lindblad-Toh K, Birney E, et al. Initial sequencing and comparative analysis of the mouse genome. *Nature* 420: 520-562, 2002.

3. Ritman EL. Current status of developments and applications of micro-CT. *Annu Rev Biomed Eng* 13: 531-552, 2011.

4. Badea CT, Fubara B, Hedlund LW, et al. 4-D micro-CT of the mouse heart. *Mol Imaging* 4: 110-116, 2005.

5. Badea CT, Hedlund LW, Mackel JF, et al. Cardiac micro-computed tomography for morphological and functional phenotyping of muscle LIM protein null mice. *Mol Imaging* 6: 261-268, 2007.

6. Detombe SA, Ford NL, Xiang F, et al. Longitudinal follow-up of cardiac structure and functional changes in an infarct mouse model using retrospectively gated micro-computed tomography. *Invest Radiol* 43: 520-529, 2008.

7. Drangova M, Ford NL, Detombe SA, et al. Fast retrospectively gated quantitative four-dimensional (4D) cardiac micro computed tomography imaging of free-breathing mice. *Invest Radiol* 42: 85-94, 2007.

8. Detombe SA, Dunmore-Buyze J, and Drangova M. Evaluation of eXIA 160 cardiac-related enhancement in C57BL/6 and BALB/c mice using micro-CT. *Contrast Media Mol Imaging* accepted: 2012.

9. Du LY, Umoh J, Nikolov HN, et al. A quality assurance phantom for the performance evaluation of volumetric micro-CT systems. *Phys Med Biol* 52: 7087-7108, 2007.

10. Sato F, Sasaki S, Kawashima N, et al. Late effects of whole or partial body x-irradiation on mice: life shortening. *Int J Radiat Biol Relat Stud Phys Chem Med* 39: 607-615, 1981.

11. Campbell J, Kalra MK, Rizzo S, et al. Scanning beyond anatomic limits of the thorax in chest CT: findings, radiation dose, and automatic tube current modulation. *AJR Am J Roentgenol* 185: 1525-1530, 2005.

12. Monceau V, Pasinetti N, Schupp C, et al. Modulation of the Rho/ROCK pathway in heart and lung after thorax irradiation reveals targets to improve normal tissue toxicity. *Curr Drug Targets* 11: 1395-1404, 2010.

13. Jackson IL, Vujaskovic Z, and Down JD. Revisiting strain-related differences in radiation sensitivity of the mouse lung: recognizing and avoiding the confounding effects of pleural effusions. *Radiat Res* 173: 10-20, 2010.

14. Johnston CJ, Manning C, Hernady E, et al. Effect of total body irradiation on late lung effects: hidden dangers. *Int J Radiat Biol* 87: 902-913, 2011.

15. Armitage SEJ, Pollmann SI, Detombe SA, et al. Least-error projection sorting to optimize retrospectively gated cardiac micro-CT of free-breathing mice. *Med Phys* 39: 1452-1461, 2012.

16. Otsu N. A threshold selection method from gray-level histograms. *IEEE Trans Syst Man Cybern (USA)* SMC-9: 62-66, 1979.

17. Morgan GW, and Breit SN. Radiation and the lung: a reevaluation of the mechanisms mediating pulmonary injury. *Int J Radiat Oncol Biol Phys* 31: 361-369, 1995.

18. Down JD, and Yanch JC. Identifying the high radiosensitivity of the lungs of C57L mice in a model of total-body irradiation and bone marrow transplantation. *Radiat Res* 174: 258-263, 2010.

19. Hong JH, Jung SM, Tsao TC, et al. Bronchoalveolar lavage and interstitial cells have different roles in radiation-induced lung injury. *Int J Radiat Biol* 79: 159-167, 2003.

20. Sharplin J, and Franko AJ. A quantitative histological study of strain-dependent differences in the effects of irradiation on mouse lung during the intermediate and late phases. *Radiat Res* 119: 15-31, 1989.

21. Travis EL, Down JD, Holmes SJ, et al. Radiation pneumonitis and fibrosis in mouse lung assayed by respiratory frequency and histology. *Radiat Res* 84: 133-143, 1980.

22. Lauk S. Endothelial alkaline phosphatase activity loss as an early stage in the development of radiation-induced heart disease in rats. *Radiat Res* 110: 118-128, 1987.

23. Lauk S, Kiszel Z, Buschmann J, et al. Radiation-induced heart disease in rats. *Int J Radiat Oncol Biol Phys* 11: 801-808, 1985.

24. Azimzadeh O, Scherthan H, Sarioglu H, et al. Rapid proteomic remodeling of cardiac tissue caused by total body ionizing radiation. *Proteomics* 11: 3299-3311, 2011.

25. Qian L, Cao F, Cui J, et al. The potential cardioprotective effects of hydrogen in irradiated mice. *J Radiat Res (Tokyo)* 51: 741-747, 2010.

26. Baker JE, Fish BL, Su J, et al. 10 Gy total body irradiation increases risk of coronary sclerosis, degeneration of heart structure and function in a rat model. *Int J Radiat Biol* 85: 1089-1100, 2009.

27. De Clerck NM, Meurrens K, Weiler H, et al. High-resolution X-ray microtomography for the detection of lung tumors in living mice. *Neoplasia* 6: 374-379, 2004.

28. Paulus MJ, Gleason SS, Kennel SJ, et al. High resolution X-ray computed tomography: an emerging tool for small animal cancer research. *Neoplasia* 2: 62-70, 2000.

5 Rapid micro-computed tomography suggests cardiac enlargement occurs during conductance catheter measurements in mice

The content of this chapter has been adapted from "Rapid micro-computed tomography suggests cardiac enlargement during conductance catheter measurements in mice" by Sarah A. Detombe, Fuli Xiang, Joy Dunmore-Buyze, James A. White, Qingping Feng, and Maria Drangova. It is currently in press with the Journal of Applied Physiology.

5.1 Introduction

Genetically modified mice, such as transgenic and gene-targeted models, are used in cardiovascular research as a way to determine the molecular basis for cardiac dysfunction. The small size and rapid heart rate have necessitated the development of tools specifically designed to track and measure cardiac function on a small scale. One widely used technique involves the measurement of real-time pressure and volume changes in the left ventricle (LV) using a micro pressure conductance catheter (CC) inserted into the heart. Baan *et al.* first presented a method for relating conductance to volume[1] using the equation $V = \rho L^2 (G - Gp)/\alpha$ where ρ is the resistivity constant, L is the length between the electrodes, α is Baan's constant, G is the total conductance measured, and G_p is the parallel conductance of the surrounding tissue. This technique was first used in large animals[2,3] and humans,[4] but with the development of miniaturized micromanometers, it was translated for use in mice.[5-8] The CC technique allows assessment of LV function by load-independent indexes (e.g. the slope of the end-systolic pressure-volume (PV) relation),[5,9] which are more sensitive to small changes in dysfunction than load-dependent measurements such as ejection fraction.[10] This

increased sensitivity is especially important when detecting changes in contractility early in disease progression.

Accurate PV relationships require an accurate absolute volume, but a number of recent studies comparing CC volumes with those derived from imaging methods have shown that catheter-based measurements tend to underestimate ventricular volumes in both healthy and diseased mice. These studies have compared CC volumes to volumes obtained from magnetic resonance imaging[11-13] or echocardiography;[14] however, in most cases the measurements were not performed simultaneously, with imaging occurring one to two days prior to the CC experiments. The differences between CC-derived volumes and imaging may be explained, in part, by differences in respiratory support (free breathing vs. intubated and ventilated)[13] or the residual functional depressive effects due to repeated anesthesia.[13] The most recent study, by Porterfield *et al.*[14] compared CC measured volumes to volumes determined from simultaneously acquired 2D echocardiographic images (using the prolate ellipse method to estimate volume) and reported discrepancies between the imaging and CC volumes that were highly dependent on the position of the conductance catheter within the LV. Retrospective review of the data reported by Porterfield also identifies a great variation in LV size between mice (end diastolic volumes ranging between 22 and 55 μL), which could be attributed to biological variability, but may represent a previously unreported enlargement of the LV during the insertion of the conductance catheter.

The present study takes advantage of a micro-computed tomography (CT) technique – retrospectively gated cardiac micro-CT – which produces high-resolution three-dimensional (3D) images of the mouse heart over the entire cardiac cycle, in scan times of just under one minute.[15,16] Using this imaging technique we were able to compare simultaneously acquired micro-CT and CC measurements of LV volumes in healthy and infarcted mice and to determine changes in LV volume and function associated with the insertion of the catheter. For the first time, these simultaneous measurements have been made without the necessity to make any geometrical assumptions, often associated with two-dimensional (e.g. 2D echocardiography) or thick-slice 3D imaging (e.g. MRI).

5.2 Methods

All studies performed were approved by the Animal Use Subcommittee of the University Council on Animal Care at The University of Western Ontario.

5.2.1 Experimental Strategy

Twenty C57BL/6 male mice, weighing 27.5g ± 4.5g, were split into two groups of ten mice each. One group underwent ligation of the left coronary artery 4 weeks prior to scanning (MI group); the other group was scanned without prior surgical intervention (Normal group). To determine the effects of catheterization on the mouse heart, each mouse was scanned three times using retrospectively gated micro-CT: 1) prior to catheterization, 2) with the catheter placed in the LV and acquired simultaneously with CC measurements, and 3) upon withdrawal of the catheter from the LV into the carotid artery. The final scan was performed to determine if any effects of the catheter on the LV were reversed upon catheter withdrawal. Details regarding each step of the procedure are described below.

5.2.2 Induction of Myocardial Infarction

Surgery was performed as previously described.[17] Briefly, animals were anesthetized with an IP injection of ketamine (50 mg/kg) and xylazine (12.5 mg/kg) prior to intubation. Atropine (0.05 mg subcutaneous) was administered prior to surgery to decrease airway secretion and post-operative mortality. After establishing mechanical ventilation, a left thoracotomy was performed, exposing the LV wall; the left coronary artery was ligated by positioning a suture between the pulmonary artery out-flow tract and the left atrium. After surgery, mice were treated with an antibiotic agent (oxytetracycline, 200 mg/L) via drinking water for 3 days; an analgesic (0.03 mg/kg buprenorphine subcutaneous) was administered to relieve pain. Mice in this group were scanned 4 weeks following ligation.

5.2.3 Animal Preparation

Prior to scanning, mice were anesthetized with 2% isoflurane in O_2 and intubated. A breathing rate of 90 breaths per minute was maintained throughout imaging and hemodynamic studies. A contrast agent (eXIA 160, Binitio Biomedical Inc, Ottawa, Canada), containing 160 mg I/mL, was administered at a dose of 7.5 μL/g body weight. The contrast agent was slowly injected via the left jugular vein over a 2-minute period approximately 10 minutes prior to the first scan. Each animal was positioned supine and three neonatal electrodes (2269T, 3M Health Care, St. Paul, MN) were placed on the animal's paws to record ECG. Physiological signals were recorded using a physiological monitoring and triggering system (BioVet; m2m Imaging Corp., Newark, NJ). Temperature was maintained between 36°C and 37°C during the entire experiment. Once the first scan was completed, the animal was catheterized (see below) and an additional 7.5 μL/g body weight contrast agent was administered over a 2-minute period prior to the remaining two scans.

5.2.4 Catheterization and Hemodynamic Measurements

Following the initial scan, the mice were catheterized using a micro-pressure conductance catheter (Millar Instruments, model SPR-839, 1.4F). The right carotid artery was cannulated and the catheter inserted and advanced into the LV. Correct placement of the catheter was determined solely by the physiologic PV loop in an effort to replicate a typical experimental environment (*i.e.* imaging was not used to provide additional guidance); final acceptance of the placement depended on loop appearance. The right jugular vein was also cannulated, and a 10-μL bolus of 15% saline was injected to measure parallel conductance; this was performed prior to the second scan. Hemodynamic data (relative volume units (RVU), pressure, dP/dt) were recorded using a Power Lab analog-to-digital converter using Chart 5 software (ADInstruments Inc., Colorado Springs, CO). A trigger signal, indicating the start of image acquisition, was also recorded to synchronize the hemodynamic measurements with the CT images; the second scan was acquired approximately 7-10 minutes following catheter insertion. The catheter was then withdrawn into the carotid artery (determined solely by hemodynamic

feedback) and a third scan was acquired immediately following catheter withdrawal (less than 2 minutes). Following the final scan, blood was collected for volume calibration, using cuvettes of a known volume to determine the linear conductance-to-volume relationship; the blood was drawn directly from the heart using a syringe flushed with heparin. This was performed separately for each mouse due to possible variability caused by the presence of contrast agent in the blood. All hemodynamic parameters were collected and analyzed using PVAN software (Millar Instruments, Houston, TX), using the RVU method, which requires only a single measurement of parallel conductance and volume calibration using the cuvette method.

5.2.5 Retrospectively Gated Micro-CT

This method has been previously described, and used to successfully evaluate cardiac function in both healthy and MI mice.[15,16] Images were acquired using a volumetric cone-beam micro-CT scanner (Locus Ultra, General Electric Healthcare, London, ON, Canada), equipped with a flat-panel detector mounted on a slip-ring gantry, enabling continuous acquisition of x-ray projections. Projection images were acquired at 80 kVp and 50 mA. To enable retrospective gating, projections were acquired over 10 rotations (5 seconds per rotation, 416 projection images per rotation at a rate of 12 milliseconds/projection) for a total scan time of 50 seconds. Using the technique described by Armitage *et al.*,[18] the projection images were sorted based on the phase within the cardiac cycle during which they were acquired, enabling subsequent reconstruction of 3D images at 12-ms intervals. For this study, between 9 and 12 3D images were reconstructed per cardiac cycle, depending on the heart rate. All images were reconstructed with voxel spacing of 150 µm x 150 µm x 150 µm (equivalent to 3.4 nL volume elements).[19]

5.2.6 Image Analysis

Image analysis was performed using MicroView software (version ABA 2.2, General Electric Healthcare, London, ON, Canada). To calculate LV volume, a threshold level that separated the myocardium from the blood pool was identified automatically;[20]

this was done separately for each scan, as contrast level in the blood changed over the course of the study. As described in prior studies,[15,16] automatic segmentation of the LV chamber from the myocardium was achieved using a region-growing approach. Chamber volume was calculated by multiplying the number of voxels defining the LV chamber (ranging between 7500 (ESV) and 16000 (EDV) in a healthy mouse) and the voxel volume (3.4 nL). LV volume was calculated for each image throughout the cardiac cycle, and the minimum and maximum were used as end-systolic volume (ESV) and end-diastolic volume (EDV), respectively. Knowledge of the ESV and EDV enabled stroke volume (SV), ejection fraction (EF), and cardiac output (CO) to be calculated.

5.2.7 Statistical Analysis

Data are presented as mean ± SD for continuous variables; all analysis was performed using Prism 4 (GraphPad Software, Inc., San Diego, CA). Agreements between the CT and CC methods were evaluated using Bland-Altman analyses, linear regressions, and calculated correlation coefficients. Paired t-tests were performed to compare functional parameters between CT and CC measurements. Differences between the three scans in the Healthy and MI groups were compared using repeated measures one-way ANOVA, followed by Tukey post-hoc tests to determine where significant differences occurred. Results were considered statistically significant at $p<0.05$.

5.3 Results

Successful imaging and hemodynamic studies were completed for all 10 of the Normal mice and 7 of MI group: one mouse was not successfully ligated, determined by a lack of infarct formation, and two did not survive catheterization. Verification of infarct formation was performed several ways: the hearts were removed and examined following blood collection, the infarcts were clearly visible on the micro-CT images as thin, distended portions at the apex of the LV, and the ejection fractions calculated from the micro-CT images indicated decreased LV function.

CC volumes were consistently underestimated compared to CT volumes, and the underestimation increased in the MI group. Bland-Altman analyses demonstrate this, with biases in the Normal group of -18.4 ± 6.5 μL for ESV and -28.9 ± 13.3 μL for EDV (Fig. 5.1), and in the MI group -51.6 ± 31.5 μL for ESV and -71.7 ± 29.5 μL for EDV (Fig. 5.2). Linear regression results (Fig. 5.3) indicated a moderate correlation between the CT and CC values in the Normal group, and a low correlation in the MI group.

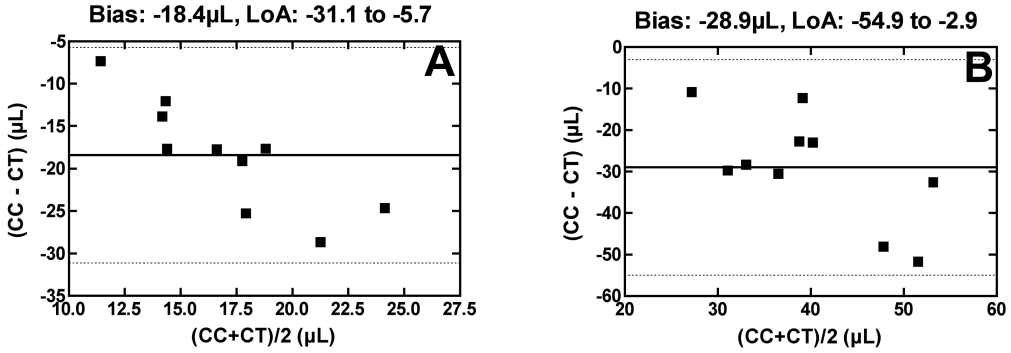

Figure 5.1: Comparison of micro-CT (CT) and conductance catheter (CC) end-systolic (A) and end-diastolic (B) volumes in Normal mice using Bland-Altman analysis. Bias is represented by the solid line, the limits of agreement (LoA = bias ± 2SD) are represented by the dotted lines.

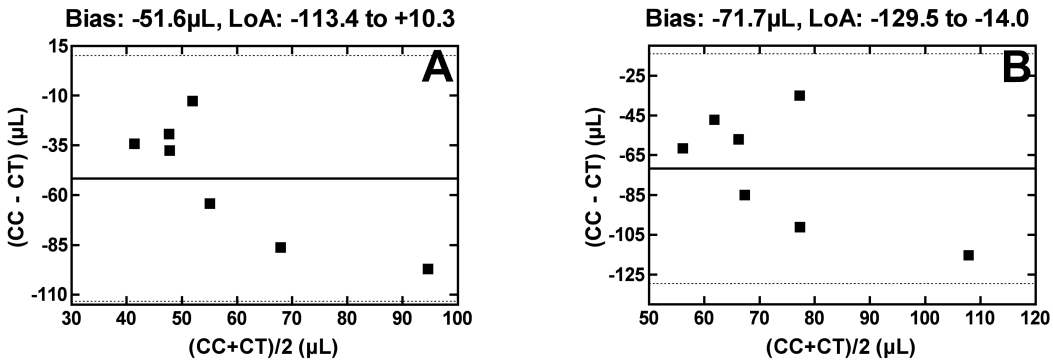

Figure 5.2: Comparison of micro-CT (CT) and conductance catheter (CC) end-systolic (A) and end-diastolic (B) volumes in MI mice using Bland-Altman analysis. Bias is represented by the solid line, the limits of agreement (LoA = bias ± 2SD) are represented by the dotted lines.

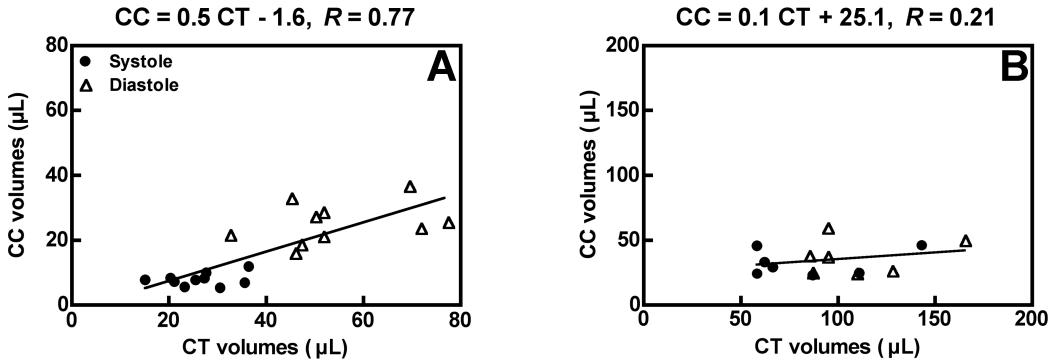

Figure 5.3: Comparison of micro-CT (CT) and conductance catheter (CC) volumes in Normal (A) and MI (B) groups using linear regression analysis.

Table 5.1 lists the averages of all the physiological parameters measured by both CT and CC methods, with corresponding p-values as determined by t-test analysis.

Table 5.1. Comparison of CT and CC methodologies in Normal and MI groups

		Measurement Methodology		P Values
		Micro-CT	*Catheter*	
ESV (μl)				
	Healthy (10)	26.3 ± 6.7	7.9 ± 1.9	<0.001
	MI (7)	83.8 ± 32.5	32.3 ± 9.9	0.005
EDV (μl)				
	Healthy (10)	54.3 ± 14.1	25.4 ± 6.4	<0.001
	MI (7)	109.3 ± 28.9	37.5 ± 13.4	<0.001
SV (μl)				
	Healthy (10)	28.1 ± 8.9	17.5 ± 5.8	0.005
	MI (7)	25.4 ± 6.3	5.3 ± 4.7	<0.001
EF (%)				
	Healthy (10)	51.2 ± 6.8	67.8 ± 9.4	0.003
	MI (7)	25.2 ± 9.8	12.5 ± 7.8	0.007
CO (ml min^{-1})				
	Healthy (10)	13.2 ± 3.8	8.2 ± 2.6	0.005
	MI (7)	11.2 ± 2.7	2.3 ± 2.0	<0.001
HR (bpm)				
	Healthy (10)	475.5 ± 38.7	475.5 ± 38.7	-
	MI (7)	441.9 ± 39.4	441.9 ± 39.4	-
$+dP/dt_{max}$ (mmHg s^{-1})				
	Healthy (10)	-	6060.1 ± 948.0	-
	MI (7)	-	4342.1 ± 1104.8	-
$-dP/dt_{min}$ (mmHg s^{-1})				
	Healthy (10)	-	6701.7 ± 735.3	-
	MI (7)	-	4594.0 ± 917.6	-

Values are means ± SD; numbers in brackets represent no. of animals. MI, myocardial infarction; ESV, end-systolic volume; EDV, end-diastolic volume; SV, stroke volume; EF, ejection fraction; CO, cardiac output; HR, heart rate; $+dP/dt_{max}$, maximal rate of LV pressure increase; $-dP/dt_{min}$, maximal rate of LV pressure decline.

The CT volumes measured prior to the insertion of the catheter (precath), during the CC measurements (cathscan), and following the withdrawal of the catheter (postcath) are plotted in Figure 5.4 for each mouse completing the study.

When changes in individual animals were tracked, several mice in each group displayed ventricle dilation following catheter insertion, demonstrated by an increased ESV and EDV in the affected mice (Fig. 5.4); in some cases the volume was doubled between the

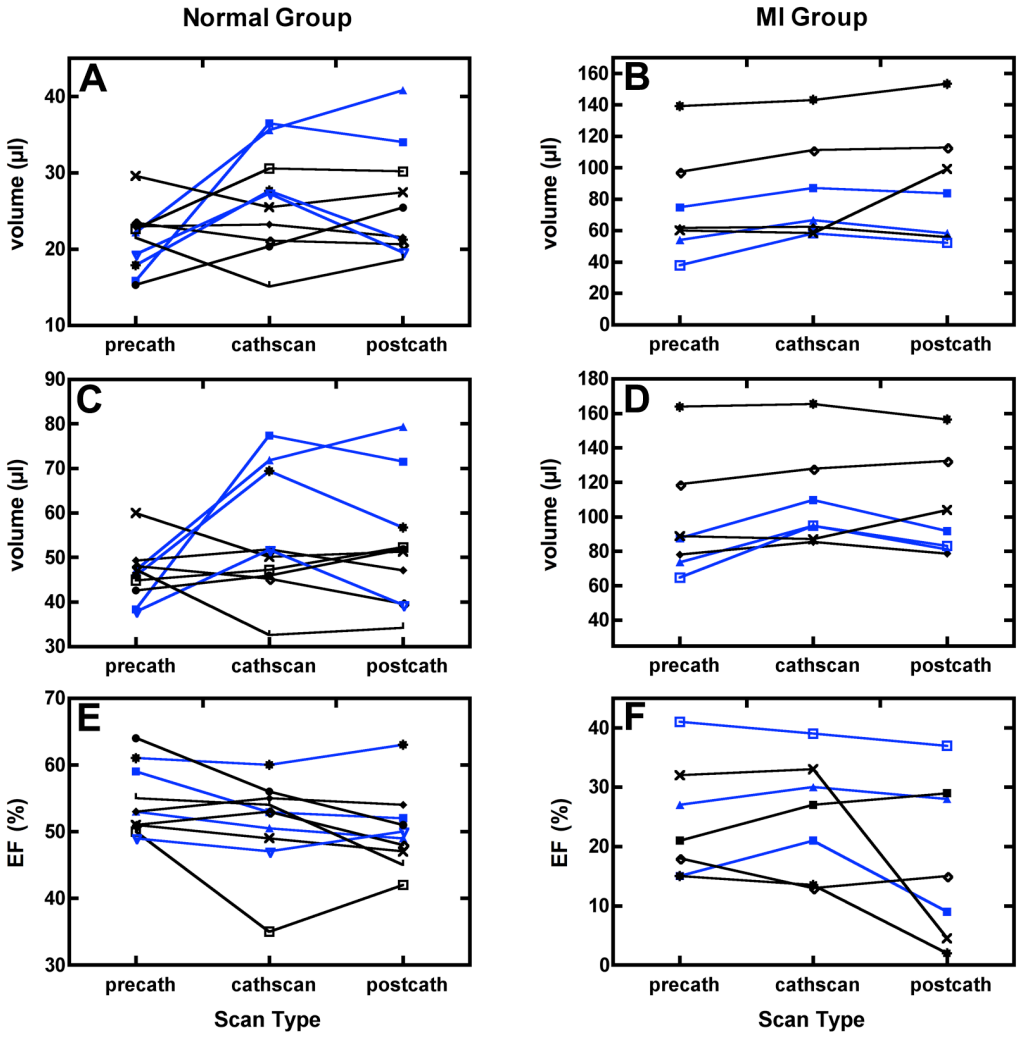

Figure 5.4: Line plots for individual mice within the Normal group and MI group. Systolic volumes (A, B), diastolic volumes (C, D), and ejection fraction (E, F) are presented. The mice with noticeable increases in LV volume are marked with blue lines.

precath image and the cathscan image, and remained increased even following catheter removal (postcath image). These changes are illustrated visually in a normal mouse and an MI mouse in Fig. 5.5 and 5.6, respectively. Volume increases did not correspond to changes in EF, however.

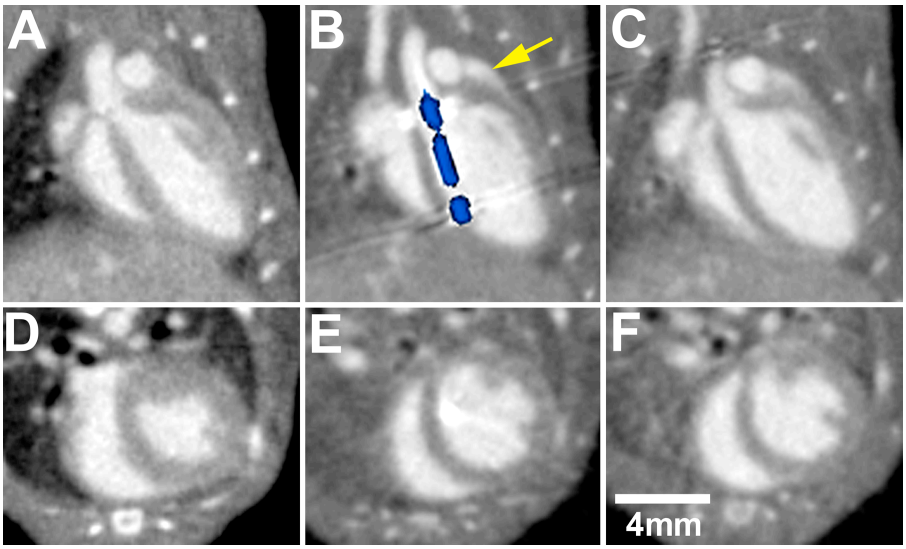

Figure 5.5: Coronal (A, B, C) and axial (D, E, F) slices (0.154 mm thick) from a 3D image of a normal mouse heart in diastole, before (A, D), during (B, E) and following catheterization (C, F). A 3D isosurface of the catheter was overlaid on the image, shown in blue. Note the large volume increase between the first (A, D) and second (B, E) scans. The yellow arrow points to the left atrium, enlarged following catheter insertion. The catheter is highly attenuating, with the electrodes causing streaking artefacts in several slices.

The averaged values for the physiological parameters measured, and the corresponding p values, are listed for the Normal group and the MI group in Tables 5.2 and 5.3, respectively. Differences between the precath and cathscan volumes were significant for the EDV of the MI group and approached significance for ESV for both Healthy and MI groups. EF differences between the three scan times were not

significantly different, except for the Normal group, which showed a decrease in EF during the postcath scan compared to the precath scan.

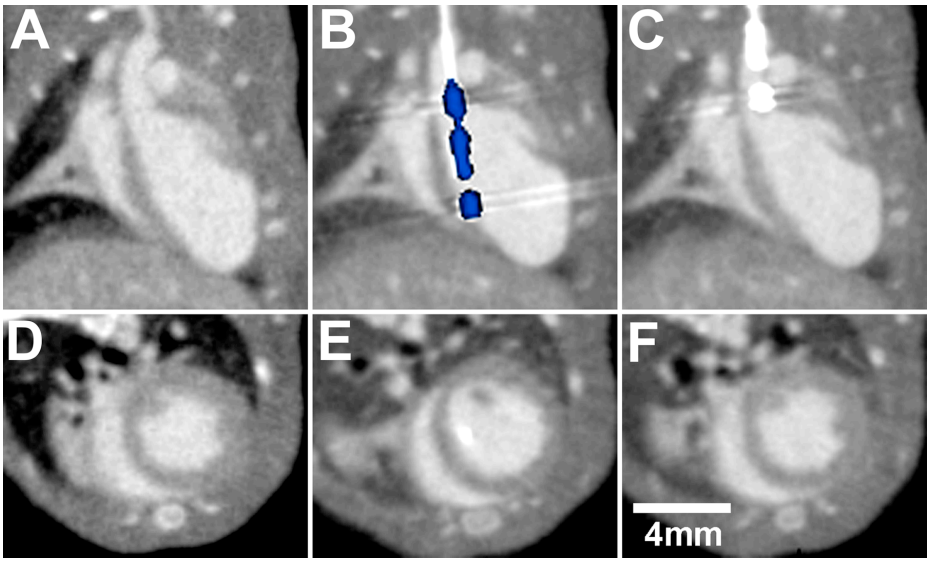

Figure 5.6: Coronal (A, B, C) and axial (D, E, F) images of an MI mouse heart in diastole, scanned before (A, D), during (B, E) and following catheterization (C, F). A 3D isosurface of the catheter was overlaid on the image, shown in blue. The infarct can be identified by the thinning wall in the apex of the heart. Note the volume increase between the first and second scans.

It is important to note that Figs 5.5B and 5.6B represent first 3D visualization of a conductance catheter within a normal and infarcted mouse heart, respectively. The placement of the catheter, highlighted as a 3D isosurface overlaid on the micro-CT images and shown in blue, is clearly seen: in both cases the catheter rests along the ventricular septum rather than in the optimal central position along the long axis. The positioning of the catheter along the septum was seen in all mice studied, with small differences corresponding to variations of cardiac anatomy and position within the thoracic cavity related to biological variability.

Table 5.2. Comparison of physiological parameters in Normal mice before, during, and following catheterization, measured using micro-CT

	Scan Type			P-value
	Precath	*Cathscan*	*Postcath*	
Normal Group (10)				
ESV (μl)	21.1 ± 4.2	26.3 ± 6.7	26.0 ± 7.2	0.066
EDV (μl)	46.1 ± 6.2	54.3 ± 14.1	52.3 ± 14.2	0.187
SV (μl)	25.1 ± 3.4	28.1 ± 8.9	26.4 ± 8.1	0.461
EF (%)	54.6 ± 5.0	51.2 ± 6.8	50.1 ± 5.7	0.026*
CO (ml/min)	11.7 ± 2.0	13.2 ± 3.8	12.3 ± 3.9	0.407
HR (bpm)	467.4 ± 56.1	475.5 ± 38.7	464.2 ± 29.1	0.743

Values are means ± SD; numbers in brackets represent no. of animals. ESV, end-systolic volume; EDV, end-diastolic volume; SV, stroke volume; EF, ejection fraction; CO, cardiac output; HR, heart rate.
*significance of precath vs. postcath

Table 5.3. Comparison of physiological parameters in MI mice before, during, and following catheterization, measured using micro-CT

	Scan Type			P-value
	Precath	*Cathscan*	*Postcath*	
MI Group (7)				
ESV (μl)	75.0 ± 33.8	83.8 ± 32.5	87.9 ± 37.1	0.072
EDV (μl)	96.5 ± 34.3	109.3 ± 28.9	103.8 ± 29.8	0.031†
SV (μl)	21.5 ± 5.7	25.4 ± 6.3	16.0 ± 10.7	0.072
EF (%)	24.1 ± 9.7	25.2 ± 9.8	17.8 ± 13.6	0.119
CO (μl/min)	10.8 ± 2.5	11.2 ± 2.7	6.9 ± 4.9	0.040‡
HR (bpm)	507.1 ± 32.0	441.9 ± 39.4	403.57 ± 65.1	0.012*

Values are means ± SD; numbers in brackets represent no. of animals. MI, myocardial infarction; ESV, end-systolic volume; EDV, end-diastolic volume; SV, stroke volume; EF, ejection fraction; CO, cardiac output; HR, heart rate.
*significance of precath vs. postcath
†significance of precath vs. cathscan
‡significance of cathscan vs. postcath

5.4 Discussion

The present study represents the first time that CC-derived LV volume measurements have been compared to volume measurements acquired simultaneously using a 3D imaging technique – retrospectively gated micro-CT – in both normal and MI

mice. The use of micro-CT provided two important advantages over previous studies comparing catheter measurements to imaging-derived measurements: 1) a single 50-second scan provided 3D images of both end-systole and end-diastole, and 2) calculation of the ventricular volumes could be made without making geometrical assumptions. The rapid scan time ensured that all CT and CC volume measurements could be made simultaneously, over a very short time period – ensuring that variations in cardiac function over time did not affect the comparison of the measurement techniques; such variations are likely to occur during prolonged periods under anesthesia, especially when studying mouse models of heart failure. Since the 3D CT images were acquired with isotropic resolution (*i.e.* equal resolution in all three dimensions) no geometric assumptions were required – the volumes were measured directly from the 3D image, without the need to calculate ellipse approximations as required with 2D echo, or to approximate apex volume, and account for large slice thicknesses or in-flow effects, as is often required with MRI. The 3D images also enable clear visualization of the entire catheter and its position within the LV: Figs. 5.5B and 5.6B represent the first time the catheter has been visualized in 3D within the ventricle of a normal mouse and MI mouse, respectively.

Overall, we demonstrated that CC volumes were significantly lower than CT volumes. The biases of the ESV and EDV were similar to those reported in a previous study where the imaging and CC methods were performed simultaneously,[14] although the ESV bias in that study was lower (-7 μL vs. -18.4 μL). The difference in measured bias at end systole can be partly explained by foreshortening of the LV long axis in the echocardiographic image, resulting in a lower echo-derived LV volume and therefore a lower bias. At end diastole the effects of foreshortening would be reduced (due to the larger overall volume of the LV), explaining the equivalent bias (-29.1 μL vs. -28.9 μL) measured by the echocardiographic and CT techniques.

The biases in the MI group were larger than in the Normal group, demonstrating that the measurement differences increased with larger volumes (Fig. 5.2 vs. Fig. 5.1), supporting the trends reported previously.[13] Correct positioning of the catheter within the LV is critical for correct volume measurements,[14] and yet visualization of the catheter *in vivo* (Fig. 5.5B and 5.6B) demonstrated that it is often placed off-center and running

along the septum. In this study, the catheter was maneuvered into position in the typical fashion, by relying on PV loop feedback to indicate correct positioning, with no additional imaging feedback. The stiffness of the catheter tip, coupled with the off-center position of the aortic valve, is likely responsible for the inability to position the tip centrally within the LV. Accurate volume measurements also require that the distance between the sensor electrodes be closely matched to the length of the LV, which was not the case when the Millar catheter was used in the MI group, accounting for the increased negative bias in the measured volumes. Catheters with varying distances between the sensor electrodes could be manufactured for use with dilated hearts, in an effort to reduce this negative bias. Additionally, by relying on PV loop feedback to position the catheter, there is the potential to position the catheter is the relatively well-contracting basal area, further accentuating the volume underestimation of MI hearts. Ultimately, accurate absolute volumes measured by conductance catheter in individual animals can only be obtained after calibration with an independent imaging method; however, within-group comparisons may still be valuable if a highly reproducible catheter positioning technique is employed.

Correlation between CT and CC volumes was moderate in the Normal group, and low in the MI group (Fig. 5.3). Previous studies comparing CC measurements to MRI-acquired volumes[12,13] reported higher correlations between the two techniques, even though the measurements were not performed simultaneously; in both cases higher correlation was achieved because the CC reported values were higher than those measured in our study. As the parallel conductance and volume calibration techniques used were similar between this study and the MRI studies, we expect that the lower reported CC values are likely due to catheter positioning. Nieslen *et al.*[12] inserted the catheter through the apex of the ventricle, which, although necessitating a thoracotomy, facilitated the positioning of the catheter along the central axis of the ventricle. Winter *et al.*,[13] on the other hand, used a different mouse strain (NOD/scid). In our experience, – performing whole-body mouse scans – the hearts of different mouse strains tend to be positioned differently within the thorax and positioning of a conductance catheter centrally within the LV may be facilitated by the heart shape and alignment with the carotid artery and aorta. Ultimately, the accuracy of catheter volumes is highly

dependent on the position within the LV, and this must be taken into account in hemodynamic studies.

The pressure-volume conductance catheter methodology has numerous advantages for continuous real-time volume measurements coupled with simultaneous pressure measurements. Ideally, this enables the evaluation of PV loops during loading interventions which results in the ability to analyze LV function in terms of systolic elastance and diastolic compliance. However, inaccurate volume readings lead to inaccurate measurements of LV function.[14] Therefore, obtaining accurate volume measurements is extremely important to take full advantage of the unique features of the conductance catheter. As has been discussed in detail previously,[14] volume measurements obtained using a conductance catheter rely on a constant parallel conductance and a constant alpha factor when in fact, these variables change in a curvilinear pattern during the cardiac cycle. Although the use of constant factors does not appear to cause difficulties in larger animals, in mice the off-center placement of the catheter exaggerates the negative effects on volume measurements. Additionally, while the relationship between conductance and volume is approximately linear, absolute volume error increases quickly when correcting for the alpha factor. This results in either an overestimation or an underestimation of the final volume measurements, depending on how alpha was calculated (Baan's equation or cuvette calibration, respectively).[21] Solutions have been proposed that continuously track the changes in parallel conductance during the cardiac cycle,[22] as well as using a dynamic correction for alpha,[23] giving a volume measurement that is less dependent on catheter positioning in the LV. While this earlier work has shown excellent agreement between catheter-measurements of volume made using Wei's technique in comparison to 2D echocardiographic measurements,[14] further verification – similar to the micro-CT experiments described in this study, which are not operator dependent – would be beneficial in ultimately verifying this newly available technology.

The rapid retrospectively gated micro-CT technique also enabled the evaluation of the effect of catheterization on the mouse heart. Earlier studies (e.g. Porterfield *et al.*) have presented results suggesting that LV enlargement may be occurring upon the insertion of the catheter (30-40% of the mice in Fig. 4[14] have noticeably larger LV

volumes). While the averaged group results (presented in Table 5.2) show significant increase only in EDV in the MI group, trends towards significant differences are seen in ESV for both normal and MI mice. More importantly, the results for individual mice, reporting LV sizes prior to and during CC insertion (Fig. 5.4), demonstrate dramatic increases in LV size (diastolic and systolic) in several of the mice in each of the two groups; in some cases LV volumes more than double following CC insertion. In these mice the increase in volume did not reverse with withdrawal of the catheter. Since a drop in EF was not associated with this myocardial dilation (Fig. 5.4), volume overload – rather than an ischemic event – is presented as a possible explanation for the LV enlargement. In some images (e.g. Fig. 5.5) left atrial enlargement was observed together with the LV enlargement, suggesting that the overload may be due to mitral insufficiency. Given the large size (0.46 mm) and stiffness of the catheter it is highly probable that catheterization through the aortic valve may occasionally damage the papillary muscle or chordae tendinae on the septal side, preventing complete mitral valve closure. While the administration of incremental volumes of contrast agent, or the injection of saline, may also be considered as possible causes for the increase in LV volume, the fact that we did not observe a transitory increase in LV end-diastolic pressure (that would be expected to accompany LV dilation) suggests that the addition of contrast agent or saline did not contribute to the LV dilation observed. Additionally, evaluation of the RVU values before and after injection of the two solutions demonstrated an insignificant change in the raw volume measurements recorded by the catheter, which further suggests it is unlikely the injected solutions caused the hypertrophy witnessed. For example, in the mouse presenting the most dramatic LV enlargement, the mean RVU before the injections was 18.6, and following the injections was 19.9.

Anesthetic administration can also have an effect on the cardiovascular system; although induction was performed at the onset of the experiment as was not altered throughout, and the LV volume increased upon catheter insertion, a cumulative influence of anesthesia exposure cannot be excluded using the experimental design outlined in this study. However, the influence of the isoflurane would be expected to be that of myocardial depression,[24] and the findings observed were that of a preservation of

contractile function. Therefore, it is unlikely that the anesthetic was a contributory factor in the LV dilation.

Our results (Tables 5.2 and 5.3) also report significant differences in CO and HR of the MI group, and in EF in the Healthy group, between the precath, cathscan, and postcath time points. These differences are attributed to accelerated heart failure during the postcath scan, a result of catheter removal from the LV, and not an indication of the catheter's effect during hemodynamic data collection.

Since a number of earlier studies have reported on the differences in volume measurement between image-derived and CC measurements, the most significant result presented in this study is the previously unacknowledged enlargement of the LV that occurs in a large fraction of mice upon the insertion of a stiff conductance catheter. While in this particular study the group average results did not reach statistical significance, the possibility that a large fraction of catheterized hearts may become dilated suggests that further evaluation of the effects of catheters on the myocardium is warranted. Variability of mouse anatomy and surgical technique may contribute dramatically to the possibility that LV enlargement will occur and may ultimately affect important preclinical results. The exact mechanism leading to LV dilation needs to be determined, perhaps using Doppler ultrasound to confirm the possible presence of mitral regurgitation. Additional information regarding the nature of the catheter's effect on the mouse heart will aid in further optimization of the technique, leading to a reliable method of ascertaining cardiac function in mice.

5.4.1 Limitations

Volume measurements acquired with a conductance catheter depend on blood conductivity, and any solution injected that alters that conductivity and is not accounted for may result in an inaccurate volume measurement. Two solutions – contrast agent and hypertonic saline – were injected during this study resulting in a potential to cause inaccurate readings. The hypertonic saline has a higher conductivity than blood plasma, and if it was administered just prior to blood collection, it may cause a problem. However, in this study the saline was injected approximately 10 minutes prior to

measurement acquisition: we waited until the volume signal had returned to baseline before proceeding with the experiment; therefore it is highly unlikely the saline injection caused the volume underestimations. The contrast agent was specifically designed to remain in the bloodstream for an extended period of time, therefore having the potential to alter blood conductivity. However, following injection, the volume measurements acquired were not significantly different from those measured before the injection, indicating that the conductance had not significantly changed. In addition, the volume measurements we report were in the same range as a number of other studies[11, 12, 14, 25, 26] that did not use a contrast agent. Therefore it is highly unlikely the contrast agent contributed to the volume underestimation we witnessed.

The catheter was left in the heart during two scans, but we believe this had no impact on cardiac function, as catheters are routinely left in the ventricle during IV occlusions, which can last 15-30 minutes. Load-independent PV relationships were not acquired, resulting in an absence of information regarding myocardial contractility. However, the large volume underestimations recorded would have made any PV relationships unreliable.[14]

5.4.2 Conclusion

Conductance catheters, although invasive, offer the potential to measure cardiac dysfunction in mice in a way not possible with imaging methodologies. However, the underestimated volumes measured, at times quite dramatic, have an impact on the sensitivity and accuracy of the data collected. The measured volume is highly reliant on catheter position, which in turn is affected by the method of insertion, and the mouse model employed in the study. Catheterization led to LV enlargement in a large fraction of mice undergoing CC evaluation which, although not significant at the 0.05 level, was potentially due to the catheter insertion combined with the mouse strain used. Such LV enlargement may affect many catheter-based studies that are performed "blindly" – *i.e.* with no knowledge of the catheter position during measurement – and further studies are required to confirm the occurrence of LV enlargement.

References

1. Baan J, van der Velde ET, de Bruin HG, et al. Continuous measurement of left ventricular volume in animals and humans by conductance catheter. *Circulation* 70: 812-823, 1984.

2. Kass DA, Yamazaki T, Burkhoff D, et al. Determination of left ventricular end-systolic pressure-volume relationships by the conductance (volume) catheter technique. *Circulation* 73: 586-595, 1986.

3. Sagawa K, Maughan WL, Suga H, et al. *Cardiac Contraction and the Pressure-Volume Relationship*. New York: Oxford University Press, 1988.

4. Kass DA, Midei M, Graves W, et al. Use of a conductance (volume) catheter and transient inferior vena caval occlusion for rapid determination of pressure-volume relationships in man. *Cathet Cardiovasc Diagn* 15: 192-202, 1988.

5. Georgakopoulos D, Mitzner WA, Chen CH, et al. In vivo murine left ventricular pressure-volume relations by miniaturized conductance micromanometry. *Am J Physiol* 274: H1416-1422, 1998.

6. Bell JR, Kennington E, Fuller W, et al. Characterization of the phospholemman knockout mouse heart: depressed left ventricular function with increased Na-K-ATPase activity. *Am J Physiol Heart Circ Physiol* 294: H613-621, 2008.

7. Shioura KM, Geenen DL, and Goldspink PH. Assessment of cardiac function with the pressure-volume conductance system following myocardial infarction in mice. *Am J Physiol Heart Circ Physiol* 293: H2870-2877, 2007.

8. Clark JE, Flavell RA, Faircloth ME, et al. Post-infarction remodeling is independent of mitogen-activated protein kinase kinase 3 (MKK3). *Cardiovasc Res* 74: 466-470, 2007.

9. Feldman MD, Erikson JM, Mao Y, et al. Validation of a mouse conductance system to determine LV volume: comparison to echocardiography and crystals. *Am J Physiol Heart Circ Physiol* 279: H1698-1707, 2000.

10. Nemoto S, DeFreitas G, Mann DL, et al. Effects of changes in left ventricular contractility on indexes of contractility in mice. *Am J Physiol Heart Circ Physiol* 283: H2504-2510, 2002.

11. Jacoby C, Molojavyi A, Flogel U, et al. Direct comparison of magnetic resonance imaging and conductance microcatheter in the evaluation of left ventricular function in mice. *Basic Res Cardiol* 101: 87-95, 2006.

12. Nielsen JM, Kristiansen SB, Ringgaard S, et al. Left ventricular volume measurement in mice by conductance catheter. Evaluation and optimization of calibration. *Am J Physiol Heart Circ Physiol* 2007.

13. Winter EM, Grauss RW, Atsma DE, et al. Left ventricular function in the post-infarct failing mouse heart by magnetic resonance imaging and conductance catheter: a comparative analysis. *Acta Physiol (Oxf)* 194: 111-122, 2008.

14. Porterfield JE, Kottam AT, Raghavan K, et al. Dynamic correction for parallel conductance, GP, and gain factor, alpha, in invasive murine left ventricular volume measurements. *J Appl Physiol* 107: 1693-1703, 2009.

15. Detombe SA, Ford NL, Xiang F, et al. Longitudinal follow-up of cardiac structure and functional changes in an infarct mouse model using retrospectively gated micro-computed tomography. *Invest Radiol* 43: 520-529, 2008.

16. Drangova M, Ford NL, Detombe SA, et al. Fast retrospectively gated quantitative four-dimensional (4D) cardiac micro computed tomography imaging of free-breathing mice. *Invest Radiol* 42: 85-94, 2007.

17. Feng Q, Lu X, Jones DL, et al. Increased inducible nitric oxide synthase expression contributes to myocardial dysfunction and higher mortality after myocardial infarction in mice. *Circulation* 104: 700-704, 2001.

18. Armitage SE, Pollmann SI, Detombe SA, et al. Least-error projection sorting to optimize retrospectively gated cardiac micro-CT of free-breathing mice. *Med Phys* 39: 1452-1461, 2012.

19. Du LY, Umoh J, Nikolov HN, et al. A quality assurance phantom for the performance evaluation of volumetric micro-CT systems. *Phys Med Biol* 52: 7087-7108, 2007.

20. Otsu N. A threshold selection method from gray-level histograms. *IEEE Trans Syst Man Cybern (USA)* SMC-9: 62-66, 1979.

21. Porterfield JE, and Pearce JA. Comparison of conductance to volume equations: the gain coefficient alpha. *Conf Proc IEEE Eng Med Biol Soc* 2009: 3043-3046, 2009.

22. Wei C, Valvano JW, Feldman MD, et al. Volume catheter parallel conductance varies between end-systole and end-diastole. *IEEE Trans Biomed Eng* 54: 1480-1489, 2007.

23. Wei CL, Valvano JW, Feldman MD, et al. Nonlinear conductance-volume relationship for murine conductance catheter measurement system. *IEEE Trans Biomed Eng* 52: 1654-1661, 2005.

24. Bovill JG. Inhalation anaesthesia: from diethyl ether to xenon. *Handb Exp Pharmacol* 121-142, 2008.

25. Ikonomidis JS, Hendrick JW, Parkhurst AM, et al. Accelerated LV remodeling after myocardial infarction in TIMP-1-deficient mice: effects of exogenous MMP inhibition. *Am J Physiol Heart Circ Physiol* 288: H149-158, 2005.

26. Pacher P, Batkai S, Osei-Hyiaman D, et al. Hemodynamic profile, responsiveness to anandamide, and baroreflex sensitivity of mice lacking fatty acid amide hydrolase. *Am J Physiol Heart Circ Physiol* 289: H533-541, 2005.

6 Summary and Future Work

6.1 Summary

Cardiac-gated micro-CT is a non-invasive imaging technique capable of producing high-resolution images of the mouse heart, in scan times of less than one minute. Cardiac structure and function can be assessed, using both qualitative and quantitative measurements, and the non-invasive nature of the technique facilitates its use in longitudinal studies.

6.1.1 Chapter 2: Longitudinal Follow-up of Cardiac Structure and Functional Changes in an Infarct Mouse Model using Retrospectively Gated Micro-computed Tomography

Chapter 2 demonstrates that retrospectively gated cardiac micro-CT can be used to precisely identify differences in left ventricular (LV) volume and heart function between myocardial infarcted (MI) and sham mice, and that these differences can be followed longitudinally in individual mice. Qualitative, structural differences were visualized between the sham and the MI mice, with the MI mice demonstrating cardiac enlargement as early as one week post-surgery; the infarct was also clearly defined as the thinning portion of the wall in the apex of the heart. These qualitative differences translated quantitatively into small changes that could be precisely measured and tracked over the four-week study. Both intra- and inter-observer variability when measuring volumes were low, indicating excellent reproducibility of measurements. Intra-subject measurements also showed good reproducibility, with variation in volumes of infarcted hearts being slightly higher than variations in sham-operated hearts; this was attributed the rounded shape of the LV in the MI mice, making identification of the LV boundary at

the base of the heart (for the purpose of drawing contours around the LV) more challenging.

Micro-CT has low soft tissue contrast, but with the addition of a contrast agent, the boundaries of the myocardial wall were clearly delineated. This enabled LV mass measurements, which showed significant differences between the sham and the MI mice; this type of measurement also provides a method for identifying the degree of cardiac hypertrophy present.

Volume and ejection fraction measurements from the micro-CT images were also compared to measurements acquired using a pressure-conductance catheter. Although the trends between the two measurement techniques were similar (*i.e.* larger volumes and lower function in MI mice), the volume measurements of the catheter were drastically lower than those of the micro-CT images. Although originally intended as a verification of the micro-CT values, the clearly inaccurate volumes of the catheter eventually led to an evaluation of the method, detailed in Chapter 5.

6.1.2 Chapter 3: Evaluation of eXIA 160 Cardiac-related Enhancement in C57BL/6 and BALB/c mice using Micro-CT

eXIA 160 is a relatively new blood-pool contrast agent; a high iodine concentration makes it possible to administer a low volume of contrast to the mice, reducing potential negative hemodynamic effects. Chapter 3 details the time-course enhancement of eXIA in both C57BL/6 and BALB/c mouse strains; overall, this agent proved to be an excellent choice for use in cardiac micro-CT studies, with similar enhancement values witnessed in both strains. A high level of enhancement (over 650 HU above the precontrast values) was measured within 5 minutes of injection; the enhancement dropped 40% within the first hour, but the values remained above 500 HU during the first 30 minutes post-injection, providing excellent contrast for a period of time sufficient to perform cardiac-gated micro-CT scans.

One of the rather unique, and unexpected, qualities of eXIA 160 was its enhancement of the myocardium, possibly a reflection of one of the ways the agent is metabolized in the mouse. Enhancement began immediately following injection, and continued to increase until peaking at four hours post-administration with a value above

270 HU. The increasing enhancement during the first hour did result in decreased contrast between the myocardium and the blood-pool, effectively shortening the period of time during which scans measuring cardiac function could be acquired. However, the myocardial enhancement also offers a number of possibilities for further study, including accurate measurement of myocardial mass independent of manual tracing, and the ability to study wall motion and wall function, not normally feasible with micro-CT. eXIA 160 can therefore act as a dual-phase cardiac contrast agent, with scans evaluating LV volume and cardiac function acquired within the first 30 minutes of injection, and later scans intended for wall motion studies acquired four hours post-injection.

6.1.3 Chapter 4: X-ray dose delivered during a longitudinal micro-CT study has no adverse effects on cardiac and pulmonary tissue in C57BL/6 mice

One of the concerns associated with using cardiac micro-CT is the x-ray dose delivered to the animal during the scan; this becomes especially relevant in longitudinal studies were the mouse is scanned multiple times. A number of studies have been performed that evaluate the effect of radiotherapy-level doses (10-20 Gy) on the mouse,[1,2] but the dose delivered and the time frame during which observation took place in these studies makes it difficult to apply the results to a micro-CT study. Chapter 4 examined the effect of the dose delivered during a cardiac micro-CT study on cardiac and pulmonary tissue in C57BL/6 mice. The mice in the Irradiated Group were scanned weekly, with each scan session comprised of three retrospectively gated scans, for a total of six weeks. The weekly entrance dose delivered to the mice was 0.84 Gy, with a total dose of 5.04 Gy delivered over the six weeks. Overall, there were no significant changes to the heart or lungs in the Irradiated Group at week six, compared to the Control Group; this was reflected both in the micro-CT scans and, more significantly, in the histological specimens of myocardial and pulmonary tissue prepared following the week six scans. There was no evidence of early inflammation occurring at a cellular level, confirming that micro-CT can be safely used in longitudinal studies without concern that the dose delivered will have adverse effects on the mouse's health.

6.1.4 Chapter 5: Rapid micro-computed tomography suggests cardiac enlargement occurs during conductance catheter measurements in mice

Conductance catheters (CC), although invasive, offer the potential to measure cardiac dysfunction in mice in a way not possible with imaging methodologies. However, in the study described in Chapter 2, CC-derived volumes were greatly underestimated compared to micro-CT derived volumes. CC volume underestimation has also been reported by several groups that compared catheter measurements to MRI-derived measurements (MRI and catheter measurements were acquired up to two days apart).[3-5] Chapter 5 details a study that makes use of the advantages of cardiac micro-CT, including the rapid scan time, and the ability to evaluate the heart both qualitatively and quantitatively from high-resolution isotropic images. The rapid scan time made it possible to scan the mouse with the catheter in place recording its pressure-volume measurements, which enabled a comparison between simultaneously acquired CT- and CC-derived volumes. The ability to scan the mouse with the catheter in place also facilitated an evaluation of the effect catheterization has on the mouse heart. This was accomplished by acquiring micro-CT scans before, during, and after catheterization.

The CC-derived volumes were found to be dramatically underestimated compared to the CT-derived volumes, confirming the results previously reported. Visualization of the catheter within the LV in the micro-CT images illustrated that the catheter is often placed off-center in the chamber; given that CC-derived volumes are highly reliant on catheter position,[6] this gives an explanation for the observed underestimation.

Catheterization of the mouse heart was found to cause LV enlargement in 40% of the mice: comparing the LV in micro-CT images acquired before catheter insertion, to the LV in images with the catheter in place, demonstrated an increase in volume that in some mice was almost doubled. Given that the ejection fraction remained the same, regardless of the severity of enlargement, it is proposed this volume increase was due to mitral regurgitation as a result of damage caused during catheter insertion. The average change in LV volume in the group of mice studied was ultimately found to be not significant at the 0.05 level; however, given that catheter placement within the LV is highly dependent on the anatomy of the mouse, which can vary between strains, the results presented may have significance to other catheter studies.

6.2 Future work

As detailed in Chapter 3, eXIA 160 has the unique property of enhancing the myocardium beyond a time when the contrast agent has been eliminated from the blood-pool, creating a reverse contrast with a bright wall and unenhanced blood. This offers a number of opportunities for evaluating the LV wall, normally challenging in micro-CT images given the low soft tissue contrast. LV mass may be more accurately measured, as the enhancement would enable automatic segmentation, rather than relying on manually traced contours. Evaluation of wall motion and wall function may also be possible; given that this would most useful in mouse models that display abnormal wall function, the first step would be to determine the extent of myocardial enhancement in such a model; for example, in a mouse model of myocardial infarction. Initial results indicate that enhancement of the infarcted area does not occur, which would limit the types of evaluation possible. However, if this agent was combined with conventional contrast agent that extravasates into the infarct, as described by Narhendorf *et al.*,[7] this may provide a solution that enables wall motion studies to be performed.

In Chapter 4, it was determined that the x-ray dose delivered during a longitudinal micro-CT study has no adverse effects on the mouse. What is unclear, however, is how the dose will affect cancer mouse models. Longitudinal evaluations of tumor growth, regression, or metastasis are necessary for evaluation new therapeutic approaches,[8, 9] and what needs to be determined is how the dose delivered during a micro-CT study will affect tumor growth. There is the potential that the radiation dose may influence the fast-growing cancer cells, confounding the investigation of treatment therapies. A study similar to the one described in Chapter 4, using a tumor model, should be carried out to investigate the possibility.

This thesis has described the use of cardiac micro-CT to quantitatively and qualitatively evaluate mouse models of heart disease in longitudinal studies. Although micro-CT excels at evaluating cardiac structure, and providing accurate volume measurements not reliant on geometric assumptions or approximations, the level of information acquired regarding function can be somewhat limited. Hemodynamic studies are not possible, which have a greater sensitivity to changes in myocardial function[10] and

are often used in physiology labs. High-frequency echocardiography, on the other hand, is an imaging method that, although providing similar resolution to micro-CT, does not visualize cardiac structure as clearly. It does, however, have the ability to measure hemodynamic function non-invasively in mice, using Doppler imaging.[11] It would therefore be beneficial to try and create a protocol for using the two imaging modalities in one study, combining the advantages of each. This has the potential of providing physiologists with a non-invasive methodology for performing the measurements they find valuable, with the added benefit of excellent structural information, as an alternative the invasive methods currently employed.

6.3 Conclusion

Cardiac-gated micro-CT is a rapid, reproducible imaging technique capable of quantifying changes in cardiac structure and function over time. This enables the longitudinal evaluation of disease progression in mouse models of cardiac disease, with the added possibility of assessing wall motion and function, due to the unique characteristics of new contrast agent. The x-ray dose delivered during the a longitudinal study is sufficiently low that no early signs of radiation damage are observed at a cellular level, indicating that micro-CT can be safely used without concern that the radiation dose will affect the outcome of the study. This imaging technique can also be used to evaluate other methods of assessing cardiac function, providing both qualitative and quantitative measurements. Overall, cardiac-gated micro-CT offers a number of advantages, and is proving to be valuable tool in cardiovascular disease research.

References

1. Jackson IL, Vujaskovic Z, and Down JD. Revisiting strain-related differences in radiation sensitivity of the mouse lung: recognizing and avoiding the confounding effects of pleural effusions. *Radiat Res* 173: 10-20, 2010.

2. Johnston CJ, Manning C, Hernady E, et al. Effect of total body irradiation on late lung effects: hidden dangers. *Int J Radiat Biol* 87: 902-913, 2011.

3. Jacoby C, Molojavyi A, Flogel U, et al. Direct comparison of magnetic resonance imaging and conductance microcatheter in the evaluation of left ventricular function in mice. *Basic Res Cardiol* 101: 87-95, 2006.

4. Nielsen JM, Kristiansen SB, Ringgaard S, et al. Left ventricular volume measurement in mice by conductance catheter. Evaluation and optimization of calibration. *Am J Physiol Heart Circ Physiol* 2007.

5. Winter EM, Grauss RW, Atsma DE, et al. Left ventricular function in the post-infarct failing mouse heart by magnetic resonance imaging and conductance catheter: a comparative analysis. *Acta Physiol (Oxf)* 194: 111-122, 2008.

6. Porterfield JE, Kottam AT, Raghavan K, et al. Dynamic correction for parallel conductance, GP, and gain factor, alpha, in invasive murine left ventricular volume measurements. *J Appl Physiol* 107: 1693-1703, 2009.

7. Nahrendorf M, Badea C, Hedlund LW, et al. High-resolution imaging of murine myocardial infarction with delayed-enhancement cine micro-CT. *Am J Physiol Heart Circ Physiol* 292: H3172-3178, 2007.

8. De Clerck NM, Meurrens K, Weiler H, et al. High-resolution X-ray microtomography for the detection of lung tumors in living mice. *Neoplasia* 6: 374-379, 2004.

9. Paulus MJ, Gleason SS, Kennel SJ, et al. High resolution X-ray computed tomography: an emerging tool for small animal cancer research. *Neoplasia* 2: 62-70, 2000.

10. Nemoto S, DeFreitas G, Mann DL, et al. Effects of changes in left ventricular contractility on indexes of contractility in mice. *Am J Physiol Heart Circ Physiol* 283: H2504-2510, 2002.

11. Liu J, and Rigel DF. Echocardiographic examination in rats and mice. *Methods Mol Biol* 573: 139-155, 2009.

Appendix A

Fast Retrospectively Gated Quantitative 4D Cardiac Micro CT Imaging of Free-breathing Mice

The content of this chapter is adapted from "Fast retrospectively gated quantitative 4D micro CT imaging of free-breathing mice", published in Investigative Radiology, vol 42 (2) February 2007, by Maria Drangova, Nancy L. Ford, Sarah A. Detombe, Andrew R. Wheatley, and David W. Holdsworth. It has been included as background for the gated micro-CT methodology used in this thesis.

Introduction

Mouse models play an important role in the study of cardiac disease and its potential treatment, and would benefit from the ability to quantify myocardial function and structure during longitudinal studies. The challenges of generating images of the beating mouse heart relate to the small size of the heart (the left ventricle of an adult mouse is less than 4 mm in diameter), the rapid respiratory rate, and the rapid cardiac cycle (up to 600 beats per minute).

Currently, magnetic resonance imaging (MRI) is available for the study of myocardial function and structure but the studies are time-consuming, requiring up to an hour to acquire 6-8 images of 1-mm thick slices through the heart, with in-plane resolution ranging between 50 and 120 μm;[1-4] more time-efficient MRI techniques to image multiple mice simultaneously are being developed.[5] Recently Dawson *et al.*[4] introduced a 3D-echocardiographic technique capable of acquiring 10-18 gated short-axis views of mouse myocardium, spaced 500 μm apart, in less than 5 minutes. However,

neither the MRI nor echocardiographic techniques offer isotropic resolution, with slice-thickness equal to the pixel dimension in plane. In a recent publication, Badea *et al.* described a micro computed tomography (micro-CT) technique for generating four-dimensional (4D) images of the murine heart with 90-µm isotropic voxel size, using a prototype micro-CT scanner.[6, 7] This micro-CT technique combines the benefits of dynamic acquisition with isotropic, 3D, high-resolution images, thereby providing 4D images of the heart that have not been possible with either echocardiography or MRI. The technique requires the animal to be mechanically ventilated, positioned vertically, and rotated throughout the scan, while triggered projection images are acquired. Scan times for this prospectively triggered acquisition are on the order of 10 minutes, depending on the heart rate and ventilation-cycle length.

The most recent technical advances in micro-CT have focused on the implementation of area detectors mounted on a clinical slip-ring gantry, making the continual acquisition of projection data possible and thereby enabling the rapid acquisition of volumetric scans.[8, 9] Such scanners have been used for rapid (8 second) anatomical imaging[10] but the lack of respiratory and cardiac gating for such systems limits their application for cardiac imaging.

In this study, we present a retrospectively gated micro-CT imaging technique that enables the acquisition of 4D cardiac images, (*i.e.* 3 spatial dimensions plus resolution in the temporal dimension) in less than one minute in free-breathing mice. We use a state-of-the-art volumetric CT scanner, which utilizes a flat-panel detector mounted on a slip-ring gantry. Combining the capabilities of this device with physiological monitoring and retrospective sorting of the projection data, we have been able to demonstrate 4D cardiac images in mice with isotropic 150-µm voxels and temporal resolution of 12 ms.. The purpose of this paper is to describe the retrospectively gated micro-CT technique and demonstrate its effectiveness in measuring cardiac functional parameters, such as left-ventricular ejection fraction (EF), stroke volume (SV) and cardiac output (CO), in a cohort of healthy mice.

Methods

Animal preparation

All animal studies were approved by the Animal Use Subcommittee of the University Council on Animal Care at our institution. Five female C57BL6 mice, weighing approximately 20 g each, were anesthetized using approximately 1.5 % Isoflurane in O_2. A micro catheter was placed in a lateral tail vein for the administration of contrast agent. Pediatric ECG electrodes (2269T, 3M Health Care, St. Paul, MN), with radiolucent carbon-fiber leads, were affixed to the paws to monitor the ECG waveform. The mice were positioned prone on a custom-made bed that was connected to a pressure transducer, which was designed to measure the motion of the diaphragm and thereby provide a respiration-gating signal. The respiration-monitoring bed is described in detail by Ford *et al.*[11] Both the ECG and respiratory signals were measured and recorded using a physiological monitoring and triggering system (BioVet, Spin Systems, South Brisbane, Australia). The mice were not intubated and were allowed to breathe freely throughout the experiment.

Approximately 5 minutes prior to scanning, a blood-pool contrast agent, Fenestra VC [50 mg I/ml] (Alerion Biomedical, Inc., San Diego, CA) was administered intravenously at a dose of 0.02 ml/g body weight, as recommended by the manufacturer. This iodinated contrast agent has been shown to provide significant enhancement of the mouse vasculature (as high as 700 HU at the administered dose)[7] for up to 2 hours post injection.[10, 12, 13]

To evaluate the reproducibility of the functional parameters obtained using this technique, each mouse was scanned three times, as described below, with repositioning between scans.

Image acquisition

Images were acquired using a volumetric cone-beam micro-CT scanner (Locus Ultra, General Electric Healthcare, London, ON, Canada). The scanner uses a 1024×1024-element flat-panel detector and a clinical x-ray tube mounted on a slip-ring

gantry to enable continuous rotation about the object. Mice were positioned at the centre of the scanner, to reduce the effect of radial blur caused by the rotation of the gantry during image acquisition. For the volumetric CT application described here, only the central 1024 × 360 detector elements are read out. Projection images were acquired at 80 kVp and 50 mA, with 0.15-mm added copper filtration, over a field of view of 14 cm (transaxial) x 5.4 cm (longitudinal). For retrospectively gated imaging, projection images were acquired over 10 complete rotations (3600°) at a rate of 5 seconds per rotation, for a total scan time of 50 seconds. For each rotation, 416 projection images spaced at 0.86° intervals were acquired, at a frame rate of 12 ms/projection. Bright- and dark-field projection images were also acquired, prior to each scan, to correct the data for detector non-uniformities. To estimate the entrance dose delivered during the scans, the entrance exposure rate at 80 kVp was measured using a 15-cm^3 ion chamber (model 96035, Keithley, Cleveland, OH) placed near the isocentre of the scanner and an electrometer (model 617, Keithley, Cleveland, OH).

In the continuous-rotation acquisition mode of the Locus Ultra, the first projection image is acquired a known-delay after the x rays are turned on. Therefore to synchronize the physiological signals with the image acquisition, an x-ray monitor, constructed by mounting a piece of x-ray fluorescent screen on a photo-diode, was placed near the edge of the x-ray field and positioned so that it detected scattered x-ray photons. The signal from the x-ray monitor was recorded simultaneously with the respiratory and ECG waveforms using the BioVet system at a rate of 1 kHz, thereby enabling the synchronization of the physiological waveforms and the acquired projection images.

Retrospective Gating and Reconstruction

Analysis of the ECG, respiratory, and x-ray monitor signals was performed using Matlab (The MathWorks, Natick, MA, USA). Figure 1 represents a sample set of ECG and respiratory waveforms recorded during acquisition, along with the main processing steps described below First, the respiratory waveform, resp(t), was analyzed to determine the periods of end expiration: after smoothing the waveform by a 30-ms boxcar window,

the first derivative dresp(t)/dt was calculated and the peaks of the respiratory waveform were determined from the zero-crossings of dresp(t)/dt (Fig. 1b).

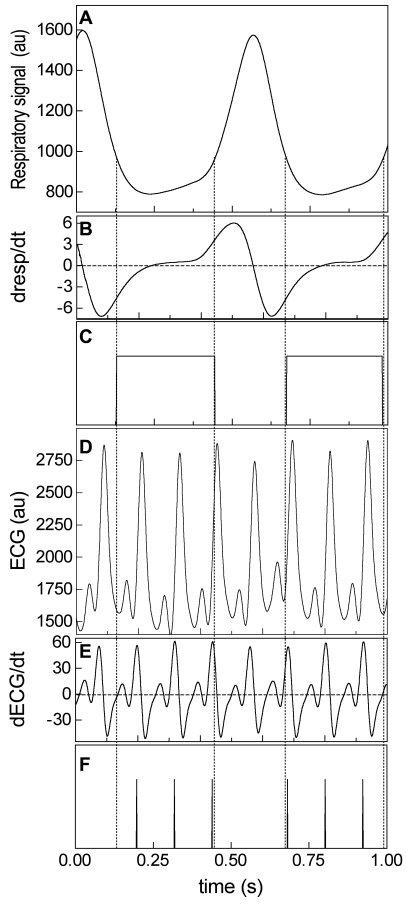

Figure 1: Sample subset of ECG and respiratory waveforms recorded during image acquisition. (a) Respiratory signal, (b) derivative of respiratory signal used to identify the peaks of resp (t), (c) the end-expiration period identified in each cycle, (d) measured ECG signal, (e) derivative of the ECG signal, and (f) the time points identified as the start of each cardiac cycle, based on the inflection point just prior to each R-wave. The start of the cardiac cycle is depicted only for cycles occurring during end expiration. Note that the waveforms shown in (a) and (d) have been smoothed by a 30 ms and 10 ms boxcar window, respectively, as described in the text.

The maximum (max) and minimum (min) respiratory excursion for each breath were then calculated and expiration was considered to be the time period over which resp(t) < (min + F (max – min)), where F is a factor selected to define the expiration period. For the studies described here, F was set to 0.2. The ECG waveform was analyzed in a similar fashion, by smoothing the ECG waveform (10 ms window), calculating the derivative of the waveform (Fig. 1d) and considering the inflection point just prior to the peak (R-wave) to be the start of the cardiac cycle.

The projection data were then sorted and only unique projections falling within a predetermined cardiac window were used to reconstruct a 3D image, corresponding to a specific time point of the cardiac cycle. Three-dimensional images were reconstructed for each frame in the cardiac cycle using the reconstruction engine of the Locus Ultra. The cardiac window width (W) was chosen to be 12 ms, based on the acquisition time for each projection; for this study, 10-14 frames were reconstructed per cardiac cycle, depending on the heart rate. Note that W does not have to equal the acquisition window width and can be selected retrospectively. However, selecting a wider W will lead to increased temporal blurring. For comparison purposes, an ungated scan was also reconstructed from the first 360° of projection images. Although an ungated scan can be reconstructed from the entire 3600° data set, we believe that, in terms of SNR, comparison of an ungated image reconstructed from one rotation (1/10 of all acquired data) to the gated images is more appropriate. All images were reconstructed on a 256 × 256 × 360 matrix, providing an isotropic voxel spacing of 150 μm × 150 μm × 150 μm.

Image Analysis

Images were analyzed using MicroView analysis software (MicroView v2.2, General Electric Healthcare, London, ON, Canada). A single operator reoriented the 3D images to align with the long/short axis of the left ventricle (LV). For LV volume calculation, an automated region-growing algorithm was used to isolate the chamber of the left ventricle and calculate volume. Otsu's automatic thresholding algorithm[14] was used to determine the threshold CT number separating the LV chamber from myocardium; for experiments reported on here, the average threshold value was 306 ± 73 HU. Automatic region growing was terminated at the aortic valve, and in regions near the base of the heart, where "bleeding" of the region into the neighbouring atria occurred, by manually drawing a region to limit the automatic region-growing operation. The same operator who re-oriented the images drew the regions used to constrain the automatic region-growing algorithm. To define the time points corresponding to systole and diastole, the LV volume was calculated throughout the cardiac cycle to determine which frames had the minimum and maximum LV volume, respectively. Left-ventricular

systolic volume (LVSV), left-ventricular diastolic volume (LVDV), stroke volume (SV = LVDV – LVSV), ejection fraction (EF = SV/LVDV) and cardiac output (CO = SV * heart rate) were calculated for each mouse.

Statistical Analysis

For all reported parameters the mean and standard deviation were calculated based on a single scan for each mouse, thereby demonstrating the inter-subject variability of the parameters in this cohort of mice. This inter-subject standard deviation was used to determine the power of future studies and the required sample sizes. To calculate the technique's reproducibility (intra-subject), the average standard deviation of the results from the three repeat scans, for each mouse, was also calculated for the functional parameters. Lastly, an unpaired t-test was performed to compare our results for the functional parameters to those published by Badea *et al.*[7]

Results

All reported results, except for the reproducibility results, are for one scan per mouse. The average heart rate in this study was 405 ± 34 beats per minute. The average respiratory rate of all mice scanned was 51 ± 46 breaths per minute; the average of four of the mice was 30± 4.7 and the fifth mouse had a respiratory rate of 131 breaths per minute, therefore accounting for the large standard deviation. For each scan, approximately 80 percent (ranging between 65% and 85%) of the 50-s acquisition occurred during expiration. Figure 2 demonstrates, for one time point in the cardiac cycle, how projection-data space was filled by adding more projection views following each rotation of the gantry. On average, 326±35 projections were available to reconstruct an image at each time point in the cardiac cycle (the maximum/minimum number of views available were 375/257); the missing views resulted in streaking artifacts (as discussed below). The entrance dose delivered for each 50-second scan was calculated to be 28 cGy, based on the entrance exposure of 0.013 $RmA^{-1}s^{-1}$ that was measured at the isocentre.

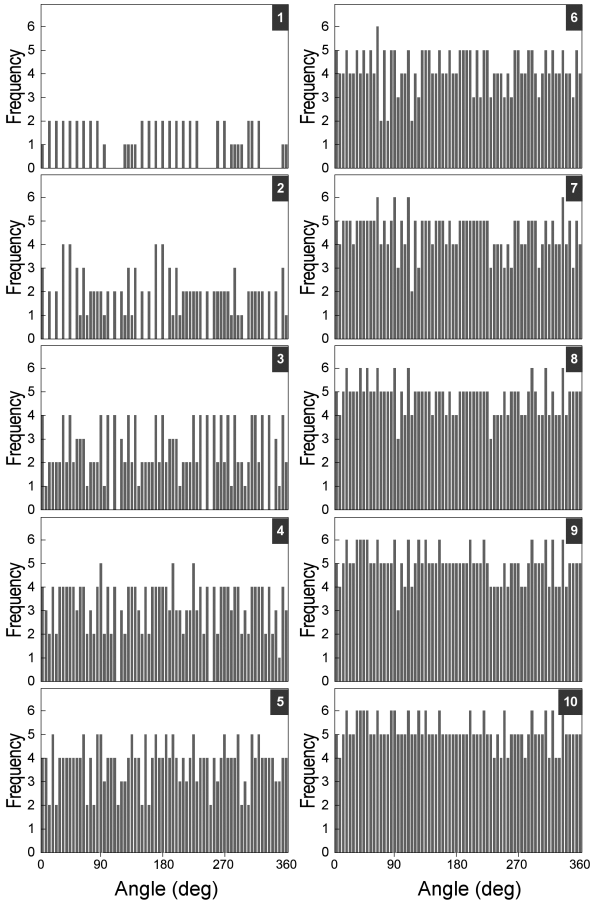

Figure 2: Histograms representing the filling of projection data space with each additional rotation of the scanner: the angular positions of each valid projections were binned into 5° histogram bins. Because the angular interval between projections was 0.86°, the maximum number of projection images per bin (frequency) was 6. The number of rotations contributing projection images to the reconstruction is identified in the top right hand corner of each graph. The histograms presented are for a single time point during the cardiac cycle of one mouse. Note that the bin width was selected for illustration purposes only and did not affect the selection of valid projection views.

Figure 3 demonstrates example systolic and diastolic images acquired for one of the mice studied. The images presented have been reformatted to depict the heart in a long-axis and short-axis view; because the acquired images have isotropic voxels, the same image quality is possible for all reformatted planes. A series of short- and long-axis images are presented in Fig. 4, corresponding to seven time points in the cardiac cycle 4(b-h) for one of the mice imaged, along with a pair of ungated images (Fig. 4(a)). Note the excessive blurring in the myocardium, as well as near the lung/liver interface, in the ungated images compared to the gated ones.

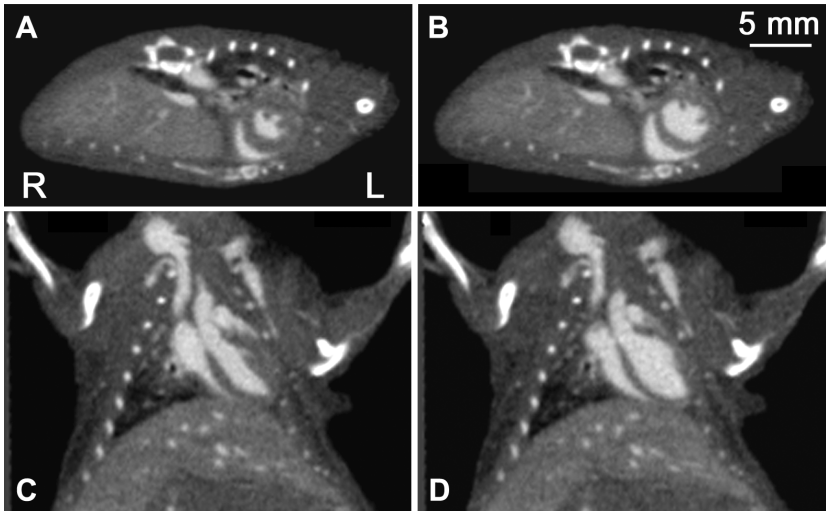

Figure 3: Reformatted mid-ventricular short (a,b) and long (c,d) axis images of a mouse heart at systole (a,c) and diastole (b,d). Note that all chambers of the heart, the aorta and structures such as the papillary muscles are easily identifiable in the images. These images represent 150-μm sections taken from the 3D volumes reconstructed at each time point. The voxel spacing in-plane is also 150 μm.

The collage in Fig. 5 is a series of contiguous 150-µm thick slices parallel to the long-axis, compiled to demonstrate the 3D nature of the reconstructed images and the detail with which cardiac structure can be identified in the 3D, high-resolution, gated images. Relevant anatomical features that are easily distinguished are identified in the figure.

The average signal-difference observed between the myocardium and the blood-pool in the gated images was 360 ± 27 HU and the average noise measured in the myocardium was 36 ± 4.6 HU, resulting in a signal-difference-to-noise ratio of 10.4 ± 1.6. The noise in the gated images increased by a factor of 1.4 when compared to the un-gated images due to the artifacts generated by the missing views. Noise was measured in an air region defined just above the mouse heart; it should be noted that the artifact level varies depending on the object, and therefore on the position of the region of interest, and was most pronounced in the air regions outside the mouse. For the mice studied, the

measured and calculated cardiac functional parameters are listed in Table 1; the table presents both the inter-subject variability as well as the intra-subject variability based on repeat scans. Note that for all functional parameters, the standard deviation derived from a single scan of multiple mice (reflecting the inter-subject variability) is the same or larger than the standard deviation for repeat scans on the same animals (reflecting underlying measurement reproducibility).

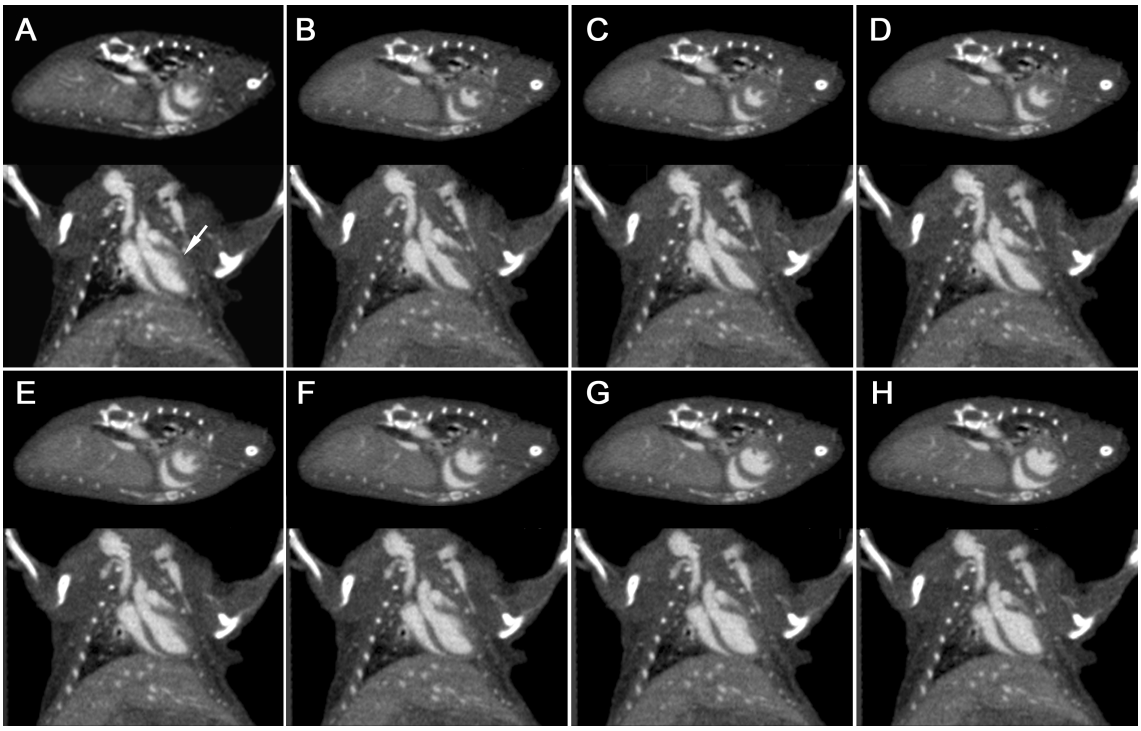

Figure 4: A series of long and short axis images are presented to demonstrate the dynamic nature of the acquisition. The images in (a) were reformatted from an ungated image obtained from the 1st of 10 rotations; Images (b) through (h) represent the heart at 12-ms intervals starting with systole in panel (b) and covering the first 90 ms of the cardiac cycle. Note the poor delineation of the myocardium in the ungated images (a), especially in the region of the left free wall (arrow), when compared to the time-resolved images.

Based on the measured inter-subject standard deviations, a sample-size calculation was performed to estimate the sensitivity to differences between study groups. With the measured inter-subject variability of 4.6%, EF differences of 9.3% between two groups of 5 animals can be determined at a significance level of 0.05 with a power of 80%; this minimum detectable difference reduces to 6% when the number of animals per

group is increased to 10. For longitudinal studies, where paired comparisons can be performed, the difference in EF that can be detected – with a sample size of 5 animals in a group and expected correlation of 0.8 between measurements (say, at weekly intervals) – reduces to 4%.

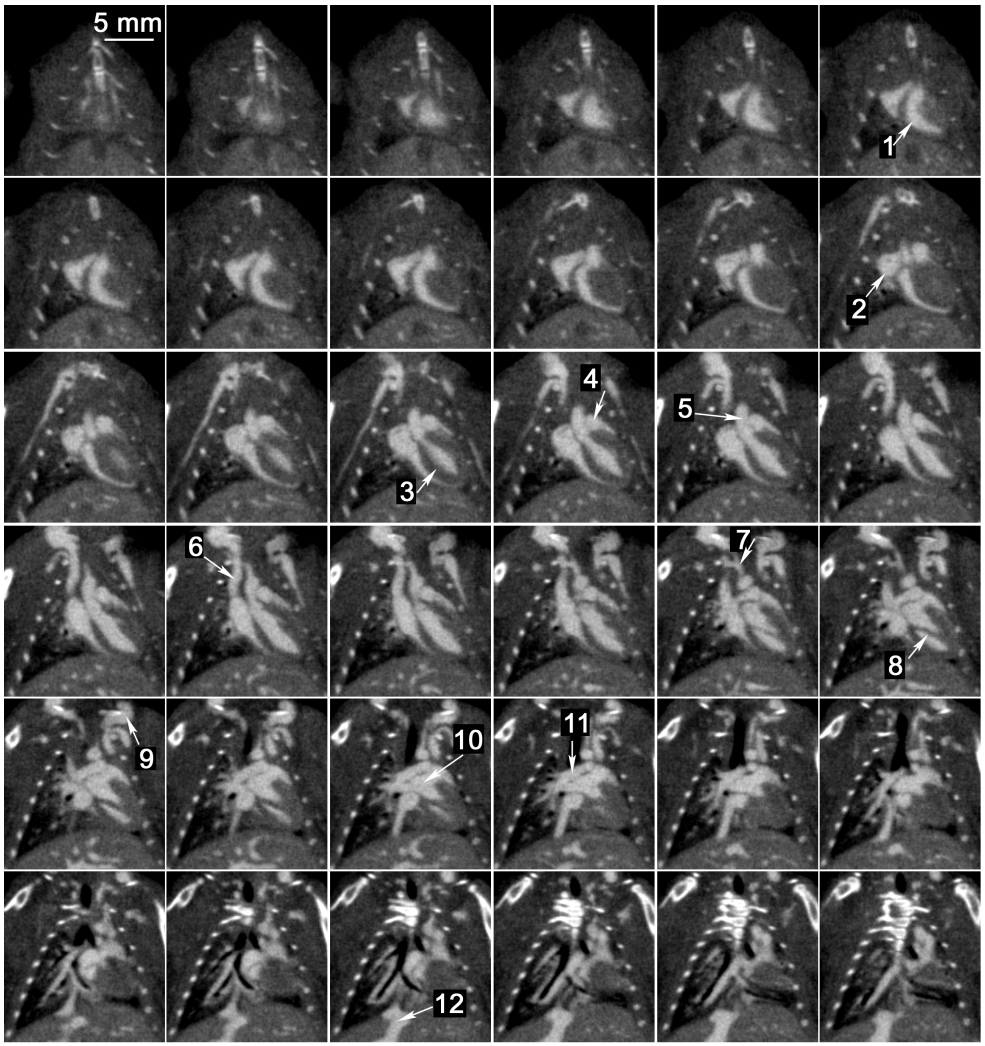

Figure 5: Collage of adjacent 150-μm thick coronal slices covering the entire extent of the heart, in the systolic phase, in the anterior-posterior direction. The collage demonstrates the isotropic resolution of the images and the high image quality over the entire volume. The image in the top left corner is the most anterior slice and the one in the lower left corner – the most posterior slice. The arrows identify the following cardiac/vascular structures: right atrium (1), right ventricle (2), left ventricle (3), left atrium (4), ascending aorta (5), superior vena cava (6), inominate artery, 0.6 mm diameter (7), papillary muscle, 0.4 mm diameter (8), left jugular vein (9), pulmonary trunk (10), right pulmonary vein and branches (11), and the inferior vena cava (12).

Table 1. Average functional parameters (mean ± SD) measured in free-breathing mice (n = 5) during a 50-s scan.

Parameter	
LV volume, systole (μl)	19.5 ± 5.2
LV volume, diastole (μl)	49.4 ± 7.6
Ejection fraction	0.61 ± 0.06
Stroke volume (μl))	29.9 ± 5
Cardiac output (ml/min)	12.4 ± 0.8

Discussion

In this paper we have presented the first use of a volumetric micro-CT scanner to acquire dynamic 3D cardiac images in free-breathing mice. The images, which took less than one minute to acquire, provide the ability to measure cardiac function in experimental mice, under typical physiological conditions, without the necessity to intubate the animals or place them in unnatural positions. The high speed of the technique makes it an ideal candidate for high-throughput studies for phenotype characterization, as well as for the study of diseased animals in short anesthesia periods, since scanning takes less than one minute. The functional measurements (LVEF, CO, *etc*.) that can be obtained in lightly anesthetized mice, from retrospectively gated micro-CT scans as described here, are equivalent to the type of measurements routinely performed clinically in humans, thereby making the technique an excellent candidate to follow cardiac function in models of disease; any findings in such models would be directly applicable to the clinical setting where the same functional measurements can be made.

This new cardiac imaging technique depends on the use of a novel slip-ring mounted micro-CT scanner. The voxel size of the reconstructed images is dependent on the scanner geometry and detector pixel size. Note that voxel spacing alone does not determine the effective spatial resolution of the system, which depends on geometric parameters, focal spot size and reconstruction algorithm. A detailed investigation of spatial resolution for this type of CT scanner has recently been published by Ross *et al.*,[15] who report the 10% cutoff of the modulation transfer function as ranging between 19 and

31 cm^{-1}; this result is consistent with our own measurements of the scanner's resolution.[16] To characterize any possible degradation in resolution (including the effects of temporal blurring) resulting from the retrospective gating, further studies are required. A technique to study the temporal resolution of a dynamic micro-CT scanning system has been previously described by our group and could be applied to this retrospective gating technique.[17]

The benefits of performing retrospective, rather than prospective, gating for mice are similar to those observed in human imaging: retrospective gating enables all time points within the cardiac cycle to be imaged and the entire cardiac cycle is imaged during one scan. Retrospective gating has most frequently been applied to human cardiac MRI, but was recently implemented in mouse cardiac MRI[5]; in that study multiple mice were imaged simultaneously, making prospectively triggered acquisition difficult. The rapid, retrospectively gated micro-CT technique described here has been applied to a single mouse in one scan, but could be adapted to multiple-mouse scanning, provided the respiratory and ECG signals of each mouse are recorded separately. However, it is not clear that the added complexity of implementing multiple-mouse micro-CT is necessary, given that a single mouse can be imaged in less than one minute. Retrospective gating is also amenable to self-gating techniques, where the raw projection data is used to determine the phase of the cardiac and respiratory cycles.[18, 19]

The cardiac functional parameters calculated based on the micro-CT images (Table 1) compare closely with previous measurements of cardiac function in mice. In the most direct comparison of the results presented here, with the measurements made by Badea *et al.* who used the same contrast agent, the measured values for LVSV, LVDV, stroke volume, and cardiac output were not significantly different from our results ($p > 0.1$ for all parameters, t-test).[7] Our EF was higher by approximately 14%, when compared to that reported by Badea,[7] but agrees well with values reported by others.[2, 4] The small difference may be attributed to differences in identifying the extent of the LV chamber in the images. The voxel spacing attained with the prototype-CT scanner described by Badea was 90 μm, compared to 150 μm for the Locus Ultra. The good agreement in physiological parameters measured by the two techniques suggests that the larger nominal voxel size is not the limiting factor in attaining accurate measurements of

cardiac function. The results reported in this study also compare closely to previous measurements using *in vivo* MRI. The slice thickness achievable using the volumetric micro-CT scanner is about 6 times smaller than the typically used MR slice thickness, leading to the ability to realign the volumetric images with the long-axis of the heart following reconstruction, with no loss in image quality. If the micro-CT images were averaged to mimic the typically used MRI slice thickness, a further reduction in dose is achievable.[20] Because of the requirement to reorient the images post-reconstruction in order to align the images with the long/short axis of the myocardium, voxel averaging would optimally be performed on the reoriented images.

Repeat measurements of the functional parameters of each mouse in three consecutive scans, performed after repositioning of each mouse, indicated very low intra-subject variability (see Table 1). For all functional parameters the intra-subject variability was lower than or the same as the inter-subject variability (calculated from one scan for each mouse), suggesting that biological variability is the dominant effect in these experiments. The inter-subject variability determined in this paper, for the different physiological parameters, can be used in the future to plan studies with the appropriate number of animals required to prove a specific hypothesis. As demonstrated in the presented power calculations, longitudinal studies – with 80% power – can be performed with as few as 5 animals per group when weekly changes of as little as 4% in EF are expected, thereby making this technique an ideal candidate for following both the progression and regression of disease.

The technique presented here is the only micro-CT technique available to image the mouse myocardium under conditions of free breathing. By not requiring intubation, this technique allows for frequent scans in longitudinal studies of cardiac function, without the possibility of inducing unnecessary damage to the mouse trachea, and reduces the amount of time during which the mouse is anesthetized, thereby reducing the adverse effects of prolonged anesthesia. Furthermore, by enabling scanning during free breathing, our technique can ensure that the function of the heart is evaluated in a physiological state that is as close as possible to the natural state of the mouse, provided anesthesia is maintained at a low level.[21-23] In the current study, the respiratory rates varied over a wide range, indicating that the technique can successfully reconstruct 4D

cardiac images under most conditions. Further studies, investigating the effect of respiratory and cardiac rate on image quality, will indicate the range of breathing rates over which image artifacts are minimized.

The 12-ms temporal window currently achieved may excessively blur the images during systole, but is similar to that used by Badea *et al.,*[7] The GE Locus Ultra is capable of rotating at speeds of up to 1 revolution per second, and acquiring projection images (albeit with a reduced longitudinal field of view) every 2 ms.. When this acquisition mode is available, we will investigate the optimal scanning protocol to maximize the number of views acquired per cardiac frame, and minimize the temporal acquisition window, while maintaining the dose to the animal at or below the currently achieved level of 28 cGy. It should also be noted that blur in the images obtained with this technique results both from the motion of the heart during the acquisition window and due to the scanner gantry motion during the acquisition of each projection; faster rotation speeds are expected to reduce added blur due to both effects, although detector lag associated with flat-panel devices[24] must also be considered. Faster rotation speed may also prove optimal in terms of providing a greater number of valid projection views (during expiration and the selected cardiac phase) during acquisition.

In the current implementation of the technique, only unique projection views are utilized, where for each cardiac time-point only data corresponding to at most one complete 360° rotation are used. However, because temporally resolved images were reconstructed over the entire cardiac cycle from a single scan, the effective dose efficiency is primarily reduced by discarding projection images acquired during inspiration. After correcting for the difference in voxel size and achieved image noise[20] between our study and the prospectively gated study by Badea *et al.,*[7] the dose delivered to the animal by our study was made only slightly higher by the exclusion of data acquired during inspiration. A small improvement in utilization of the acquired data could be achieved by averaging volumes reconstructed using all "valid" projections, or if projection data occurring during temporally adjacent cardiac or respiratory frames is used as well; further investigation is required to evaluate the effect on image blurring and the ability to measure cardiac functional parameters. Depending on the application, the dose efficiency could be improved if the mice were ventilated and only cardiac gating was

implemented. Furthermore, the currently used rotation speed may not be the optimal gantry-rotation speed to use in terms of dose-optimization. Faster gantry rotation and detector readout would improve the temporal resolution of the scans, as described above, and may lead to improved utilization of the x-ray dose as well.

Although retrospective gating results in the delivery of slightly more dose to the animal than is used to reconstruct the images, the dose to the animal is acceptable and within the limits set by previously performed studies, as summarized below. The 28 cGy entrance dose reported in the current study will result in a mean absorbed dose of approximately 14 cGy in a 2-cm diameter mouse,[25] which is similar to that reported in previous ungated,[10, 26] prospectively gated,[6, 7, 11, 27] or retrospectively gated[28-30] live-animal CT studies in mice. Although this dose is significantly greater than the dose reported for clinical diagnostic CT thorax exams in humans (2 to 3.5 cGy),[31, 32] it remains far lower than the radiation dose associated with conventional therapeutic exposures – 5000 cGy total, delivered in dose fractions of up to 1000 cGy.[33] The adverse effects of irradiating the thorax include pneumonitis, fibrosis, and neoplasia, but over the short term, pneumonitis and fibrosis are likely to be the major concerns. Fortunately, mice repair sub-lethal damage quickly, with repair half-times that range from 0.4 to 4 hours.[34, 35] Given the repair kinetics in the mouse lung following therapeutic dose levels,[34-36] it has been proposed in previous studies that a time interval of 6-8 hours be used between repeat exposures of over 100 cGy, in order to allow the majority of tissue repair to be completed.[37] Thus, we do not anticipate adverse effects in future longitudinal CT-based studies of cardiac function in mice, given the relatively low entrance exposure reported in this study.

The ability to obtain retrospectively gated cardiac data in this study has depended on the availability of an intra-vascular contrast agent, Fenestra VC, which has a long biological half-life,[38] and provides constant maximum vessel opacification over a period of about 2 hours in mice.[10] The volume of contrast agent injected in this study represented a significant fraction (~25%) of the blood volume of a mouse and may potentially have had an impact on mouse cardiac function. Studies to determine whether the volume of contrast agent injected has an effect on cardiac function will need to be performed by repeat scanning at with lower administered doses, while maintaining

sufficient contrast between the chambers and the myocardium. Other contrast agents with long circulation life-time *in vivo* are becoming available, and can allow multi-modal imaging using the same contrast agent, but may suffer from low iodine loading resulting in higher injected volumes.[39] Contrast agents with a higher iodine concentration would enable the volume of administered contrast agent to be reduced, while maintaining the contrast between the blood pool and tissue. Recently Mukundan *et al.* described a new liposomal-nanoscale iodinated contrast agent with almost double the iodine concentration (85 – 100 mg I/ml) compared to that of Fenestra VC, while demonstrating that the contrast remains within the vasculature for more than 3 hours, with enhancement after 2 hours of approximately 600 HU.[40] Use of this contrast agent in the retrospectively gated cardiac micro-CT studies could enable reduction of the delivered volume of contrast agent, or a reduction in x-ray dose, while maintaining SNR Furthermore, it might also be possible to acquire the retrospectively gated cardiac images during a constant infusion of clinical, non-ionic, extra-cellular contrast agent, with concentrations of iodine as high as 350 mg/ml. Badea *et al.* showed that by infusing 1 ml of Isovue-370 continuously over one hour, contrast enhancement of ~500 HU was achieved after 1 hr.[7] A similar approach might be applicable here, but would require further evaluation to determine the exact protocol required to provide a constant opacification of the vasculature during the 50-second scan. Aside from the higher iodine concentration of conventional, rapidly clearing contrast agents, the benefit to being able to use such agents in retrospectively gated micro-CT would extend the applicability of the technique to larger animals; currently the use of intra-vascular contrast agents in rats and rabbits is prohibitively expensive.

The image quality of the retrospectively gate cardiac images is high and amenable to automated image analysis. In this study, automated region growing was used to determine the volumes of the chambers, with minimal user intervention near the base of the heart. Ventricular wall mass and thickness, both important parameters used clinically, can also be determined from the images but would require further software development, given the low contrast between the heart wall and the surrounding tissues, such as the chest wall.

Future applications in mice will include studies of induced myocardial infarction and to monitor therapy, thereby making this an invaluable tool for the study of cardiovascular disease in pre-clinical models. Although others believed that cardiac CT in mice might not be possible,[41] we have shown that not only is it possible,[7] but can be performed in free breathing mice in scan times shorter than one minute.

Conclusion

Combining retrospective cardiac and respiratory gating with the high-speed acquisition of x-ray projection images over multiple rotations, using a high-speed volumetric micro-CT scanner, has enabled us to obtain 4D images, with 150-μm isotropic voxel spacing, of the hearts of free-breathing mice. Sufficient contrast is provided between the myocardium and blood pool through the intravenous injection of an intra-vascular contrast agent. This technique promises to become an important tool in the study of cardiac disease, since it provides a highly reproducible rapid means to quantify cardiac function in acute and longitudinal studies.

References

1. Ruff J, Wiesmann F, Hiller KH, et al. Magnetic resonance microimaging for noninvasive quantification of myocardial function and mass in the mouse. *Magn Reson Med* 40: 43-48, 1998.

2. Schneider JE, Cassidy PJ, Lygate C, et al. Fast, high-resolution in vivo cine magnetic resonance imaging in normal and failing mouse hearts on a vertical 11.7 T system. *J Magn Reson Imaging* 18: 691-701, 2003.

3. Cassidy PJ, Schneider JE, Grieve SM, et al. Assessment of motion gating strategies for mouse magnetic resonance at high magnetic fields. *J Magn Reson Imaging* 19: 229-237, 2004.

4. Dawson D, Lygate CA, Saunders J, et al. Quantitative 3-dimensional echocardiography for accurate and rapid cardiac phenotype characterization in mice. *Circulation* 110: 1632-1637, 2004.

5. Bishop J, Feintuch A, Bock NA, et al. Retrospective gating for mouse cardiac MRI. *Magn Reson Med* 55: 472-477, 2006.

6. Badea C, Hedlund LW, and Johnson GA. Micro-CT with respiratory and cardiac gating. *Med Phys* 31: 3324-3329, 2004.

7. Badea CT, Fubara B, Hedlund LW, et al. 4-D micro-CT of the mouse heart. *Mol Imaging* 4: 110-116, 2005.

8. Kiessling F, Greschus S, Lichy MP, et al. Volumetric computed tomography (VCT): a new technology for noninvasive, high-resolution monitoring of tumor angiogenesis. *Nat Med* 10: 1133-1138, 2004.

9. Greschus S, Kiessling F, Lichy MP, et al. Potential applications of flat-panel volumetric CT in morphologic and functional small animal imaging. *Neoplasia* 7: 730-740, 2005.

10. Ford NL, Graham KC, Groom AC, et al. Time-Course Characterization of the Computed Tomography Contrast Enhancement of an Iodinated Blood-Pool Contrast Agent in Mice Using a Volumetric Flat-Panel Equipped Computed Tomography Scanner. *Invest Radiol* 41: 384-390, 2006.

11. Ford NL, Nikolov HN, Norley CJ, et al. Prospective respiratory-gated micro-CT of free breathing rodents. *Med Phys* 32: 2888-2898, 2005.

12. Bakan DA, Lee FT, Jr., Weichert JP, et al. Hepatobiliary imaging using a novel hepatocyte-selective CT contrast agent. *Acad Radiol* 9 Suppl 1: S194-199, 2002.

13. Bakan DA, Weichert JP, Longino MA, et al. Polyiodinated triglyceride lipid emulsions for use as hepatoselective contrast agents in CT: effects of

physicochemical properties on biodistribution and imaging profiles. *Invest Radiol* 35: 158-169, 2000.

14. Otsu N. A threshold selection method from gray-level histograms. *IEEE Trans Systems, Man, and Cybernetics* smc-9: 62-66, 1979.

15. Ross W, Cody DD, and Hazle JD. Design and performance characteristics of a digital flat-panel computed tomography system. *Med Phys* 33: 1888-1901, 2006.
16. Du LY, Lee TY, and Holdsworth DW. Image quality assessment of a pre-clinical flat-panel volumetric micro-CT scanner. *Proceedings of SPIE; Medical Imaging: Physics of Medical Imaging* 6142: 614216, 2006.

17. Drangova M, and Fenster A. A laboratory CT scanner for dynamic imaging. *Med Phys* 21: 731-740, 1994.

18. Hiba B, Richard N, Janier M, et al. Cardiac and respiratory double self-gated cine MRI in the mouse at 7 T. *Magn Reson Med* 55: 506-513, 2006.

19. Lehmann GC, Holdsworth DW, and Drangova M. Angle-independent measure of motion for image-based gating in 3D coronary angiography. *Med Phys* 33: 1311-1320, 2006.

20. Ford NL, Thornton MM, and Holdsworth DW. Fundamental image quality limits for microcomputed tomography in small animals. *Med Phys* 30: 2869-2877, 2003.
21. Roth DM, Swaney JS, Dalton ND, et al. Impact of anesthesia on cardiac function during echocardiography in mice. *Am J Physiol Heart Circ Physiol* 282: H2134-2140, 2002.

22. Rottman JN, Ni G, Khoo M, et al. Temporal changes in ventricular function assessed echocardiographically in conscious and anesthetized mice. *J Am Soc Echocardiogr* 16: 1150-1157, 2003.

23. Schaefer A, Meyer GP, Brand B, et al. Effects of anesthesia on diastolic function in mice assessed by echocardiography. *Echocardiography* 22: 665-670, 2005.
24. Siewerdsen JH, and Jaffray DA. Cone-beam computed tomography with a flat-panel imager: effects of image lag. *Med Phys* 26: 2635-2647, 1999.

25. Boone JM, Velazquez O, and Cherry SR. Small-animal X-ray dose from micro-CT. *Mol Imaging* 3: 149-158, 2004.

26. Johnson EM, Price RE, Rivera B, et al. Intraperitoneal administration of an iodine-based contrast agent to improve abdominal micro-computed tomography imaging in mice. *Contemp Top Lab Anim Sci* 44: 20-27, 2005.

27. Hu J, Haworth ST, Molthen RC, et al. Dynamic small animal lung imaging via a postacquisition respiratory gating technique using micro-cone beam computed tomography. *Acad Radiol* 11: 961-970, 2004.

28. Walters EB, Panda K, Bankson JA, et al. Improved method of in vivo respiratory-gated micro-CT imaging. *Phys Med Biol* 49: 4163-4172, 2004.

29. Cavanaugh D, Johnson E, Price RE, et al. In vivo respiratory-gated micro-CT imaging in small-animal oncology models. *Mol Imaging* 3: 55-62, 2004.

30. Cody DD, Nelson CL, Bradley WM, et al. Murine lung tumor measurement using respiratory-gated micro-computed tomography. *Invest Radiol* 40: 263-269, 2005.

31. Campbell J, Kalra MK, Rizzo S, et al. Scanning beyond anatomic limits of the thorax in chest CT: findings, radiation dose, and automatic tube current modulation. *AJR Am J Roentgenol* 185: 1525-1530, 2005.

32. Mayo JR, Aldrich J, and Muller NL. Radiation exposure at chest CT: a statement of the Fleischner Society. *Radiology* 228: 15-21, 2003.

33. Camphausen K, Moses MA, Beecken WD, et al. Radiation therapy to a primary tumor accelerates metastatic growth in mice. *Cancer Res* 61: 2207-2211, 2001.

34. van Rongen E, Travis EL, and Thames HD, Jr. Repair rate in mouse lung after clinically relevant radiation doses per fraction. *Radiat Res* 141: 74-78, 1995.

35. Vegesna V, Withers HR, and Taylor JM. Repair kinetics of mouse lung. *Radiother Oncol* 15: 115-123, 1989.

36. Travis EL, Thames HD, Watkins TL, et al. The kinetics of repair in mouse lung after fractionated irradiation. *Int J Radiat Biol Relat Stud Phys Chem Med* 52: 903-919, 1987.

37. Parkins CS, Whitsed CA, and Fowler JF. Repair kinetics in mouse lung after multiple X-ray fractions per day. *Int J Radiat Biol* 54: 429-443, 1988.

38. Weichert JP, Lee FT, Jr., Longino MA, et al. Lipid-based blood-pool CT imaging of the liver. *Acad Radiol* 5 Suppl 1: S16-19, 1998.

39. Zheng J, Perkins G, Kirilova A, et al. Multimodal contrast agent for combined computed tomography and magnetic resonance imaging applications. *Invest Radiol* 41: 339-348, 2006.

40. Mukundan S, Jr., Ghaghada KB, Badea CT, et al. A Liposomal Nanoscale Contrast Agent for Preclinical CT in Mice. *AJR Am J Roentgenol* 186: 300-307, 2006.

41. Yea Y, Zhu J, and Wang G. Geometric studies on variable radius spiral cone-beam scanning. *Med Phys* 31: 1473-1480, 2004.

Appendix B

Ethics Approval for Animal Subjects

10.16.09

This is the Original Approval for this protocol
A Full Protocol submission will be required in 2013

Dear Dr. Drangova:

Your Animal Use Protocol form entitled:

Optimized Micro-CT of the Redent Heart and Coronary Vasculature

Funding Agency HSFO - Grant # T6293 has been approved by the University Council on Animal Care.

This approval is valid from **10.16.09 to 10.31.13** with a yearly renewal required each year.

The protocol number for this project is **2009-077**

1. This number must be indicated when ordering animals for this project.
2. Animals for other projects may not be ordered under this number.
3. If no number appears please contact this office when grant approval is received.
   If the application for funding is not successful and you wish to proceed with the project, request that an internal scientific peer review be performed by the Animal Use Subcommittee office.
4. Purchases of animals other than through this system must be cleared through the ACVS office. Health certificates will be required.

ANIMALS APPROVED FOR 4 Years

Species	Strain	Other Detail	Pain Level	Animal # Total for 4 Years
Mouse	As outlined in Protocol	25g male	C	130
Rat	As outlined in Protocol	300g male	C	30

REQUIREMENTS/COMMENTS
Please ensure that individual(s) performing procedures on live animals, as described in this protocol, are familiar with the contents of this document.

The holder of this Animal Use Protocol is responsible to ensure that all associated safety components (biosafety, radiation safety, general laboratory safety) comply with institutional safety standards and have received all necessary approvals. Please consult directly with your institutional safety officers.

c.c. J Dunmore-Buyze, M Pickering, W Lagerwerf

11.01.10
***This is the 1st Renewal of this protocol**
*A Full Protocol submission will be required in **2013**

Dear Dr. **Drangova**

Your Animal Use Protocol form entitled:

Optimized Micro-CT of the Rodent Heart and Coronary Vasculature

has had its yearly renewal approved by the Animal Use Subcommittee.

This approval is valid from **11.01.10 to 11.01.11**

The protocol number for this project remains as **2009-077**

1. This number must be indicated when ordering animals for this project.
2. Animals for other projects may not be ordered under this number.
3. If no number appears please contact this office when grant approval is received.
   If the application for funding is not successful and you wish to proceed with the project, request that an internal scientific peer review be performed by the Animal Use Subcommittee office.
4. Purchases of animals other than through this system must be cleared through the ACVS office. Health certificates will be required.

REQUIREMENTS/COMMENTS
Please ensure that individual(s) performing procedures on live animals, as described in this protocol, are familiar with the contents of this document.
The holder of this *Animal Use Protocol* is responsible to ensure that all associated safety components (biosafety, radiation safety, general laboratory safety) comply with institutional safety standards and have received all necessary approvals. Please consult directly with your institutional safety officers.

c.c. J. Dunmore, W. Lagerwerf, M. Pickering

Western

March 27, 2007

This is the Original Approval for this protocol
A Full Protocol submission will be required in 2011

Dear Dr. Feng:

Your Animal Use Protocol form entitled:
Modulation of Myocardial Function in Myocardial Infarction, Sepsis and Diabetes
Funding Agency CIHR - Grant #MOP-14653; CIHR partnership Grant - MOP-64395; HSFO - T-5306

has been approved by the University Council on Animal Care. This approval is valid from **March 27, 2007 to March 31, 2008.** The protocol number for this project is **2007-011-03**.

1. This number must be indicated when ordering animals for this project.
2. Animals for other projects may not be ordered under this number.
3. If no number appears please contact this office when grant approval is received.
   If the application for funding is not successful and you wish to proceed with the project, request that an internal scientific peer review be performed by the Animal Use Subcommittee office.
4. Purchases of animals other than through this system must be cleared through the ACVS office. Health certificates will be required.

ANIMALS APPROVED FOR 1 YR.

Species	Strain	Other Detail	Pain Level	Animal # Total for 1 Year
Mouse	Various Strains	3-6 months - M/F	D	2200
Rat	Sprague Dawley	200-300 gms - M/F	D	200

STANDARD OPERATING PROCEDURES
Procedures in this protocol should be carried out according to the following SOPs. Please contact the Animal Use Subcommittee office (661-2111 ext. 86770) in case of difficulties or if you require copies.
SOP's are also available at http://www.uwo.ca/animal/acvs
310 Holding Period Post-Admission
320 Euthanasia
321 Criteria for Early Euthanasia/Rodents
330 Post-Operative Care/Rodent
343 Surgical Prep/Rodent/Recovery Surgery
360 Blood Collection/Volumes/Multiple Species

REQUIREMENTS/COMMENTS
Please ensure that individual(s) performing procedures on live animals, as described in this protocol, are familiar with the contents of this document.

c.c. Approved Protocol Q. Feng, W. Lagerwerf, T. Kirkpatrick
Approval Letter - W. Lagerwerf, T. Kirkpatrick

Appendix C

Copyright Agreements

This thesis contains material from previously published manuscripts in Investigative Radiology (Chapter 2 and Appendix A), and Contrast Media and Molecular Imaging (Chapter 3); the copyright agreements for the three papers are included. Chapter 4 is adapted from a manuscript currently in press with the Journal of Applied Physiology. Appropriate reference to the published sources is given in the co-authorship section.

WOLTERS KLUWER HEALTH LICENSE TERMS AND CONDITIONS

Apr 30, 2012

This is a License Agreement between Sarah A Detombe ("You") and Wolters Kluwer Health ("Wolters Kluwer Health") provided by Copyright Clearance Center ("CCC"). The license consists of your order details, the terms and conditions provided by Wolters Kluwer Health, and the payment terms and conditions.

All payments must be made in full to CCC. For payment instructions, please see information listed at the bottom of this form.

License Number	2870421086427
License date	Mar 15, 2012
Licensed content publisher	Wolters Kluwer Health
Licensed content publication	Investigative Radiology
Licensed content title	Longitudinal Follow-up of Cardiac Structure and Functional Changes in an Infarct Mouse Model Using Retrospectively Gated Micro-Computed Tomography
Licensed content author	Sarah Detombe, Nancy Ford, Fuli Xiang, et al
Licensed content date	Jan 1, 2008
Volume Number	43
Issue Number	7
Type of Use	Dissertation/Thesis
Requestor type	Individual
Title of your thesis / dissertation	Applications of Rapid Cardiac Micro-CT
Expected completion date	Apr 2012
Estimated size(pages)	160
Billing Type	Invoice
Billing address	Imaging Research Laboratories Robarts Research Institute London, ON N6A 5K8 Canada
Customer reference info	
Total	0.00 USD
Terms and Conditions	

JOHN WILEY AND SONS LICENSE TERMS AND CONDITIONS

Apr 30, 2012

This is a License Agreement between Sarah A Detombe ("You") and John Wiley and Sons ("John Wiley and Sons") provided by Copyright Clearance Center ("CCC"). The license consists of your order details, the terms and conditions provided by John Wiley and Sons, and the payment terms and conditions.

All payments must be made in full to CCC. For payment instructions, please see information listed at the bottom of this form.

License Number	2896630845581
License date	Apr 26, 2012
Licensed content publisher	John Wiley and Sons
Licensed content publication	Contrast Media & Molecular Imaging
Licensed content title	Evaluation of eXIA 160 cardiac-related enhancement in C57BL/6 and BALB/c mice using micro-CT
Licensed content author	Sarah A. Detombe,Joy Dunmore-Buyze,Maria Drangova
Licensed content date	Mar 14, 2012
Start page	240
End page	246
Type of use	Dissertation/Thesis
Requestor type	Author of this Wiley article
Format	Print and electronic
Portion	Full article
Will you be translating?	No
Order reference number	
Total	0.00 USD
Terms and Conditions	

TERMS AND CONDITIONS

This copyrighted material is owned by or exclusively licensed to John Wiley & Sons, Inc. or one of its group companies (each a "Wiley Company") or a society for whom a Wiley Company has exclusive publishing rights in relation to a particular journal (collectively WILEY"). By clicking "accept" in connection with completing this licensing transaction, you agree that the following terms and conditions apply to this transaction (along with the billing and payment terms and conditions established by the Copyright Clearance Center Inc., ("CCC's Billing and Payment terms and conditions"), at the time that you opened your Rightslink account (these are available at any time at http://myaccount.copyright.com)

WOLTERS KLUWER HEALTH LICENSE TERMS AND CONDITIONS

Apr 30, 2012

This is a License Agreement between Sarah A Detombe ("You") and Wolters Kluwer Health ("Wolters Kluwer Health") provided by Copyright Clearance Center ("CCC"). The license consists of your order details, the terms and conditions provided by Wolters Kluwer Health, and the payment terms and conditions.

All payments must be made in full to CCC. For payment instructions, please see information listed at the bottom of this form.

License Number	2870421232067
License date	Mar 15, 2012
Licensed content publisher	Wolters Kluwer Health
Licensed content publication	Investigative Radiology
Licensed content title	Fast Retrospectively Gated Quantitative Four-Dimensional (4D) Cardiac Micro Computed Tomography Imaging of Free-Breathing Mice
Licensed content author	Maria Drangova, Nancy Ford, Sarah Detombe, et al
Licensed content date	Jan 1, 2007
Volume Number	42
Issue Number	2
Type of Use	Dissertation/Thesis
Requestor type	Individual
Title of your thesis / dissertation	Applications of Rapid Cardiac Micro-CT
Expected completion date	Apr 2012
Estimated size(pages)	160
Billing Type	Invoice
Billing address	Imaging Research Laboratories Robarts Research Institute London, ON N6A 5K8 Canada
Customer reference info	
Total	0.00 USD
Terms and Conditions	

Vita

Name: Sarah Anne Detombe

Post-secondary Education and Degrees:

The University of Western Ontario
London, ON, Canada
2005-2012, Ph.D., Medical Biophysics
Thesis: "Applications of Rapid Cardiac Micro-CT"
Supervisor: Dr. Maria Drangova

Queen's University
Kingston, ON, Canada
1998-2005, B.Sc., Honours in Life Sciences
(2-year absence while employed at RCMP)
Fourth-year Thesis: "Development of a HeLa cell-free system for use in studying checkpoint pathways"

Awards and Scholarships:

First Prize Poster Award
Ontario Preclinical Imaging Consortium - Imaging Network of Ontario
2011

CIHR Frederick Banting and Charles Best Canada Graduate Scholarship
2009-2010

Heart and Stroke Foundation Doctoral Award
2009-2010, Declined

Ontario Graduate Scholarship
2009-2010, Declined

Schulich Graduate Scholarship
The University of Western Ontario
2007-2010, Tuition Deferral

Student Travel Award
World Molecular Imaging Congress
2009

Ontario Graduate Scholarship
2007-2009

Best Overall Poster
Imaging Network of Ontario Symposium
2007

Western Graduate Research Scholarship
2005-2007, Tuition Deferral

Heart and Stroke Master's Studentship
2005-2007

CIHR Vascular Research Fellowship
2005-2007

Dean's Honour List
Queen's University
2001

Entrance scholarship
University of Ottawa
1998, Declined

Professional Work Experience:

Forensic Laboratory Technologist
RCMP Forensic Lab Services
Ottawa, ON, Canada
2001-2003

Summer Student Researcher
Supervisor: Dr. James Donnelly
Ottawa Hospital, Civic Campus
Ottawa, ON, Canada
1999 & 2000

Co-op Student Researcher
Supervisor: Dr. James Donnelly
Ottawa Hospital, Civic Campus
Ottawa, ON, Canada
1998

PUBLICATIONS/PRESENTATIONS

Peer-reviewed Papers

Published

1. **Detombe SA**, Dunmore-Buyze J, Drangova M. Evaluation of eXIA 160 Cardiac-related Enhancement in C57BL/6 and BALB/c mice using Micro-CT. *Contrast Media Mol Imaging* 7: 240-246, 2012.

2. Armitage SE, Pollman SI, **Detombe SA**, Drangova M. Least-error projection sorting to optimize retrospectively gated cardiac micro-CT of free-breathing mice. *Med Phys* 39: 1452-1461, 2012.

3. **Detombe SA**, Ford NL, Xiang FL, Lu X, Feng Q, Drangova M. Evaluating Cardiac Structure and Function in an Infarct Mouse Model using Retrospectively Gated Micro-CT. *Invest Radiol* 43: 520-529, 2008.

4. Graham KC, **Detombe SA**, MacKenzie LT, Holdsworth DW, MacDonald IC, Chambers AF, Drangova M. Contrast-enhanced Micro-Computed Tomography using Intraperitoneal Contrast Injection for the Assessment of Tumor-burden in Liver Metastasis Models. *Invest Radiol* 43: 488-495, 2008.

5. Drangova M, Ford NL,***** **Detombe SA,*** Wheatley AR, Holdsworth DW. Fast retrospectively gated quantitative 4D cardiac micro-CT imaging of free-breathing mice. *Invest Radiol* 42: 85-94, 2007. ***** NLF and SAD contributed equally

6. Donnelly JG, **Detombe SA**, Hindmarsh JT. Single-Strand Conformational Polymorphism and Denaturing Gradient Gel Electrophoresis in Screening for Variegate Porphyria: Identification of Two New Mutations. *Ann Clin Lab Sci* 32: 107-113, 2002.

In Press

1. **Detombe SA**, Xiang F, Dunmore-Buyze J, White JA, Feng Q, Drangova M. Rapid micro-computed tomography suggests cardiac enlargement occurs during conductance catheter measurements in mice. *J Appl Physiol*. In press, 2012.

Submitted

1. **Detombe SA**, Dunmore-Buyze J, Petrov IE, Drangova M. X-ray dose delivered during a longitudinal micro-CT study has no adverse effects on cardiac and pulmonary tissue in C57BL/6 mice. *Submitted to Phys Med Biol*, April 2012.

Conference Proceedings

1. **Detombe SA**, Dunmore-Buyze J, Petrov IE, Drangova M. Evaluating the dose effects of a longitudinal micro-CT study on pulmonary tissue in C57BL/6 mice. *Proc. SPIE Medical Imaging* 8313, 2012.

2. Holdsworth DW, **Detombe SA**, Chiodo C, Fricke ST, Drangova M. Implementation and assessment of an animal management system for small-animal micro-CT / micro-SPECT imaging. *Proc. SPIE Medical Imaging* 7965, 2011.

3. **Detombe SA**, Dunmore-Buyze J, Drangova M. Time-course characterization of an aqueous colloidal polydisperse contrast agent in mice using micro-computed tomography. *Proc. SPIE Medical Imaging* 7965, 2011.

4. Ford NL, **Detombe SA**, Wheatley AR, Holdsworth DW, Drangova M. Optimization of Retrospective Respiratory-gated High Speed Micro-CT for Free-breathing Mice, *Proc. SPIE Medical Imaging* 6143: 24-31, 2006.

Invited Presentations

1. **Detombe SA,** Xiang F, De Zordo T, So A, Dunmore-Buyze J, Feng Q, Lee TY, Drangova M. Evaluation of Cardiac Function in Mice using Micro-Computed Tomography. Imaging Network of Ontario, February 2010, Toronto ON.

2. **Detombe SA**, Ford NL, Xiang FL, Lu X, Feng QP, Drangova M. Applications of retrospectively gated cardiac micro-CT. Robarts Imaging Student Seminar Series, July 2008, London, ON.

3. **Detombe SA**, Ford NL, Xiang FL, Lu X, Feng QP, Drangova M. Applications of retrospectively gated cardiac micro-CT. Alan C. Burton Research Day, March 2008, London, ON.

4. Ford NL, Wheatley AW, **Detombe SA**, Holdsworth DW, Drangova M. Retrospectively gated imaging using a high-speed, flat-panel equipped cone beam micro-CT scanner, Annual Congress of the Canadian Association of Physicists, June 17-20, 2007, Saskatoon, SK.

5. **Detombe SA**, Ford NL, Xiang FL, Lu X, Feng QP, Drangova M. Evaluating cardiac structure and function in an infarct mouse model using retrospectively gated micro CT. ORDCF Micro CT Workshop, July 2006, London, ON.

6. Drangova M, Ford NL, **Detombe SA**, Holdsworth DW. Retrospectively gated cardiac micro CT. ORDCF Micro CT Workshop, July 2006, London, ON.

Conference Presentations/Published Abstracts

Proffered Presentations

1. **Detombe SA**, Dunmore-Buyze J, Petrov IE, Drangova M. Evaluating the dose effects of a longitudinal micro-CT study on pulmonary tissue in C57BL/6 mice. *Oral Presentation at SPIE Medical Imaging Conference, San Diego CA, Feb 2012.*

2. Holdsworth DW, **Detombe SA**, Chiodo C, Fricke ST, Drangova M. Implementation and assessment of an animal management system for small-animal micro-CT / micro-SPECT imaging. *Oral Presentation at SPIE Medical Imaging Conference, Orlando FL, Feb 2011.*

3. **Detombe SA**, Dunmore-Buyze J, Drangova M. Time-course characterization of an aqueous colloidal polydisperse contrast agent in mice using micro-computed tomography. *Oral Presentation at SPIE Medical Imaging Conference, Orlando FL, Feb 2012.*

4. **Detombe SA**, Xiang FL, Dumore-Buyze J, Feng Q, Drangova M. Direct Comparison of Retrospectively Gated Cardiac Micro-CT and Conductance Catheter Measurements in Mice. *Poster at Canadian Cardiovascular Congress*, Edmonton, AB, October 2009.

5. **Detombe SA**, Xiang FL, Dumore-Buyze J, Feng Q, Drangova M. Direct Comparison of Retrospectively Gated Cardiac Micro-CT and Conductance Catheter Measurements in Mice. *Poster at World Molecular Imaging Congress, Montreal, QC, September 2009.*

6. **Detombe SA**, Ford NL, Xiang FL, Lu X, Feng Q, Drangova M. Evaluating Cardiac Structure and Function in an Infarct Mouse Model using Retrospectively Gated Micro-CT, *Poster at Society for Molecular Imaging Conference, Providence, RI, September 2007.*

7. **Detombe SA**, Ford NL, Xiang FL, Lu X, Feng Q, Drangova M. Evaluating Cardiac Structure and Function in an Infarct Mouse Model using Retrospectively Gated Micro-CT, *Poster at London Imaging Discovery Day, London, ON, June 2007.*

8. **Detombe SA**, Ford NL, Xiang FL, Lu X, Feng Q, Drangova M. Evaluating Cardiac Structure and Function in an Infarct Mouse Model using Retrospectively Gated Micro-CT, *Poster at Second Biennial Heart Failure Colloquium, London, ON, May 2007.*

9. **Detombe SA**, Ford NL, Xiang FL, Lu X, Feng Q, Drangova M. Evaluating Cardiac Structure and Function in an Infarct Mouse Model using Retrospectively Gated Micro-CT, *Poster at Imaging Network of Ontario Symposium, Toronto, ON, March 2007.*

10. **Detombe SA**, Ford NL, Wheatley A, Holdsworth DW, Drangova M. Retrospectively-gated Cardiac Micro-CT Imaging in Mice, *Poster at Society for Molecular Imaging Conference, Waikoloa, Hawaii, September 2006.*

11. **Detombe SA**, Ford NL, Wheatley A, Holdsworth DW, Drangova M. Retrospectively-gated Cardiac Micro-CT Imaging in Mice, *Poster at London Imaging Discovery, London, ON, June 2006.*

12. **Detombe SA**, Ford NL, Wheatley A, Holdsworth DW, Drangova M. Retrospectively-gated Cardiac Micro-CT Imaging in Mice, *Poster at Margaret P. Moffat Graduate Research Day, London, ON, May 2006.*

13. **Detombe SA**, Ford NL, Wheatley A, Holdsworth DW, Drangova M. Retrospectively-gated Cardiac Micro-CT Imaging in Mice, *Poster at Imaging Network of Ontario Symposium, Toronto, ON, April 2006.*

14. Ford NL, Graham KC, **Detombe SA**, Wheatley A, Chambers AF, Holdsworth DW, Drangova M. Contrast-enhanced imaging using a high-speed, flat-panel equipped micro-CT scanner, *Oral presentation at Imaging Network of Ontario Symposium, Toronto, ON, April 2006.*

15. Ford NL, Wheatley A, **Detombe SA**, Holdsworth DW, Drangova M. Retrospective Respiratory-Gated Volume Micro-CT: a First Step Towards Cardiac Gated Imaging of Rodents, *Poster at Imaging Network of Ontario Symposium, Toronto, ON, April 2006.*

16. Ford NL, **Detombe SA**, Wheatley A, Holdsworth DW, Drangova M. Optimization of Retrospective Respiratory-gated High Speed Micro-CT for Free-breathing Mice, *Oral presentation at SPIE Medical Imaging Conference, San Diego, CA, Feb. 2006.*

17. Donnelly JG, **Detombe S**, Hindmarsh JT. Variegate Porphyria: Use of Single Strand Conformational Polymorphism To Screen for Mutations in the Protoporphyrinogen Oxidase Gene. *Poster at American Association of Clinical Chemistry Meeting, San Francisco, CA, July 2000.*

18. Hindmarsh JT, Donnelly JG, **Detombe SA**, Bulman DE. Variegate Porphyria: Use of single strand conformational polymorphism rapid screening and direct sequencing to identify asymptomatic carriers of mutations in the protoporphyrinogen oxidase gene. *Poster at Millennium Meeting on Porphyrins and Porphyrias, Institut Pasteur, Paris, Fr., 2000.*

19. Donnelly JG, French-Merkley V, **Detombe SA**. Association of the methionine synthase A2756G mutation and fetal wastage. *Poster at American Association of Clinical Chemistry Meeting, Chicago, IL, July 2001.*

20. Donnelly JG, Shirley F, **Detombe SA**. Relationship between factor v leiden and the factor v r2 haplotype (A4070G). *Poster at American Association of Clinical Chemistry Meeting, Chicago, IL, July 2001.*

21. Donnelly JG, **Detombe SA**. Use of heteroduplex formation and single strand conformational polymorphism to screen for mutations in the protoporphyrin oxidase gene (PPO). *Poster at American Association of Clinical Chemistry Meeting, Chicago, IL, July 2001.*

22. Donnelly JG, Isotalo PA, **Detombe SA**. Frequency and multigenic associations of polymorphisms in methionine synthase, cystathionine beta synthase and methionine synthase reductase genes in a neonatal population. *Poster at American Association of Clinical Chemistry Meeting, Orlando, FL, July 2002.*

23. Donnelly JG, Isotalo PA, **Detombe SA**. Multigenic association of mutations in the methylenetetrahydrofolate reductase and methionine synthase genes in failed pregnancy. *Poster at American Association of Clinical Chemistry Meeting, Orlando, FL, July 2002.*

24. Donnelly JG, **Detombe SA**, Joutovsky A. Patterns of Common Polymorphisms in the Homocysteine Remethylation Pathway in Failed Pregnancy. *Poster at American Association of Clinical Chemistry Meeting, Philadelphia, PA, July 2003.*

Published Abstracts

1. **Detombe SA**, Xiang FL, Dumore-Buyze J, Feng Q, Drangova M. Direct Comparison of Retrospectively Gated Cardiac Micro-CT and Conductance Catheter Measurements in Mice. *Mol Imaging Biol* 12 (Suppl 1): S392-S393, 2010.

2. **Detombe SA**, Xiang FL, Dumore-Buyze J, Feng Q, Drangova M. Direct Comparison of Retrospectively Gated Cardiac Micro-CT and Conductance Catheter Measurements in Mice. *Can J Cardiol* 25 (Suppl B): no. 145, 2009.

3. **Detombe SA**, Ford NL, Xiang FL, Lu X, Feng Q, Drangova M. Evaluating Cardiac Structure and Function in an Infarct Mouse Model using Retrospectively Gated Micro-CT. *Joint Mol Imaging Conference Abstract Book,* 2007.

4. **Detombe SA**, Ford NL, Wheatley A, Holdsworth DW, Drangova M. Retrospectively Gated Cardiac Micro-CT Imaging in Mice. *Mol Imaging* 5: 309-310, 2006.

5. Donnelly JG, **Detombe SA**, Joutovsky A. Patterns of Common Polymorphisms in the Hcy Remethylation Pathway in Failed Pregnancy. *Clin Chem* 49: P2 supp. S. A87, 2003.

6. Donnelly JG, Isotalo PA, **Detombe SA**. Frequency and multigenic associations of polymorphisms in methionine synthase, cystathionine beta synthase and methionine synthase reductase genes in a neonatal population. *Clin Chem* 48: P2 supp. S. F30, 2002.

7. Donnelly JG, Isotalo PA, **Detombe SA**. Multigenic association of mutations in the methylenetetrahydrofolate reductase and methionine synthase genes in failed pregnancy. *Clin Chem* 48: P2 supp. S. F31, 2002.

8. Donnelly JG, **Detombe SA**. Use of heteroduplex formation and SSCP to screen for mutations in the PPOX gene. *Clin Chem* 47: P2, supp. S. 324, 2001.

9. Donnelly JG, French-Merkley V, **Detombe SA**. Association of the methionine synthase A2756G mutation and fetal wastage. *Clin Chem* 47: P2 supp. S. 345, 2001.

10. Donnelly JG, Shirley F, **Detombe SA**. Relationship between factor V leiden and the factor V r2 haplotype (A4070G). *Clin Chem* 47: P2 supp. S. 346, 2001.

11. Donnelly JG, **Detombe S**, Hindmarsh JT. Variegate Porphyria: Use of SSCP to Screen for Mutations in the PPOX Gene. *Clin Chem* 46: P2 supp. S. 799, 2000.

12. Hindmarsh JT, Donnelly JG, **Detombe SA**, Bulman DE. Variegate Porphyria: Use of SSCP rapid screening and direct sequencing to identify asymptomatic carriers of mutations in the PPOX gene. *Cell Mol Biol* 48: 1-123, 2000.